UNCLASSIFIED

Classification Changed to
UNCLASSIFIED
JPL-Letter to Authority NASA-Langley
on Nov. 4, 1970, signed by W. E Hogsett
Date: Jan. 4, 1971
By: R. Castrain

Space Programs Summary No. 37-31, Volume I

for the period November 1, 1964 to December 31, 1964

The Lunar Program

(Title Unclassified)

JET PROPULSION LABORATORY
LIBRARY
FEB 18 1965

475

Copy No._____

CALIFORNIA INSTITUTE OF TECHNOLOGY

JET PROPULSION LABORATORY
CALIFORNIA INSTITUTE OF TECHNOLOGY
PASADENA, CALIFORNIA

January 31, 1965

CONFIDENTIAL
GROUP 4 Downgraded and declassified
LAB B03821
UNCLASSIFIED
166751

UNCLASSIFIED
CONFIDENTIAL

Preface

The *Space Programs Summary* is a six volume, bimonthly publication designed to report on JPL space exploration programs, and related supporting research and advanced development projects. The subtitles of all volumes of the *Space Programs Summary* are:

Vol. I. The Lunar Program (Confidential)

Vol. II. The Planetary–Interplanetary Program (Confidential)

Vol. III. The Deep Space Network (Unclassified)

Vol. IV. Supporting Research and Advanced Development (Unclassified)

Vol. V. Supporting Research and Advanced Development (Confidential)

Vol. VI. Space Exploration Programs and Space Sciences (Unclassified)

The *Space Programs Summary,* Volume VI consists of an unclassified digest of appropriate material from Volumes I, II, and III; an original presentation of the JPL (1) quality assurance and reliability efforts, and (2) environmental- and dynamic-testing facility-development activities; and a reprint of the space science instrumentation studies of Volumes I and II.

W. H. Pickering, *Director*
Jet Propulsion Laboratory

Space Programs Summary No. 37-31, Volume I

Copyright © 1965, Jet Propulsion Laboratory, California Institute of Technology

Prepared under Contract No. NAS 7-100, National Aeronautics & Space Administration

This document contains information affecting the national defense of the United States, within the meaning of the Espionage Laws, Title 18, U.S.C., Sections 793 and 794, the transmission or revelation of which in any manner to an unauthorized person is prohibited by law.

UNCLASSIFIED
CONFIDENTIAL

UNCLASSIFIED

Contents

I. *Ranger* Project 1
A. Introduction 1
B. Project Engineering 2
C. Guidance and Control 3
D. Supporting Activities and Engineering Facilities 5
E. TV Subsystem Development 6

II. *Surveyor* Project 8
A. Introduction 8
B. System Engineering 9
C. Scientific Experiments 11
D. Flight Control 26
E. Electrical Power Supply 34
F. Engineering Mechanics 37
G. Propulsion 47
H. Thermal Control 52
I. Spacecraft Vehicle and Mechanisms for Basic Bus 60
J. Reliability and Quality Assurance 65
K. System Testing 69
L. System Analysis 78
M. Launch Operations 83
N. Space Flight Operations 84

UNCLASSIFIED

UNCLASSIFIED

I. *Ranger* Project

A. Introduction

The *Ranger* Project was established to develop a space flight technology for transporting engineering and scientific instruments to the Moon and planets. Of the nine *Ranger* launchings, using *Atlas D–Agena B* vehicles, now planned, seven flights have been made.

Rangers 1 and *2* (Block I) were not lunar-oriented, but were engineering evaluation flights to test the basic systems to be employed in later lunar and planetary missions. Several scientific experiments were carried on a non-interference basis. Both spacecraft performed satisfactorily within the constraints of the obtained satellite orbit. *Rangers 3*, *4*, and *5* (Block II) carried a gamma-ray instrument, a TV camera, and a rough-landing seismometer capsule; each of these flights experienced failures.

The objective of the *Ranger* Block III (*Rangers 6* through *9*) flights is to obtain pictures of the lunar surface, at least an order of magnitude better than those obtainable with Earth-based photography, which will be of benefit to both the scientific program and the U.S. manned lunar flight program. The *Ranger 6* spacecraft, which was launched from the Air Force Eastern Test Range on January 30, 1964, and impacted the Moon essentially on target on February 2, 1964, did not accomplish the primary flight objective due to a failure of the TV subsystem to transmit pictures. An extensive analysis of the TV subsystem failure was conducted, new and reworked hardware was assembled as the *Ranger 7* TV subsystem, and extensive testing of the reassembled TV subsystem was performed. The *Ranger 7* spacecraft was launched from the Air Force Eastern Test Range on July 28, 1964, and impacted the Moon on target on July 31, 1964. The mission flight objective was accomplished. The outstanding events of the mission were the precision of the trajectory correction and the transmission of 4304 video pictures of the lunar surface.

The updating operations and scheduled tests for the *Ranger* proof test model (PTM) were completed. The PTM will be maintained in the *Ranger 8* and *9* configuration for use in evaluating any problems that might develop during these missions. *Rangers 8* and *9* are in various stages of assembly; subsystem and system tests are being performed.

UNCLASSIFIED

UNCLASSIFIED CONFIDENTIAL

B. Project Engineering

1. Ranger 8 Assembly and Testing Operations

System Test 3 (the last in the series) was conducted October 26, 1964. The spacecraft was exposed to both onboard and off-board RF sources. The "usual" interference was noted on the data encoder Address 90 measurements, but was not considered a problem.

Preparation for the explosive safe area (ESA) simulation tests, begun October 27, included an operational test of the flight secondary Sun sensors located on the solar panels. All checks indicated proper operation. The midcourse propulsion subsystem was also installed in the spacecraft with live pyrotechnics on that date.

Tests and operations from October 28 to November 9 were as follows: TV full-power RF test; Lockheed Missiles and Space Company (LMSC) adapter and shroud arrival and inspection; electrical checks on adapter wiring; determination of preload values for mating of spacecraft feet to LMSC adapter; matchmate of spacecraft to LMSC adapter; shroud omni-antenna coupler adjustment; RF transmission loss measurements; TV shroud light compatibility checks; operational checkout of spacecraft at ESA (simulated); precountdown and countdown dummy runs; pyrotechnic subsystem verification (RF link with electromagnetic interference); attitude-control and midcourse propulsion pressure transducer calibration with data encoder; replacement of attitude-control derived-rate module with flight unit and partial subsystem test; rework of TV subsystem to ensure flight status prior to environmental tests; and final checks and remate of the TV subsystem on the spacecraft bus.

Following the reassembly of the TV subsystem, an evaluation of camera operation indicated unacceptable performance from Camera P4. To allow time for further evaluation, the TV subsystem was assembled to the bus, and weight and center-of-gravity measurements were performed. The following day, the TV subsystem problem investigation was resumed. After several tests, a miswired ground on Camera P4 was corrected, and a shutter on Camera P2 was replaced. A replacement Camera P4 and associated electronics were installed and checked out November 12.

Vibration testing of the RA-8 spacecraft was conducted November 16 to 20. This testing included the following operations: modal verification, x-axis noise vibration; x-axis low- and high-frequency vibration; the complete y-axis vibration series (performed with no direct-access cabling attached to the spacecraft); torsional vibration; adjustment of attitude-control pressure vessel Belleville springs to flight value; preparation for z-axis vibration, including blast mat installation and pressurization of the attitude-control gas subsystems to approximately flight pressures; z-axis vibration; depressurization of the gas subsystems; and post-vibration modal verification.

No problems were encountered during the antenna deflection test and post-vibration system test which followed. During the pre-mission test verification, a problem was encountered in transferring the spacecraft power from "external" to "internal." Investigation revealed an out-of-tolerance switch in the power switch and logic module, necessitating replacement of the module.

The RA-8 midcourse sequence of Mission Test 1 at high temperatures was conducted December 2, and the terminal sequence December 4. Two problems occurred during the test: (1) The TV subsystem backup clock was out of the allowable 5-min tolerance, and telemetry pulses indicated that the clock was unstable; and (2) the resolution of Camera P4 was out-of-tolerance.

Mission Test 2 at low temperatures was begun December 4. In order to determine the magnitude of the Camera P4 resolution problem, a special TV subsystem turn-on test was run prior to the midcourse sequence. This test was performed with the TV subsystem temperature at 25°C, the highest expected in flight, to determine the resolution of Camera P4 at this temperature. The resolution improved to within specification value, and the decision was made to continue the test and not replace or refocus the camera. The midcourse sequence was completed on December 5, and cruise-mode conditions were re-established the following day. The terminal sequence of Mission Test 2 will be discussed in the next issue of the *SPS*, Vol. I.

2. Ranger 9 Assembly and Testing Operations

The RA-9 mechanical assembly operations completed November 13 included a satisfactory quantitative leak check on the attitude-control gas subsystem in the Spacecraft Assembly Facility pit. Ground wiring and electrical integrity checks and initial power application were successfully performed. All subsystem tests and calibrations with telemetry were completed by November 30, except for the pressure transducer calibrations and the TV subsystem test. The significant problems during the checks,

UNCLASSIFIED CONFIDENTIAL

UNCLASSIFIED

now under study, were an open fuse in a data encoder module and excessive noise on the communications ground receiver phase error.

The TV subsystem arrived at the Spacecraft Assembly Facility on December 4. Post-shipment verification tests and camera gain checks indicated that all camera gains were 15 to 25% high and would require readjustment prior to mating of the TV subsystem to the spacecraft bus.

A system test was performed on December 4 without the TV subsystem. The only significant anomaly in this test was a B2-1 event noted on the telemetry while motion checks on the spacecraft were being performed. The event apparently was the result of a gyro capacitor charge event by the central computer and sequencer (CC&S). This condition was found to be coincident with the system test fixture motor-start transient, which somehow was coupled into the CC&S.

A power survey on December 5 revealed a noise level higher than specification on the Command Converter 4A5 6-v dc output. The unit was replaced with a spare 4A5, and the noise level was then within specification.

craft operations. One failure has been encountered to date in spacecraft operations at the environmental testing facility. The external/internal power order switch in the power switch and logic module failed to transfer properly. Investigation revealed two problems associated with the failure. Measurements of the input voltage to the motor winding used to activate the switch indicated a low out-of-tolerance condition due to line drop in the test complex. The low-voltage condition did not allow the switch to transfer completely. This was corrected by appropriate engineering-change-requirement action. Secondly, although the switch would transfer with proper voltage applied, the transfer time was excessive. Investigation of this problem indicated a manufacturing defect. The assembly was subsequently replaced and spacecraft testing continued, with no further problems occurring in the power subsystem throughout the environmental testing.

One other engineering change requirement which was incorporated involved the power Case VI assembly. It was decided to lower the expected average operating case temperature during the flight of subsequent *Rangers*. This reduction in temperature was accomplished by altering the thermal shield and paint pattern for the case. The combination of the normal high solar intensity during the launch period and the expected lower power efficiency would have caused the power booster-regulator operating temperature to approach the upper operation limit.

C. Guidance and Control

1. Spacecraft Power Subsystem

All *Ranger* power flight hardware has been retested to verify proper performance prior to spacecraft testing operations. This requalification was considered necessary due to the relatively long and inactive period between *Rangers* 7 and 8. The retest consisted of applicable portions of the normal power systems bench test, i.e., efficiency and operational limits testing, including a margin test, ripple and spike measurements, and failure-mode testing. The data were reviewed and checked for conformance to specifications and also for degradation from prior performance and, in all cases, were acceptable.

The power subsystem, certified as flightworthy, was delivered to the Spacecraft Assembly Facility for space-

2. Attitude-Control-Subsystem Gyro and Electronic Modules

a. Functional description. The *Ranger* attitude-control subsystem requires angular rate and position information about each of the three major axes: pitch, yaw, and roll. Angular rate information is used during the acquisition and cruise periods for stabilization of the subsystem. The angle information is also required during the maneuver period for midcourse correction.

The gyro subassembly derives this information by a unique application of three single-degree-of-freedom floated integrating gyros. These gyros, the Minneapolis–Honeywell Regulator Company Model GG49-E19, are filled with a low-viscosity high-density fluid which provides full flotation at 115°F. A low-viscosity fluid has been selected which permits operation of the gyros without heaters. Both damping and precession-axis restraint are accomplished by a torque feedback loop. The restraint

UNCLASSIFIED

UNCLASSIFIED
CONFIDENTIAL

provided by this electronic loop remains relatively constant, independent of changes in fluid viscosity due to temperature.

b. Testing of gyro modules. Following the *Ranger 7* mission in July 1964, the flight spare gyro and gyro electronics modules Serial No. 303 were returned from the launch station. This complete inertial sensor system will be maintained as the first spare system for *Ranger 8*. As of mid-December 1964, this system has accumulated approximately 800 hr of testing time, as indicated by the spin motor running-time meter mounted on the module. To further strengthen backup capability and to reduce down-time in the event of any necessary gyro module rework, additional single gyro testing has been proceeding normally for the past 2 mo. The present plan is to qualify and flight-acceptance-test at least four gyros. The gyro module Serial No. 310, which was not complete at the end of the Block III build schedule at Nortronics Corporation, has been completed at JPL and is being prepared for flight-acceptance testing as an additional spare for both the *Ranger 8* and *9* flight systems.

Between the *Ranger 7* firing and the *Ranger 8* and *9* systems tests begun in October, several confidence checks were made on the flight gyro and electronics modules (Serial Nos. 306, 308, and 309 for *Ranger 8*, *Ranger 9*, and the *Ranger 9* spare, respectively). These confidence checks were necessary due to the 5 mo of inactive storage expected for these systems. The results of these tests on commanded-turn-rate calibration and gyro performance, as well as the calibrations of the gyro electronics and accelerometer modules, indicate that no significant deviations from previous data points have taken place.

c. Detection of sync point of gyro motors. A gyro spin motor sync problem was detected on the *Ranger 9* gyro module. Extensive testing of the pitch gyro Serial No. G35 indicated that, at spacecraft ambient temperatures of 70 to 85°F, the blockhouse operational-support-equipment (OSE) operator could not be certain of a visual meter indication that this gyro was positively coming up to the synchronous speed of 24,000 rpm. The spacecraft three-phase 400-cps power supplies are expected to have output voltages as low as 22.0 v rms on gyro starting and 23.8 v rms with the gyro running under these cold start conditions. As a result of this problem, 28 single gyros not mounted in modules were tested for the cold start condition. Starting voltages as low as 23 v and temperatures as low as 50°F, as well as various combinations of higher temperatures and voltages, were investigated.

An unusual instrumentation method was used for detecting the actual sync point of these gyro motors. The typical laboratory method uses a small shunt or an AC current meter in one of the three input leads to the three-phase spin motor. A small but abrupt change in this current is the normal indication of the motor reaching sync speed. However, at low temperatures and voltages, the pull in the motor is so slow that no positive indication is given as to when the motor actually reaches 24,000 rpm. Therefore, a new method was devised which uses a miniature vibration accelerometer made by Endevco Corporation. This small accelerometer is attached by double-sided adhesive tape to the top of the gyro. The output of the accelerometer is fed first to a very-high-input impedance preamplifier, then through an amplifier sharply tuned to 400 cps, and finally to an oscilloscope. The accelerometer actually picks up the very small amount of vibration caused by the spin motor flywheel not being in perfect balance. The output frequency from the accelerometer is compared with the motor power frequency by means of a lissajous pattern on the oscilloscope. When the resultant pattern stops rotating, the motor is then in sync. This method is so sensitive that it is even possible to see the motor change its sync point by one segment on the stator.

The results of these tests indicate that each gyro has a threshold combination of temperature and voltage where a definite indication can be visually observed by the OSE operator. This visual observation used under prelaunch conditions is actually a small up-down kick of the meters used for indication of the gyro rebalance output.

In an effort to reduce the possibility of prelaunch hold uncertainty due to the OSE operator not observing the gyro motors come into synchronism, a request was made for two changes to the system: (1) the addition of a strip chart recorder to the blockhouse monitoring equipment to supplement the OSE operator's visual indication of motor sync and to provide a permanent record of the gyro motor runup, and (2) better control of the spacecraft thermal environment so that the cold start condition will be limited to a minimum spacecraft ambient temperature of not less than 75°F. At this temperature, even those gyros which are slow to pull in will yield a fair indication of motor sync. Also, it has been agreed that, if the sync indication is missing, the gyros will be left on for at least 10 min, shut off, and allowed to run down, and the process will then be repeated a second time. This will allow the gyro to self-heat, which will increase the likelihood of the motor coming into sync the second time.

UNCLASSIFIED

UNCLASSIFIED
CONFIDENTIAL

D. Supporting Activities and Engineering Facilities

1. Environmental Test Program

From mid-October to mid-December 1964, 27 experimental, 13 type-approval, and 28 flight-acceptance tests associated with the *Ranger* Block III Project were completed by the JPL Environmental and Dynamic Testing Laboratory (Table 1).

Table 1. *Ranger* usage of JPL Environmental and Dynamic Test Laboratory from mid-October to mid-December 1964

Facility	Number of tests
Vibration	36
Acoustic	0
Centrifuge	3
Shock	1
Handling shock	1
Temperature	9
Explosive atmosphere	0
Vacuum	18
Total	68

2. Space Simulators

One of the hazards of testing a spacecraft in a vacuum chamber results from an unexpected or uncontrolled increase in chamber pressure. Somewhere in the pressure range of 1 to 10^{-3} torr, a corona breakdown occurs between points with a high potential difference. This can and has resulted in damage to portions of the spacecraft under test when the chamber pressure unexpectedly passes through this range.

Experience has indicated that reliance upon manual cutoff of electrical power to critical circuits is usually inadequate to prevent damage, unless the pressure rise is quite slow (an improbable occurrence). The solution to the problem is to provide an automatic pressure sensing system which de-energizes the spacecraft high-voltage power before the pressure increases to the danger level.

The pre-set actuation point for the shutdown system in the JPL 25-ft Space Simulator was established at 5×10^{-4} torr. The pressure-measuring device selected for the system is an ionization gage. This, however, presents additional problems from the viewpoint of probable instrument failure as compared to the probability of a vacuum system failure. For this reason, three ionization gages are used in a circuit which requires the simultaneous measurement of a pressure above the prescribed limit. A block diagram of the system is presented in Fig. 1.

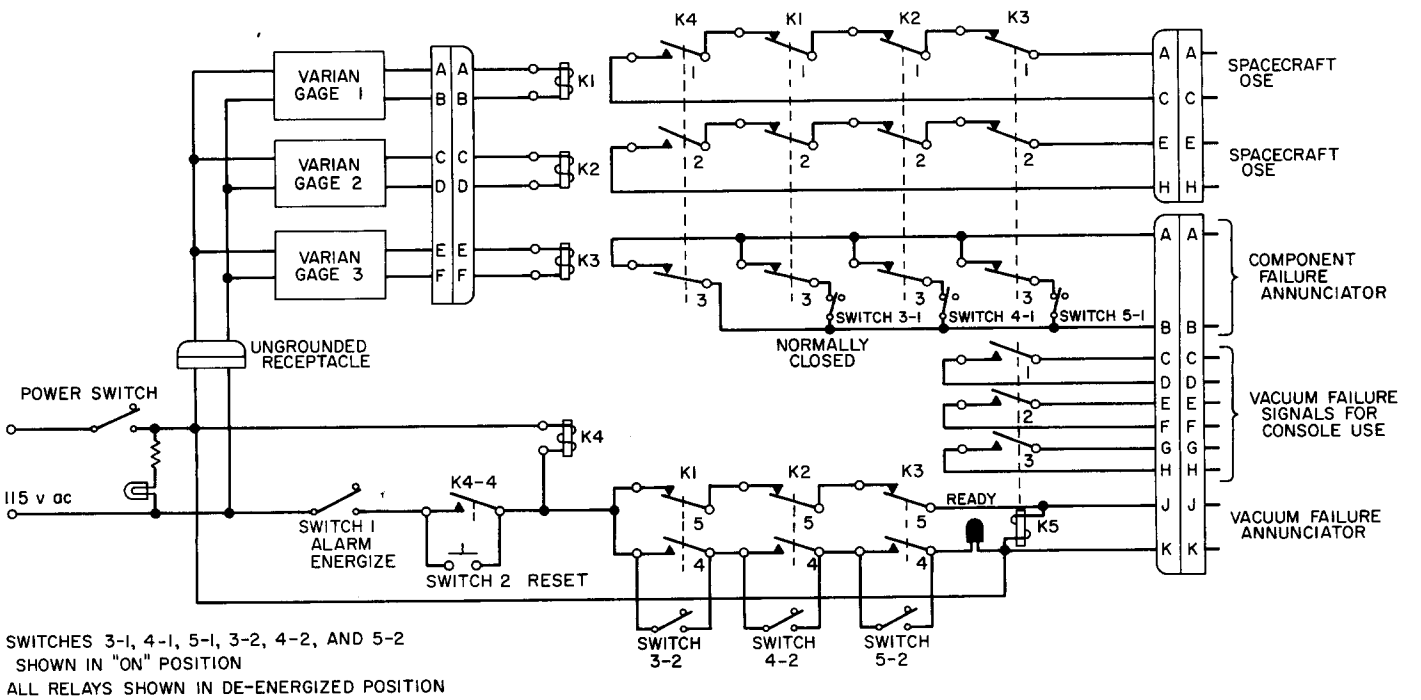

Fig. 1. Automatic vacuum failure alarm system

UNCLASSIFIED
CONFIDENTIAL

UNCLASSIFIED

Since it is desired to limit the shutdown of the spacecraft power to a failure of the vacuum system, an AC relay, K4, connected across the 115-v power to the instruments prevents a shutdown due to console power failure.

Each Varian Associates ionization-gage control unit has a built-in alarm circuit which will actuate a relay contact at some pre-set pressure level. These relays, designated K1, K2, and K3, are set to actuate at 5×10^{-4} torr. A normally closed contact is used to provide a system which requires the instrument to be operating and sensing a satisfactory pressure (i.e., less than 5×10^{-4} torr) in order to open the relay contact. If a particular Varian Associates ionization-gage system fails, it can be taken out of the circuit by turning its power off.

E. TV Subsystem Development

The following material relating to the TV subsystem development was abstracted from the RCA report: *Ranger TV Subsystem, Block III, Twentieth Bimonthly Progress Report,* December 1, 1964, covering the period from September 16 to November 15, 1964.

1. System Engineering

a. FM III-3 (Ranger 8). Flight Model (FM) III-3 completed testing operations at RCA and was shipped to JPL, arriving October 18, 1964. The following tests were successfully completed after its arrival: post-shipment test, matchmate test, Systems Tests 2 and 3, backup function test, launch complex electrical checkout, explosive-safe-area full-power test, TV subsystem shroud light compatibility test, explosive-safe-area operational checkout, precountdown dummy run, countdown dummy run, extension system verification test with pyrotechnics, communications verification test, and camera verification test.

b. FM III-4 (Ranger 9). Initial electrical integration and testing of FM III-4 was begun. Operation was normal during the communications alignment and calibration procedure performed October 15 and 16. Camera microphonics tests were performed from October 21 to 30 to evaluate a new technique of isolating each camera shutter from each camera head at the interface. Significant reduction of shutter microphonics was indicated. The flight Cameras P1 through P4 and F_a were installed. Calibration of Camera F_a was completed, and calibration of Cameras P1 through P4 was begun November 11.

c. Spare. Assembly of components and harnesses on the spare structure was completed, and abbreviated electrical tests were performed on the TV subsystem (less cameras). The spare was then shipped to JPL.

2. Cameras

Testing of FM III-3 revealed the following problems: camera-to-camera microphonic coupling, other excessive noise, and variations in resolution. The camera-to-camera microphonics has been reduced by the replacement of the shutter mounting gasket with a new design which isolates the shock at the end of each shutter stroke. These shock-isolating shutter gaskets have been installed on all cameras for FMs III-3 and -4.

The variation in resolution of FM III-3 cameras was investigated in a series of special tests. The independent effects of changes in focus current and mesh voltage were measured, and these changes were found to be far too small to justify the large changes in resolution. The focusing methods used on the cameras were evaluated. During testing, it was found that the focal length changed appreciably in an air-to-vacuum environment and that thermal expansion at elevated temperatures added to the defocusing. Work is continuing on methods to obtain the best possible focus for the cameras.

The evaluation of the partial-scan vidicons was completed, with the last three vidicons being rejected because of mask error. The full-scan vidicon procurement effort was also completed, with 21 vidicons received. These vidicons are presently being evaluated. The mechanical qualifications tests of the 1500-line-mesh full-scan vidicon have been successfully completed. Studies of the spectral response of the *Ranger* vidicons are continuing.

3. Telecommunications

A detailed checkout of all telecommunications equipment on FM III-3 was performed at JPL. All equipment was determined to be within specification, with performance very similar to that obtained during acceptance tests and initial checkout of FM III-3 at RCA. Acceptance testing of all assemblies for FM III-4 was completed, and the equipment was delivered for integration. Testing of the telecommunications equipment on FM III-4 showed all equipment within specification and ready for the start of environmental tests.

Modification of the proof-test-model transmitters and transmitter power supplies to the Resdel intermediate-power-amplifier configuration and acceptance testing of

UNCLASSIFIED

UNCLASSIFIED

the two transmitters for the second set of spares are continuing.

4. Systems Control and Electrical Power

Following a malfunction of the TV subsystem operating with the ground support equipment, it was decided to check Capacitors C1 and C2 of all flight command control units for leakage resistance. Units from FMs III-3 and -4 and the two spares were checked and found to be within specification.

A modification to provide greater resolution of the cruise-mode current was completed on all units of all current-sensing groups. All, except for the qualification test units, have been tested and returned to use. Tests on the qualification test units are under way.

All of the high-current and low-current voltage regulators for FMs III-3 and -4 have been tested and integrated into the respective TV subsystems.

Four new batteries to be used to support FM III-4 during thermal-vacuum tests at JPL are in production at the vendor's facility. There are enough batteries on hand to meet all other anticipated test requirements for FMs III-3 and -4.

Seven of the 13 flight and flight spare batteries for FMs III-3 and -4 were removed from storage at the vendor's facility and activated. One of these will be used as a flight lot qualification test unit, and the other six will be used as flight and flight spare units for FM III-3. The six batteries remaining in storage will be used as flight and flight spare batteries for FM III-4.

5. Thermal Control

From September 19 to October 7, four series of thermal-vacuum tests were performed. Actually, the tests were electrical verification tests in which the terminal-mode operations of the TV subsystem were exercised in a simulated space environment, with each test run starting from a predetermined average cruise-mode temperature. A thermal-balance test was not required since the TV subsystem had been thermally tested prior to electrical modification. These previous tests showed that FM III-3 had thermal characteristics similar to those of FM III-2 (*Ranger* 7). The temperature data obtained during the thermal-vacuum tests were normal.

In preparation for thermal-vacuum testing at JPL, the thermal shrouds of FM III-3 were painted to flight configuration. This is a deviation from the normal procedure of painting the shrouds after completion of thermal-vacuum testing. However, the requirement to use solar simulation rather than electrical heating of the spacecraft during the "no-cables" test at JPL necessitated this action. Extreme care in handling must be exercised if the TV subsystem is to be shipped directly to the Air Force Eastern Test Range without repainting after thermal-vacuum testing.

The thermal finishes employed on the TV subsystem during the *Ranger* 7 mission provided desirable cruise-mode temperatures to all portions of the TV subsystem. There is no reason to change the average temperature of the over-all spacecraft or to alter the thermal distribution within the TV subsystem for the *Ranger* 8 mission. One exception to this will be the application of a white paint to the antenna ring, resulting in a slightly lower temperature in the cameras.

Terminal-mode temperatures of FM III-3 will be affected to a limited degree by changes in equipment from the *Ranger* 7 design. The only equipment changes made thus far are in the intermediate power amplifiers of the transmitter assemblies and in the battery mounting bars. The configuration of intermediate power amplifiers incorporating the Resdel cavity was found to operate considerably cooler than the configuration used on FM III-2. The change in construction material of the battery support bars will have little or no effect on battery temperatures.

During the final hours of the *Ranger* 7 flight, a temperature increase of 7 or 8°F was noted in the camera-lens-housing telemetry. It has been found that the flux density of thermal energy as the spacecraft approaches the lunar surface is sufficient to cause the encountered temperature increase. The *Ranger* 8 spacecraft can be expected to encounter a rise in temperature of 7.5 to 8.5°F in the area of the camera lens housing during the last 3 hr of flight.

6. Ground Support Equipment

The design is complete of a modification to the trailing-edge sync circuitry to provide more dependable operation during normal mode and during the Camera P1 free-running mode. Modification of the ground support equipment is being performed as the units become available. Modifications to the high-voltage power supplies, system test console, and ground power supply cabinet are also being incorporated.

UNCLASSIFIED

UNCLASSIFIED
CONFIDENTIAL

II. *Surveyor* Project

A. Introduction

The *Surveyor* Project will take the next step in developing lunar technology by attempting soft landings on the Moon with a group of test missions whose objective is to demonstrate successful soft landing by post-landing spacecraft operation. An engineering payload including elements of redundancy, increased diagnostic telemetry, touchdown instrumentation, and survey TV will be used.

Following the test missions, the general objective is to conduct lunar exploration to extend our knowledge of the nature of the Moon and to discover and verify the suitability of sites for *Apollo* spacecraft landings. These flights will carry a scientific payload selected from the following experiments: two-camera TV, micrometeorite ejecta, single-axis seismometer, alpha-particle scattering, soil properties (surface sampler), and touchdown dynamics.

Through 1966 spacecraft will be injected into the lunar trajectory by direct ascent, using single-burn *Atlas–Centaur* vehicles. For launches prior to 1966 a 50-m/sec midcourse correction capability will exist. Launches performed in 1966 will require a 30-m/sec midcourse correction capability.

Hughes Aircraft Company is under contract to develop and manufacture the first seven spacecraft.

The major portion of the following material relating to the *Surveyor* spacecraft system was derived from material prepared by the Hughes Aircraft Company; articles prepared by the JPL Technical Sections are identified by footnotes to the article titles. The principal model designations and vehicles discussed are defined in Table 1.

UNCLASSIFIED
CONFIDENTIAL

UNCLASSIFIED

Table 1. Model and vehicle designations

Designation	Description
SC-1—4	Flight spacecraft with engineering payload
SC-5—7	Flight spacecraft with scientific payload
A-21	Model designation for spacecraft with engineering payload (SC-1—4)
A-21A	Model designation for spacecraft with scientific payload (SC-5—7)
T-21	Model A-21 prototype system test spacecraft
T-21A	Model A-21A prototype system test spacecraft
T-2	Simplified spacecraft for evaluation of terminal descent propulsion and flight control
S-2	Test spaceframe for vibration, shock, and static structural tests
S-6, -7	Test spaceframe for vernier propulsion system tests
S-8	Test spacecraft for flight control buzz tests

B. System Engineering

1. A-21 Spacecraft Configuration

The first four flight spacecraft (Model A-21) are designed to carry an engineering instrument payload to evaluate spacecraft performance and lunar soft-landing characteristics. The current A-21 weight summary is shown in Table 2. The A-21 balance summary showing the center-of-gravity location is given in Table 3.

Table 2. A-21 spacecraft weight summary

Item	Current design weight, lb
Total separated weight	2172.81
Basic bus	703.33
Usable propellant	1406.91
Engineering payload	62.57

Table 3. A-21 spacecraft weight and balance summary

Condition	Weight, lb	Vertical center of gravity Z location[a]	Lateral X location	Center of gravity Y location
Spacecraft after Centaur separation	2172.81	12.10	+0.13	−0.11
Maximum touchdown	648.71	16.88	+0.15	−0.11
Minimum touchdown	608.51	17.55	+0.16	−0.04

[a]Inches above landing gear hinge line (spacecraft station 47.48)

2. A-21A Spacecraft Configuration

The fifth, sixth, and seventh flight spacecraft will have a scientific instrument payload for the measurement and evaluation of lunar surface characteristics. The configuration with the scientific payload is designated A-21A. The latest A-21A spacecraft weight summary is shown in Table 4.

Table 4. A-21A spacecraft weight summary

Item	Current design weight, lb
Total separated weight	2150.00
Basic bus	704.27
Usable propellant	1381.81
Scientific payload	63.92

3. Functional Description of A-21 System

A functional description of the A-21 spacecraft, which shows the detailed system functional relationships and assists in system test, mission operations, postflight evaluation, failure mode analysis, and spacecraft familiarization, has been updated. The sixth issue of the A-21 Functional Description was released December 1, 1964 and comprises three volumes:

(1) Volume I contains system and subsystem level functional block diagrams and theory of functional operation for the *Surveyor* system and six *Surveyor* subsystems.

(2) Volume II contains updated revisions of the basic publication with functional schematic diagrams and theory of functional operation.

(3) Volume III contains a concise data sheet for each telemetry signal of the A-21 spacecraft. The data sheet describes, by functional representation, how the signal is generated and scaled, and interconnected to the units used for signal processing. Included on each data sheet is a brief description of the signal, its significance, and its characteristics such as telemetry range, scale factor, and expected value.

4. Transient Effect Studies

An extensive analytical study was undertaken to determine the design changes required to eliminate all undesirable effects of transients at each connector pin of several subsystem units and at the silicon controlled rectifiers (SCR) installed in the units. The effect of these transients on the *Surveyor* units was broken up into two

UNCLASSIFIED

UNCLASSIFIED

categories. The first category is unit survival. A unit is considered not to survive if any function of the unit has undergone degradation. This resulted in establishing reasonable stress levels for all classes of components. The second category is unit malfunction. The unit is considered to malfunction if: (1) it has been destroyed or causes another unit to be destroyed, (2) it has changed modes of operation, (3) it results in another unit changing modes of operation, or (4) it results in the activation of a Deep Space Instrumentation Facility (DSIF) command circuit.

The transient study was applied to each connector pin on the following units: flight control, receiver/transponder, Transmitters A and B, approach and survey TV, TV auxiliary, altitude marking radar, auxiliary battery control, boost regulator, battery charge regulator, engineering mechanisms auxiliary, thermal control and Heaters A and B. The ability of the unit to survive and not malfunction was determined. In addition, the threshold level for destruction or malfunction was determined on existing hardware.

All SCR circuits were given special attention to determine that no parameter had been overlooked in the initial design and that adequate margins for operation had been used. The necessary circuit changes for transient protection and to correct circuit deficiencies in the SCR circuits were explored. This exploration included the number of components added, the approximate increase in weight, and a brief statement concerning the packaging problem.

Most of this study was primarily analytical. However, a transient generator was obtained and some experimental verification of the effects of the transients and suitability of suppression networks was verified.

A study plan on the engineering mechanisms auxiliary (EMA) unit was completed. The investigation provided supplementary information for the desensitizing program. The EMA was subjected to power bus switching transients while varying the waveshape of the command pulses.

The following circuits were monitored during the switching period to establish pulse rise, fall, amplitude, width, and duty factor which cause changes in switching response phenomena:

(1) EMA input bus voltages.

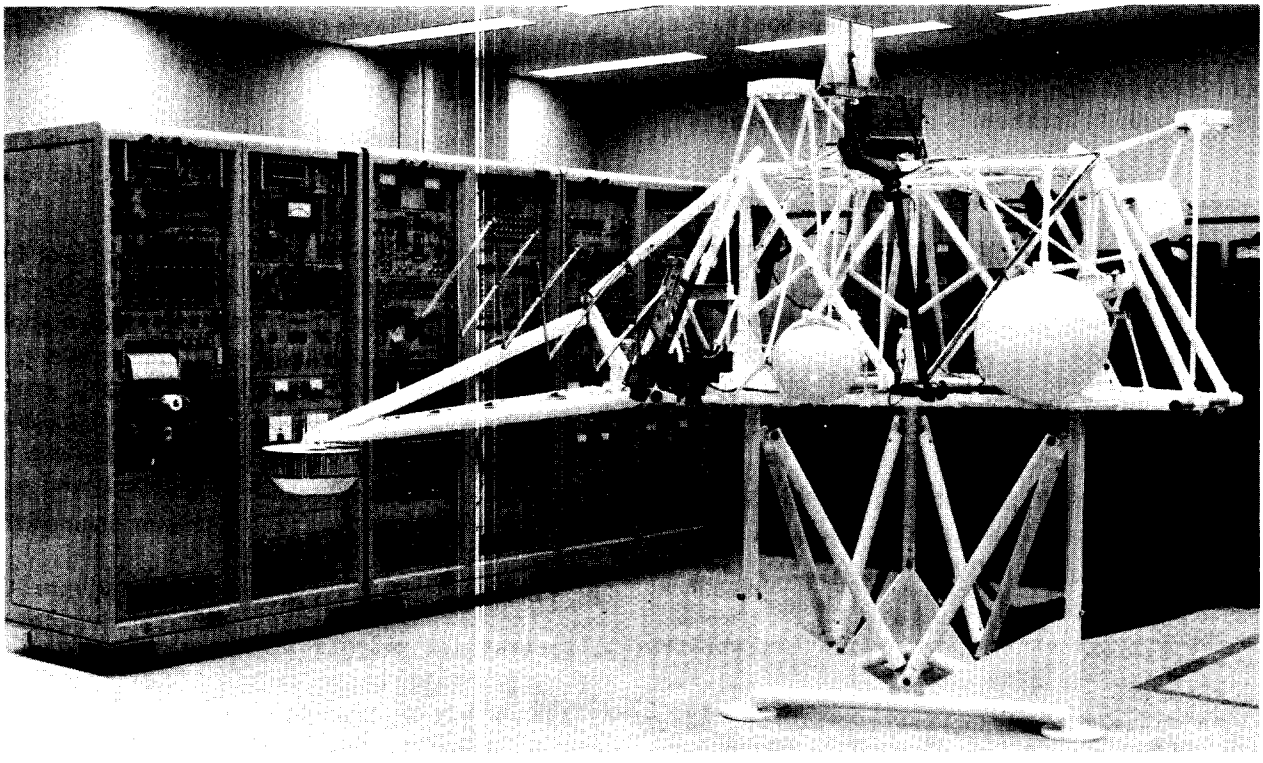

Fig. 1. Payload Systems Laboratory test configuration with scientific instruments installed

UNCLASSIFIED

UNCLASSIFIED

(2) EMA heater output lines, with and without heater loads.

(3) EMA squib lines.

(4) EMA constant current generator output lines.

(5) Accelerometer amplifier voltage output line.

(6) Flight control squib gate line.

Recommendations to desensitize electronic circuits against transients will be based on analysis of the results of these two studies.

C. Scientific Experiments

1. Payload Systems Laboratory

Fabrication of the Hughes Aircraft Company Payload Systems Laboratory test configuration has been completed. This configuration (Figs. 1 and 2) consists of the following major elements:

(1) PSL scientific instrument test rack.

(2) M-13 simulated spaceframe and mounting stand.

(3) Scientific payload spacecraft harness.

(4) Junction box assembly.

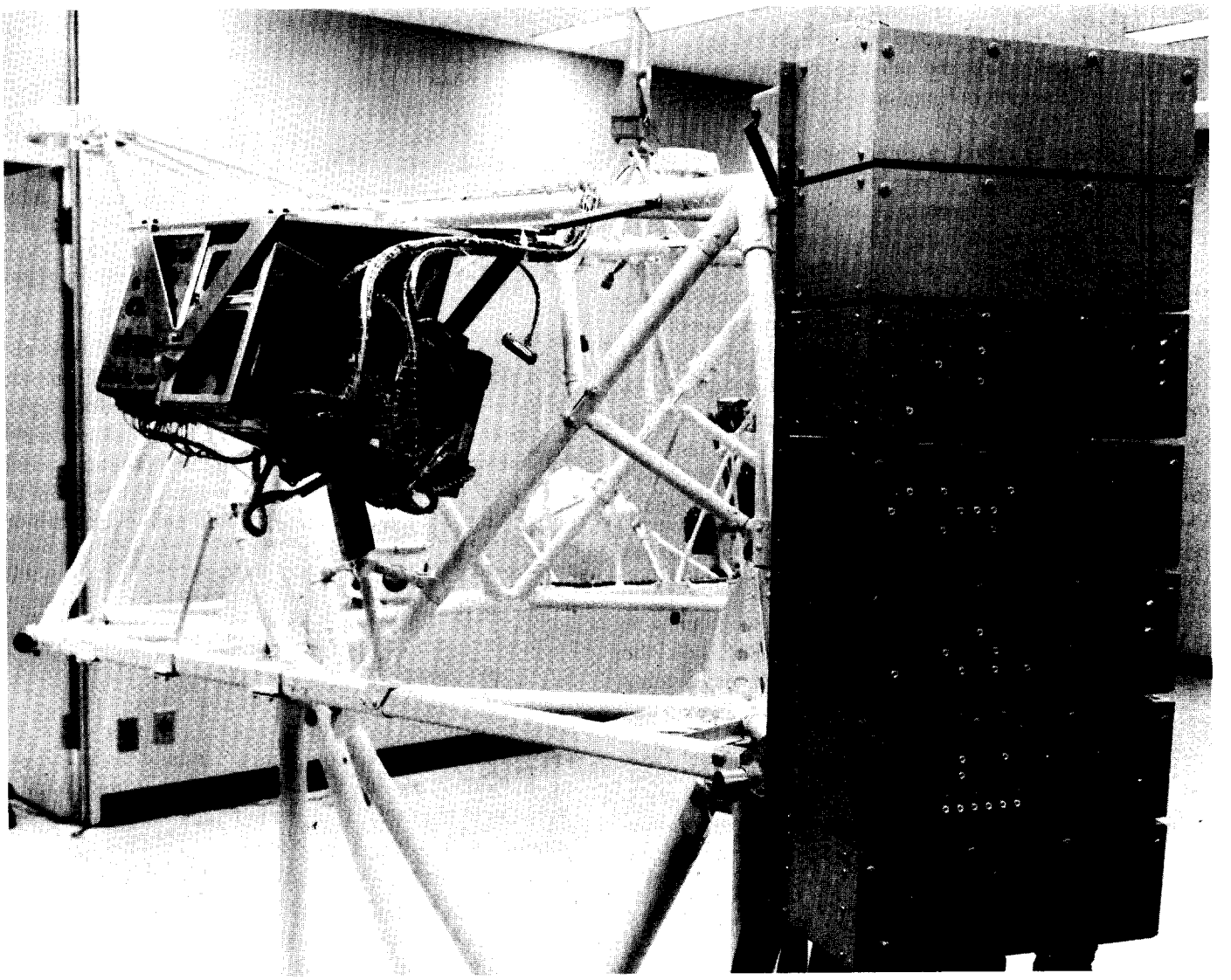

Fig. 2. Payload Systems Laboratory J-box assembly and spaceframe with scientific instruments installed

CONFIDENTIAL UNCLASSIFIED

UNCLASSIFIED
CONFIDENTIAL

(5) Interconnecting cables.

(6) Test tees.

(7) J-box (spacecraft/test cables).

Scientific instruments and auxiliaries have been received for each experiment subsystem. Experiment checkout and integration tests have started. All the instruments and auxiliaries have been installed on the M-13 spaceframe as shown in Figs. 1 and 2.

2. Television Subsystem

a. T-21 television subsystem. During the upgrade period (reported in *SPS 37-30*, Vol. I) when the azimuth end stop change was made to the survey camera, minor failures were corrected on both TV cameras, and both units were functionally tested. On return of the equipment to the spacecraft the telecommunications integration phase of the system functional test was completed.

A problem was noted in three telemetry signals from the approach camera. These signals (Camera 4 ON, Camera 4 Vidicon Temperature Control ON, and Vidicon Faceplate Temperature) saturated when connected to the signal processing equipment. Investigation disclosed that the camera was incapable of accepting the required current from signal processing due to high output impedance. Correction of the problem was accomplished by replacing four resistors with lower value components and removing one diode from the camera.

b. SC-1 television subsystem. After completion of the group test phase (in which the camera and auxiliary were integrated with the spacecraft harness, spacecraft power, and with the systems test equipment), the cameras were returned to the unit area. The following modifications are to be incorporated:

(1) Addition of azimuth end stops which limit the maximum azimuth rotation of the mirror assembly to 360 deg.

(2) Revised mounting for capacitor C-1 on the electronic conversion unit.

(3) Correction of a camera-auxiliary interface problem.

(4) Replacement of the variable focal length lens assembly with a unit containing modifications for correction of the iris end stop weakness and the focus cell thread seizure.

(5) Replacement of the filter wheel assembly with a unit containing revised shaft and rivets.

When the camera and TV auxiliary were connected, one telemetry signal (Shutter Mode ON-OFF) was shifted approximately 2.7 v negatively. Investigation disclosed that the relatively high output impedance of the camera, in conjunction with the negative return in the auxiliary, resulted in a current flow from the camera to the auxiliary. (See circuit diagram in Fig. 3.) This current developed a voltage drop which resulted in a voltage offset in the signal. To solve the problem, the output impedance of the camera may be reduced by changing the values of R1 and R2.

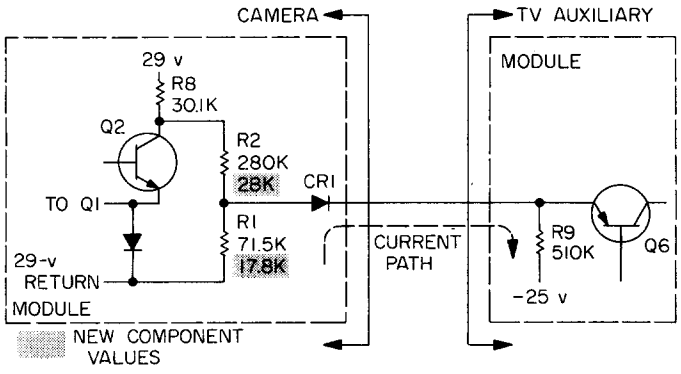

Fig. 3. SC-1 TV subsystem shutter mode telemetry signal

c. TV mirror assembly. It has been determined that calibration of the TV mirror assembly in a thermal-vacuum environment is feasible. The calibration is required to establish position repeatability accuracies of the mirror assembly under varying temperature conditions in a thermal-vacuum environment. At present the mirror angles are determined at room ambient conditions only.

The major problem is to establish reference lines of sight which are not affected by the test environment. It is required, therefore, that the precision angle measuring equipment not be subjected to the environment. This problem is solved by using a vacuum chamber which has an optical quality window and a precision autocollimating theodolite outside the chamber. Inside the chamber the mirror assembly is mounted on a fixture which is capable of rotating it in elevation and azimuth and a reference mirror which is aligned relative to the mirror assembly azimuth bearing surface.

The principle of the test is to look through the window into the vacuum chamber and autocollimate off the camera's mirror. When the mirror is stepped to the next

UNCLASSIFIED

UNCLASSIFIED

position, the theodolite is realigned to again autocollimate off the mirror. The difference between the two theodolite positions is equal to the mirror step size. The absolute position of the mirror is established by autocollimating off the reference mirror and comparing the reading with the one obtained from the mirror assembly. Because of access limitations, only a limited number of steps may be determined in a sequence. When the mirror has rotated to the point where the theodolite cannot achieve autocollimation, the fixture inside the chamber is activated to rotate the mirror assembly back into the working range of the theodolite. Because the theodolite basically measures the difference in mirror positions, the fixture inside the chamber need not be calibrated.

d. TV camera thermal analysis. The survey camera thermal model has been redefined, resulting in 109 nodes interconnected by 227 conduction terms and 178 radiation terms. This model was used to predict the capability of the camera heaters to bring the camera to operating temperature under worst case conditions during the transit phase. Initial nodal steady-state temperatures during transit were calculated as a result of the transit analysis previously performed. Studies of the survey camera on the Moon's surface during the last few hours of the lunar night are in process.

Results of these studies indicate that modifications must be made to the survey camera to ensure that the heaters will be capable of raising the electronics to their minimum operating temperature of −20°F during either transit or lunar night conditions. While these are not requirements of the mission, it is desirable to provide this capability if the penalty is not excessive. Camera modifications under investigation include increasing the heater input power, increasing the chassis and electronics conversion unit thermal isolation, and changing the exterior painted surface to a combination of polished aluminum and white paint. Preliminary studies indicate that an exterior surface composed of white paint and polished aluminum will make possible camera operation with heaters during the transit and lunar night environments.

A thermal model for the approach TV camera is being definitized. The model consists of 63 nodes interconnected by conduction and radiation terms. As a consequence of the preliminary results of the transit analysis, a study was initiated to determine if the individual components of the camera were tested to adequate thermal rates and levels. One component, the deflection yoke, was felt to be tested marginally. An investigation of the manufacturing techniques and test procedures was initiated and a test at low temperatures was started. Although the testing has not been completed, preliminary results show that the yokes will survive the expected temperature rate of change and minimum expected temperature levels during both transit phase and lunar night phase.

A total of six deflection yokes were subjected to acceptance testing of inductance, resistance, and deflection linearity. Each was installed in a test camera and resolution was measured. Following the electrical parameter measurements the yokes were divided into two groups of three yokes each and subjected to thermal testing. One group was lowered at a rate of 5°F or less per minute from room temperature to −185°F. A second group was lowered to −255°F in a manner similar to the first. The coil resistance was measured at intervals during the test and was observed to change as much as 50%; however, no catastrophic failures occurred.

e. Variable focal length lens assembly. Type-approval testing has determined that the present variable focal length lens assembly is adequate to meet minimum requirements in all drive functions except the focus cell assembly. However, testing and redesign continue so as to provide a unit of considerably higher reliability.

Binding and galling of the focus cell threads recurred in the second lens type-approval test. Investigation showed that fabrication techniques were questionable and that quality inspection and cleaning of the threads was inadequate. Correction of these deficiencies should eliminate the problem.

A "Higbee Cut" at the start end of the threads is being incorporated and the thread crests are being cut to reduce the bearing area. Tests with dummy cell assemblies of different aluminum alloys are being initiated to establish the effect of wear on materials with different hardness.

According to specifications, zoom cell assembly torque after the 1000-cycle run-in period was marginal. This was due to a breakdown of the hard anodize at the edge of the drive slot and nonlinear zoom slot. Microscopic examination showed these slots to be rough and cracked after the run-in period. Sample slots, with radii from 0.000 to 0.015 in., are being processed to see if crazing can be reduced. Additional tests are being conducted on assemblies which have been fabricated from commercial lenses having the same slot configurations. These tests

UNCLASSIFIED

UNCLASSIFIED
CONFIDENTIAL

consist of running steel drive pins against variously treated slot surfaces. Wear characteristics will be determined at room ambient conditions.

3. Touchdown Dynamics Experiment

A study to investigate the technical problems and program implications associated with the inclusion of the touchdown dynamics experiment in the *Surveyor* payload was initiated by Hughes Aircraft Company in response to a formal request from JPL.

Experiment objectives require that the subsystem has a capability of retrieving, storing, and relaying 21 channels of data which are developed immediately prior to and during a *Surveyor* landing. The data to be retrieved, stored, and transmitted to Earth via telemetry are as follows:

(1) Three mutually orthogonal components of translational acceleration (derived from three accelerometers).

(2) Three mutually orthogonal components of angular velocity (derived from three gyros).

(3) Axial forces in six landing leg struts and three shock absorbers (derived from the nine strain gages).

(4) Angular position of each landing leg (derived from three potentiometers).

(5) The initial contact time of each footpad and crushable block (derived from the six switches).

Utilizing data derived from the various elements of the subsystem, the objectives of the touchdown dynamics experiment are:

(1) Determine linear and angular acceleration, velocity, and displacement of spacecraft reference axes during touchdown, and express these motions in lunar inertial reference system.

(2) Obtain information on bearing strength of lunar surface.

(3) Obtain information on shearing resistance and/or coefficient of friction of lunar surface for both static and dynamic conditions.

(4) Obtain information on penetration of spacecraft into lunar surface.

(5) Obtain information on lunar surface contours in landing area.

The weights of the three major units, the sensors, and the associated wiring harness are estimated as follows:

Sensors (rate gyros, strain gages, etc.)	12.0
Tape recorder and associated electronics	9.5
Auxiliary	2.0
Harness	2.5
	26.0 lb

4. Soil Mechanics Surface Sampler[1]

a. Introduction. The *Surveyor* soil mechanics surface sampler instrument consists of a motorized lazy-tongs mechanism equipped with an accelerometer and strain-gage sensors for measuring the forces developed during manipulation. The basic mechanism was originally designed by Hughes Aircraft Company (HAC) as a device for obtaining a sample of lunar surface soil and delivering it to a grinder for processing preparatory to analysis by other instruments. It was felt that with minor modifications plus suitable sensors, this surface sampler mechanism could be converted into an acceptable soil mechanics instrument. Developmental tests to date have verified this to the satisfaction of the principal investigator and the cognizant JPL personnel.

b. Description. Fig. 4 shows the prototype unit, Serial X-4, mounted on the HAC Payload Systems Laboratory simulated spacecraft. The mechanism comprises five bays of 14-in. link members carrying a clam-shell scoop at the outboard end and supported at the base by a yoke motorized for motion in azimuth and elevation. Extension is accomplished by base springs and retraction by a motor-driven spool which carries the draw tape. A fourth motor opens and closes the scoop door.

Motion capabilities are 150 deg in azimuth, 70 deg in elevation, and 12 to 60 in. in extension. This permits the scoop to be deployed for picking, scraping, digging, or sample collecting from a sector of the lunar surface approximately 35 ft^2 in area—all of which is within the field of view of one or both of the survey TV cameras. The instrument dexterity will also permit it to clear an area of surface debris for observation by another analytical instrument, or to redeploy some other instrument, thus increasing its capabilities.

Each motor is reversible and may be commanded in coarse (2-sec) or fine (0.1-sec) increments. This permits a

[1]Prepared by JPL Technical Section 322.

UNCLASSIFIED
CONFIDENTIAL

UNCLASSIFIED

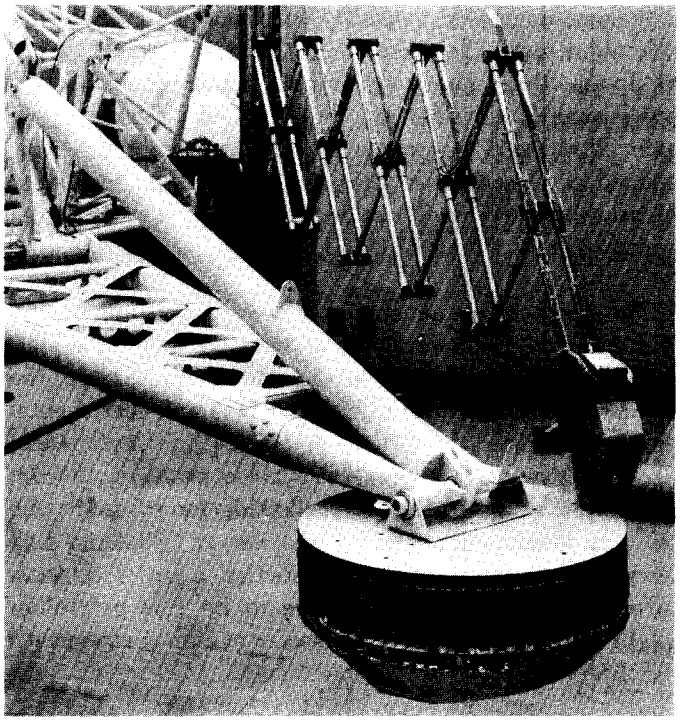

Fig. 4. Prototype soil mechanics surface sampler X-4 mounted on HAC Payload Systems Laboratory simulated spacecraft

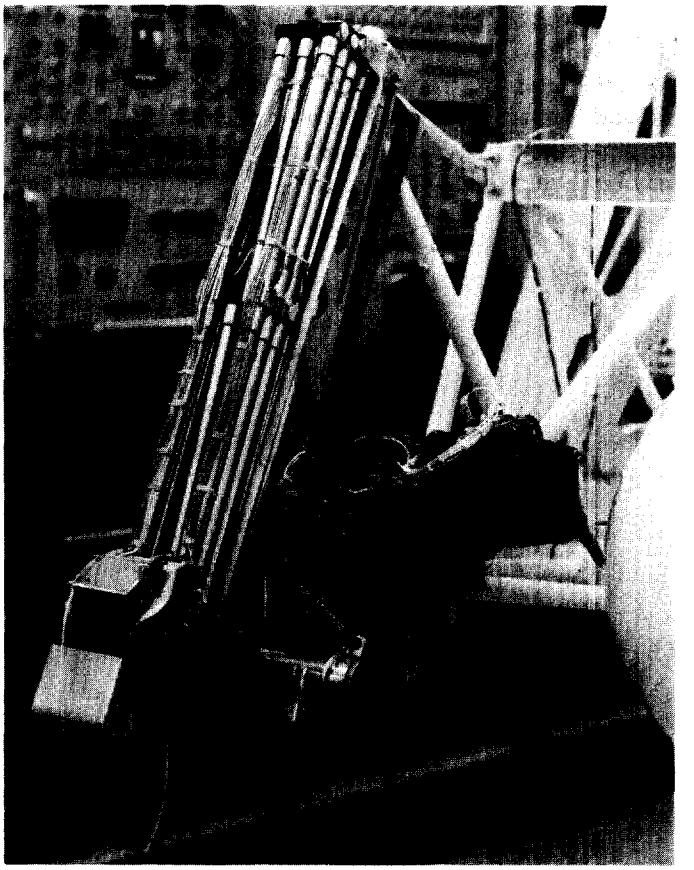

Fig. 5. Stowed surface sampler showing the accelerometer, amplifier, potentiometers, and microswitches

wide degree of control of the scoop in mapping the local lunar surface or in repositioning the scoop for repeated digging or picking tests. Closing the scoop also changes the "footprint" configuration for bearing strength tests from a sharp tool–steel blade to a rectangular flat plate about 1 by 2 in. The force capabilities of the motors are in excess of 1 lb each direction in azimuth, 1 lb in extension, 20 lb in retraction, and 3 lb up or down in elevation. The scoop door can develop a 7-lb crushing force at the lip.

c. Transducers. Seven transducers are provided for measuring forces, acceleration, and position of the scoop tip. These are three precision, sector-type potentiometers for indicating extension, elevation, and azimuth position; a pair of microswitches for monitoring the scoop door position; two sets of bonded strain-gage bridges with separate power supplies and amplifiers for measuring forces; and a piezoelectric acceleration sensor with an associated charge sensitive amplifier for picking decelerations. The accelerometer, amplifiers, two potentiometers, and the microswitches may be seen in Fig. 5 along with the extension motor-gear assembly. Fig. 4 shows the elevation strain-gage bridge attached to the center root member of the linkage. The other strain-gage bridge is mounted on a small strain–multiplying cantilever beam at the base of the scoop. This is hidden from view, but is at the point where the draw tape attaches to the scoop.

d. Operation. The experimental operation of this instrument is planned to include a series of scraping, picking, and pressing operations in addition to the surface mapping mentioned above. The principal investigator is having a soil "catalog" prepared which will show typical signatures for various types of loose and solid materials that may be encountered.

Relative hardness of solid materials and the approximate character of granular soils may be determined by picking at a given spot. This is accomplished by elevating the scoop and then releasing a solenoid-operated clutch integral with the elevation motor assembly. A combination of torsion spring and gravity then drives the scoop onto the lunar surface while the accelerometer

CONFIDENTIAL UNCLASSIFIED

UNCLASSIFIED
CONFIDENTIAL

monitors the deceleration trace for 2 sec following release of the clutch. This signal and the output of the elevation potentiometer are transmitted to the Deep Space Instrumentation Facility as analogs from which the velocity at impact—as well as the character of the deceleration—may be determined.

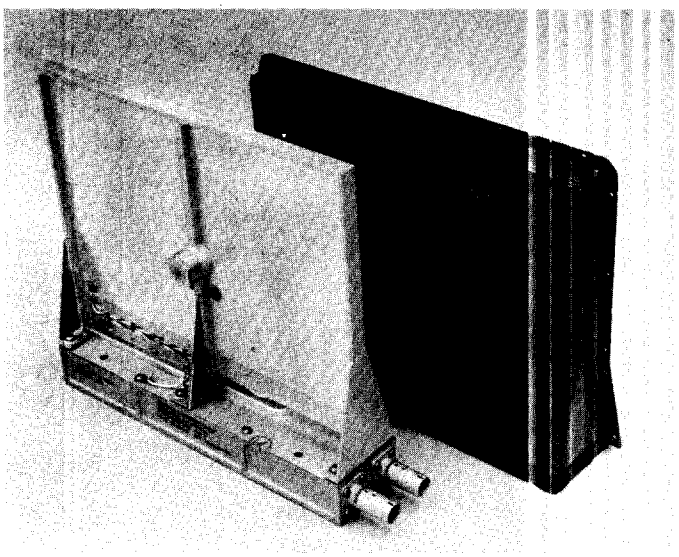

Fig. 6. Micrometeorite ejecta detector sensor and protective cover

A large degree of flexibility is provided for these deceleration tests. Elevation height may be varied from 0 to about 40 in. above the nominal lunar surface, the accelerometer amplifier may be switched for high or low gain (20:1), and the scoop may be used with the door opened or closed for a sharp edge or a large foot area. Measurable peak decelerations may thus be varied from approximately 0.1 to 20,000 Earth g.

The force measurements are essentially static, being read from a commutator along with the potentiometer, switch, and other outputs at the rate of 1/sec. Here, the scoop is positioned on the lunar surface and incremental motions of shear (draw tape) or bearing (downward elevation) are made. The gear trains are non-reversible from the output shafts so that the following force read is the one just developed. Skipping, jumping, or crunching may be variable and unpredictable so that a series of measurements will most likely have to be run before an intelligent estimate of the character of the lunar surface can be read.

5. Micrometeorite Ejecta Detection Experiment[2]

The thermal analysis of the micrometeorite ejecta detector (MED) sensor assembly discussed previously

[2]Prepared by JPL Technical Section 322.

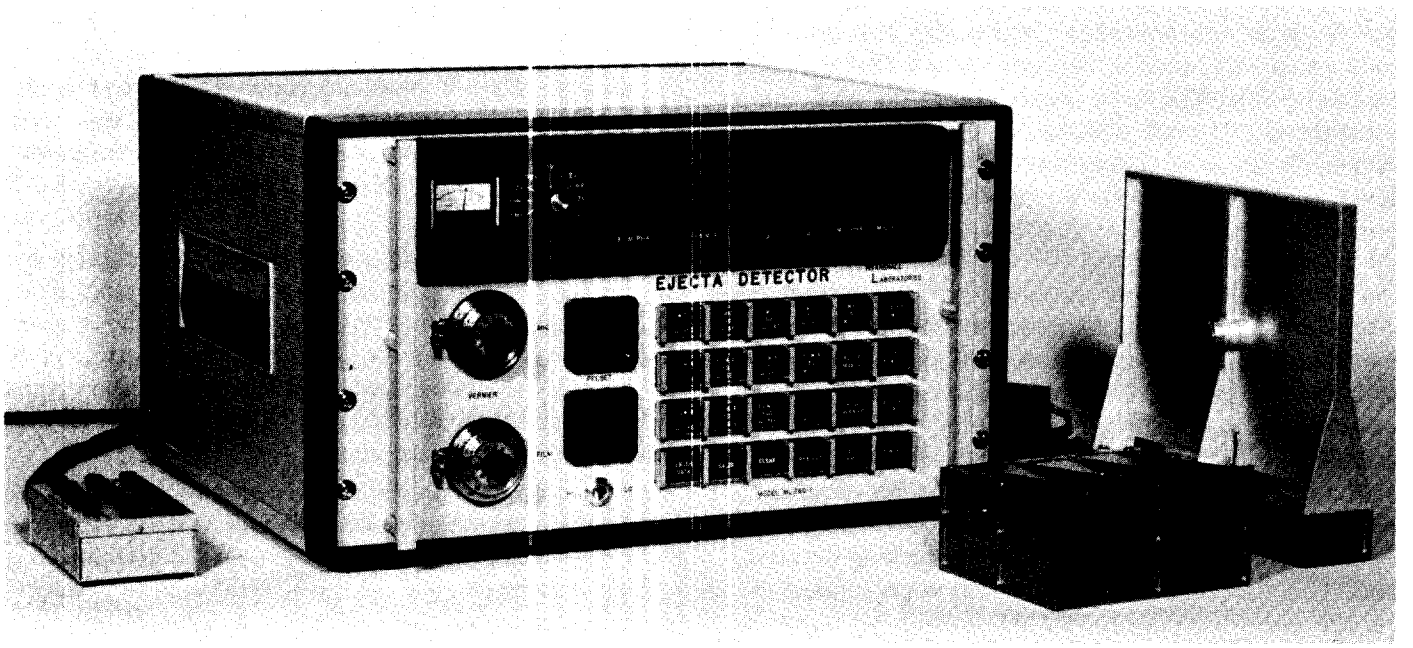

Fig. 7. Type-approval test micrometeorite ejecta detector sensor and electronics with the bench check-out equipment

UNCLASSIFIED
CONFIDENTIAL

CONFIDENTIAL UNCLASSIFIED

in *SPS 37-29* was completed. The analysis indicated that painting of all sensor surfaces, except for the sensor thin films, with white inorganic paint is extremely important. Without the paint the maximum lunar day temperature of the sensor electronics was calculated to be 450°F, but with the white inorganic paint applied this temperature would be reduced to 213°F. The analysis also indicated that the 1-w sensor heater would extend the experiment operation time at lunar day terminator by only 6 hr.

Problems associated with applying the Hughes Aircraft Company (HAC) inorganic paint were avoided by utilizing the JPL organic/inorganic white paint and painting scheme. In addition, the upper limit of the operational temperature range of the sensor electronics had to be increased from 180 to 217°F, which required a slight redesign and retrofit of the prototype instruments.

Sensor covers to protect the sensor thin films and acoustic transducer from contact with foreign materials during testing and handling have been fabricated for each prototype sensor. The sensor covers also act to shield the acoustic transducer from acoustical noise. Fig. 6 shows a typical MED sensor and protective cover.

Fig. 7 shows the MED type-approval unit operating with the MED bench checkout equipment (BCE). The BCE is capable of simulating all the spacecraft commands to the experiment in addition to monitoring the instrument performance. The 19-bit data readout is automatically displayed in digital form and in the proper format every time the calibration or readout command is initiated.

a. Micrometeorite ejecta detector auxiliary. In response to a JPL request, HAC has submitted an engineer-

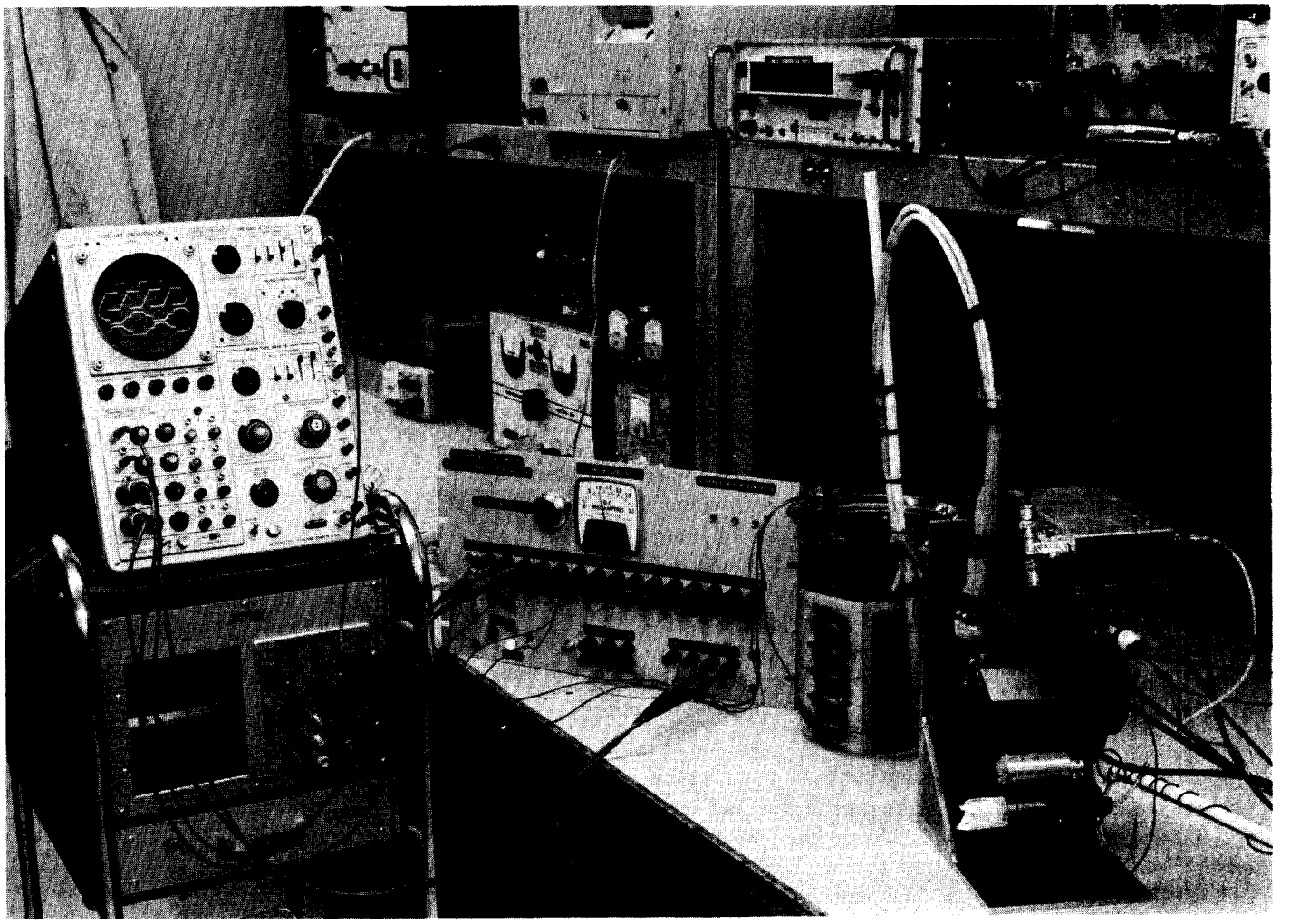

Fig. 8. Diffractometer test setup

CONFIDENTIAL UNCLASSIFIED

UNCLASSIFIED

ing change proposal which will provide current limiting for the experiment. This proposal provides for a redesign of the MED auxiliary 29-v-dc switch circuit to limit instrument current to less than 200 ma in case of a malfunction in the power circuits. The proposal also covered fusing of the 22-v heater circuit.

6. *Advanced Surveyor: X-Ray Diffractometer*[3]

a. Introduction. Philips Electronic Instruments produced the first approach to the design of an X-ray diffractometer for an on-site lunar-rock powder analysis. The latest prototype instrument (P-5) consists of three major packages: power supply, scan drive logic, and goniometer. High-voltage (25-kv) cables and connectors are required between the packages. The P-5 instrument has a total weight of approximately 25 lb, of which 15 lb is the goniometer weight and 9 lb is the power supply weight. The total volume is estimated to be approximately 1000 in.^{3} The required continuous power is about 65 w, with a constant current of 2.2 amp and a transient current at turn-on of about 4 amp.

Based on the acceptable functional performance of the P-5 approach and the knowledge that the instrument design could be optimized, it was decided to proceed with a redesign of the diffractometer electronics. The primary objectives of the redesign effort are: (1) to reduce instrument weight and required power, (2) to unitize packaging, and (3) to improve reliability. The redesign is based on the use of integrated circuitry and an enclosed oil-immersed high-voltage power supply (i.e., no high-voltage cables or connectors).

b. High-voltage (25-kv) power supply. The 25-kv power supply was redesigned and tested with all high-voltage components and connections operating in an oil bath. This technique eliminates all arcing. The test setup is shown in Fig. 8. The bottom two traces on the oscilloscope are the waveform across the high-voltage transformer primary. (Note the duty cycle and core collapse curve.) The anode current is shown to be 1 ma on the front panel meter.

Fig. 9 shows the high-voltage aquarium, a gallon beaker containing the high-voltage transformer and rectifier–multiplier assembly. This beaker is filled with transformer oil. The two cables tied to the Teflon support rod lead to the X-ray tube. The method of attaching

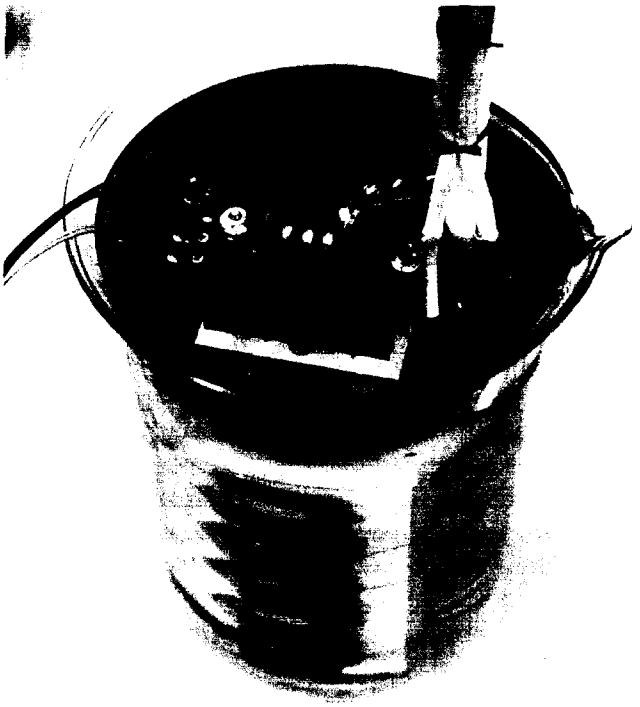

Fig. 9. High-voltage aquarium

these cables to the X-ray tube for testing the feasibility of using oil as an insulator in the vicinity of a hot X-ray tube is shown in Fig. 10. The large shrink tubing contains the oil.

The breadboarded electronics for the high-voltage power supply and motor drive system is shown in Fig. 11. A metal, hermetically sealed, oil-filled package has been designed to contain the supply. Fabrication of the high-voltage package will be completed during January 1965.

Power supply efficiency has been increased from 60 to 83%. The anode current is regulated over the temperature range of −50 to 100°C to 0.1% of 1 ma. This accuracy is also maintained over a power supply variation of ±5%. The current is regulated using pulse-width modulation techniques instead of the previous Class A method. Integrated circuits are used to mechanize the preamplifier, pulse-width modulator, and pre-driver.

c. Power amplifier and anode current control loop. The output of the pulse duration modulator (PDM) is applied to two *and* gates along with an *on, off* function and a bi-phase drive (Fig. 12). Without the PDM, the output of the power amplifiers would be a 4-kc square

[3] Prepared by JPL Technical Section 322.

UNCLASSIFIED CONFIDENTIAL

UNCLASSIFIED
CONFIDENTIAL

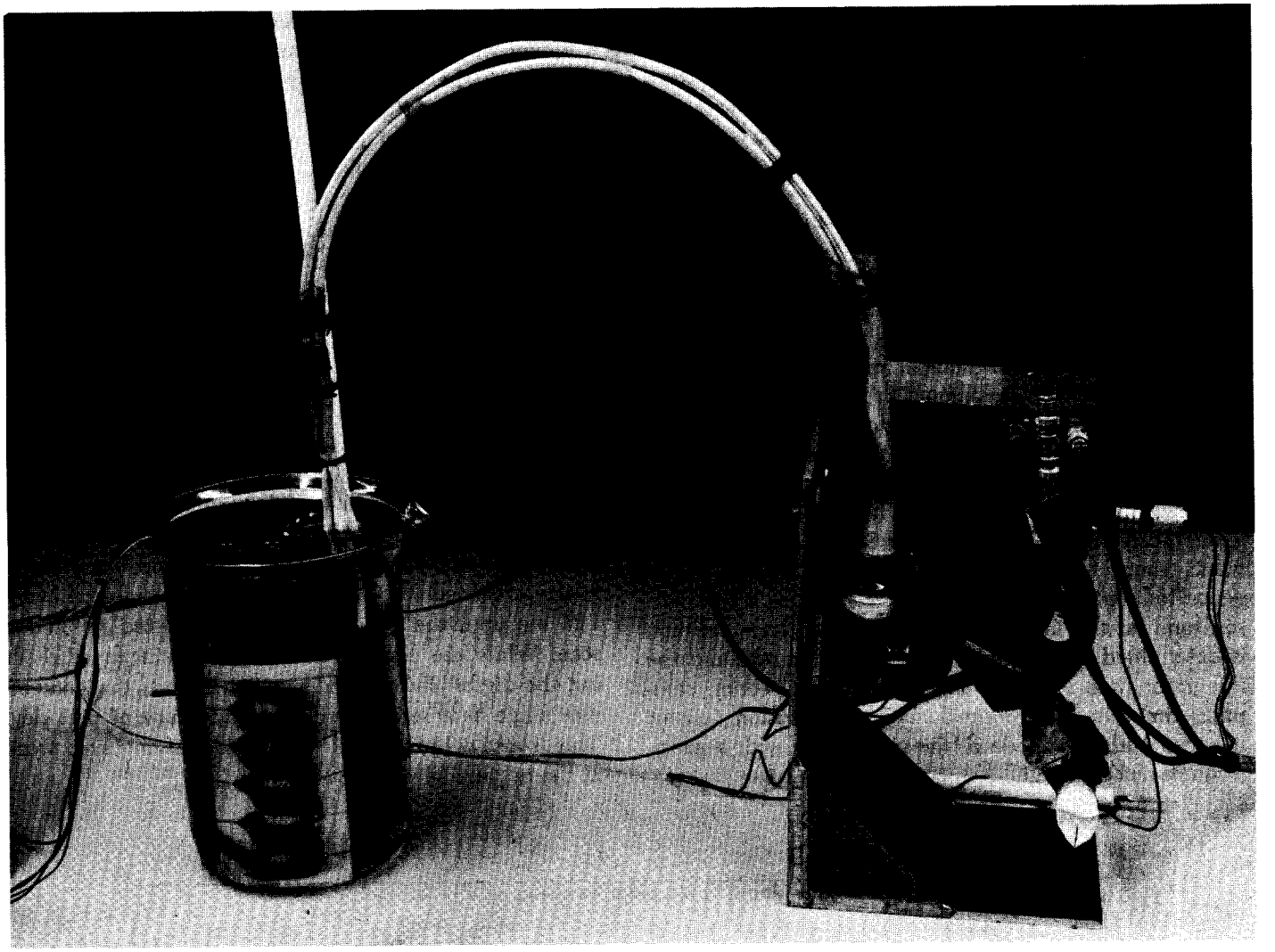

Fig. 10. Goniometer and high-voltage aquarium

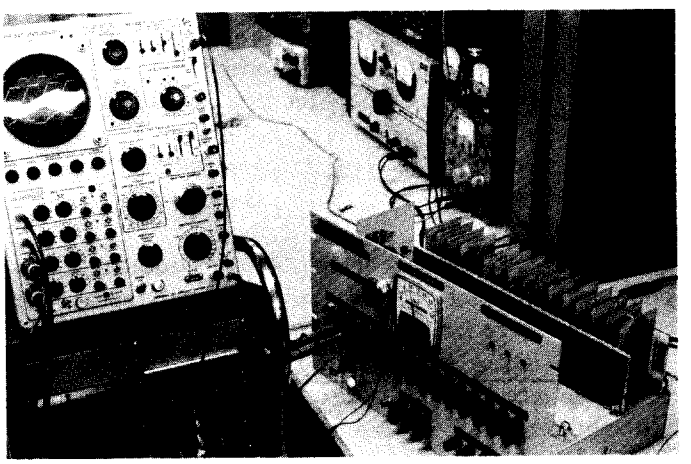

Fig. 11. Flight electronics simulator

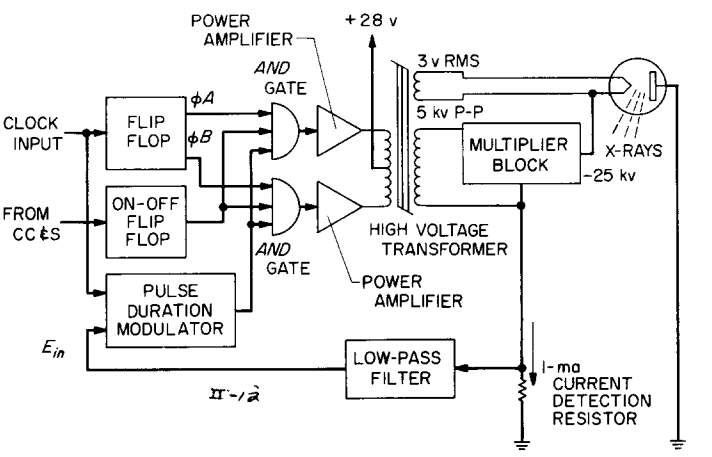

Fig. 12. Power amplifier and anode current control loop block diagram

CONFIDENTIAL
UNCLASSIFIED

UNCLASSIFIED

wave driving the high-voltage transformer. As the filament of the X-ray tube heats up and 25 kv is applied, the anode current flows through a resistor, which in turn develops a voltage directly proportional to the anode current. The voltage across an 8.5-KΩ resistor is applied to the PDM, which then varies the duty cycle of the square wave across the transformer. The rms value of this square wave controls the filament temperature, thereby keeping the anode current constant at 1 ma through the action of the PDM. Since the multiplier block is essentially a peak-sensitive rectifier, the high voltage does not vary. In practice, though, it varies approximately 5% and in such a manner as to be self-regulated against line voltage changes. It can be seen in Fig. 13 that the anode current and anode voltage are essentially independent of supply voltage.

d. Pulse duration modulator. The PDM makes use of Texas Instruments Incorporated Series 52 linear networks connected as shown in Fig. 14. The integrator generates a triangular wave which is used as a comparison ramp at the input of the comparator. Its amplitude is determined by the clock-input repetition rate and the integrator time constant. The preamplifier section compares the voltage developed across a precision resistor in series with the anode of the X-ray tube with a precision reference voltage.

The output of the comparator, operated open loop, is a square wave whose rising and falling edges are generated when the ramp voltage equals the output of the preamplifier and rises above or below it. Fig. 15 shows the equivalent PDM input offset drift as a function of temperature.

e. Counter–scanner. The data-handling system for the X-ray diffractometer consists of a 13-bit ripple-through counter (Fig. 16) and a series of *and* gates. The counter is driven by the output of the pulse-height discriminator (PHD). The *and* gates are driven by a 4-bit counter, which counts at a rate determined by the clock countdown system (64 pps). The counter is allowed to accumulate the pulses from the PHD for 1 sec. The input is then inhibited, and the scanner converts the accumulated count into a 13-bit serial word with a sync word at the beginning (Fig. 17). At the end of the 250-msec scan period, the counter is reset to zero and the goniometer is advanced 0.01 deg. This process is repeated every 1.25 sec until the goniometer has completed its 83-deg scan. While the counter is counting, the scanner reads out the digital shaft encoder and transmits the goniometer angle as a serial word to an accuracy of 0.01 deg. This is also a 13-bit word with an identifying sync word at the beginning.

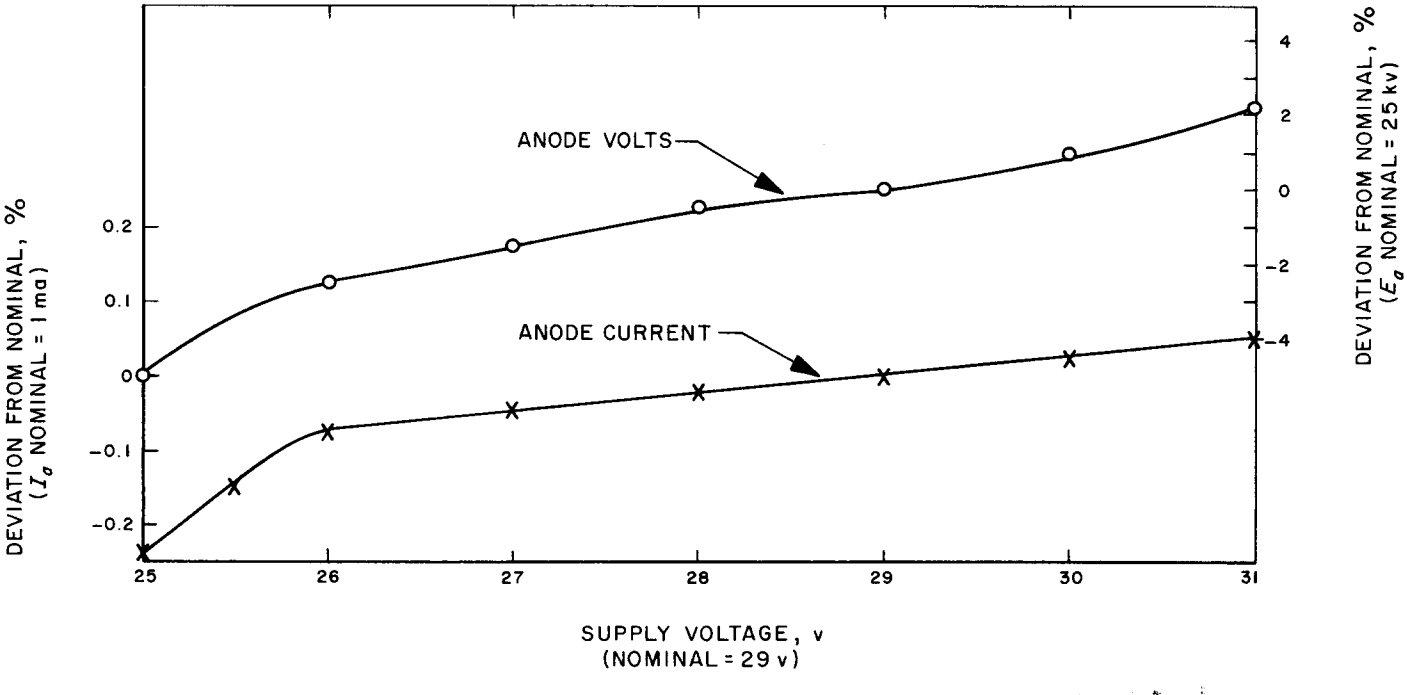

Fig. 13. Variation of anode current and high voltage with supply voltage

UNCLASSIFIED

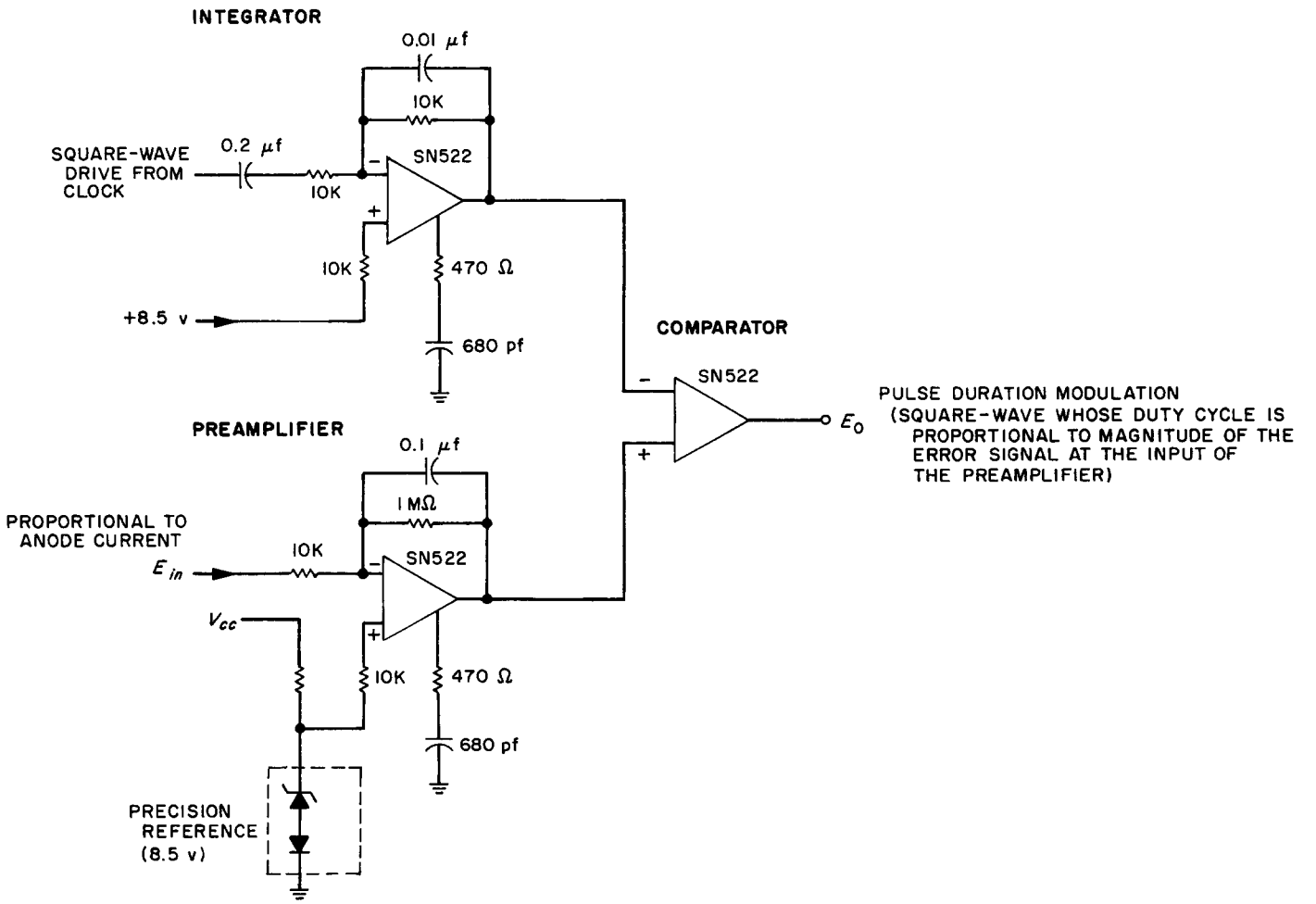

Fig. 14. Pulse duration modulator block diagram

f. Pulse-height discriminator. A PHD (Fig. 18) has been mechanized using two Texas Instruments linear networks and one Texas Instruments Series 51 gate network. The function of this device is to perform a pulse-height discrimination on the pulses appearing at the output of the proportional preamplifier. By setting the threshold control to eliminate noise and the window control to eliminate high-energy pulses, only those pulses generated by diffracted X-rays are allowed to pass through to the counter.

If Comparator 1 fires due to a pulse of amplitude greater than the setting of the threshold control, the pulse propagates through Gates 1 and 2 to the counter. If Comparators 1 and 2 fire due to a pulse of height greater than the window control setting, the pulse is prevented from passing through Gate 2. The settings of both the threshold and the window are remotely programmable. The variation of threshold and window voltages with temperature is shown in Fig. 19.

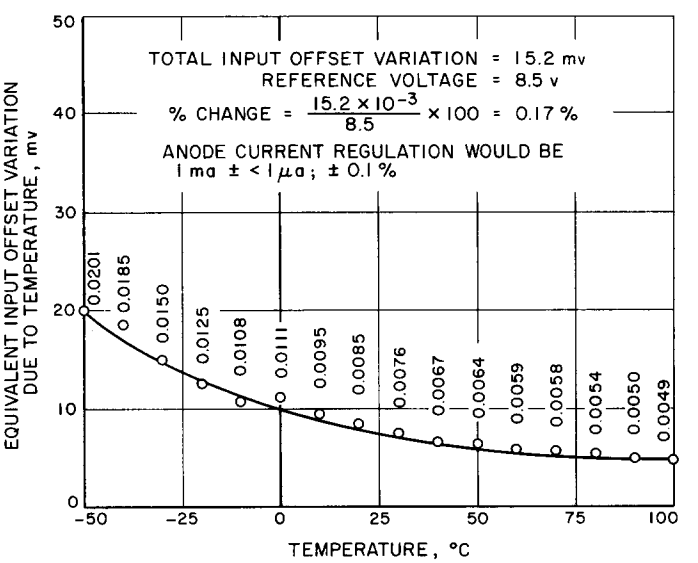

Fig. 15. Results of temperature cycling of pulse duration modulator

UNCLASSIFIED

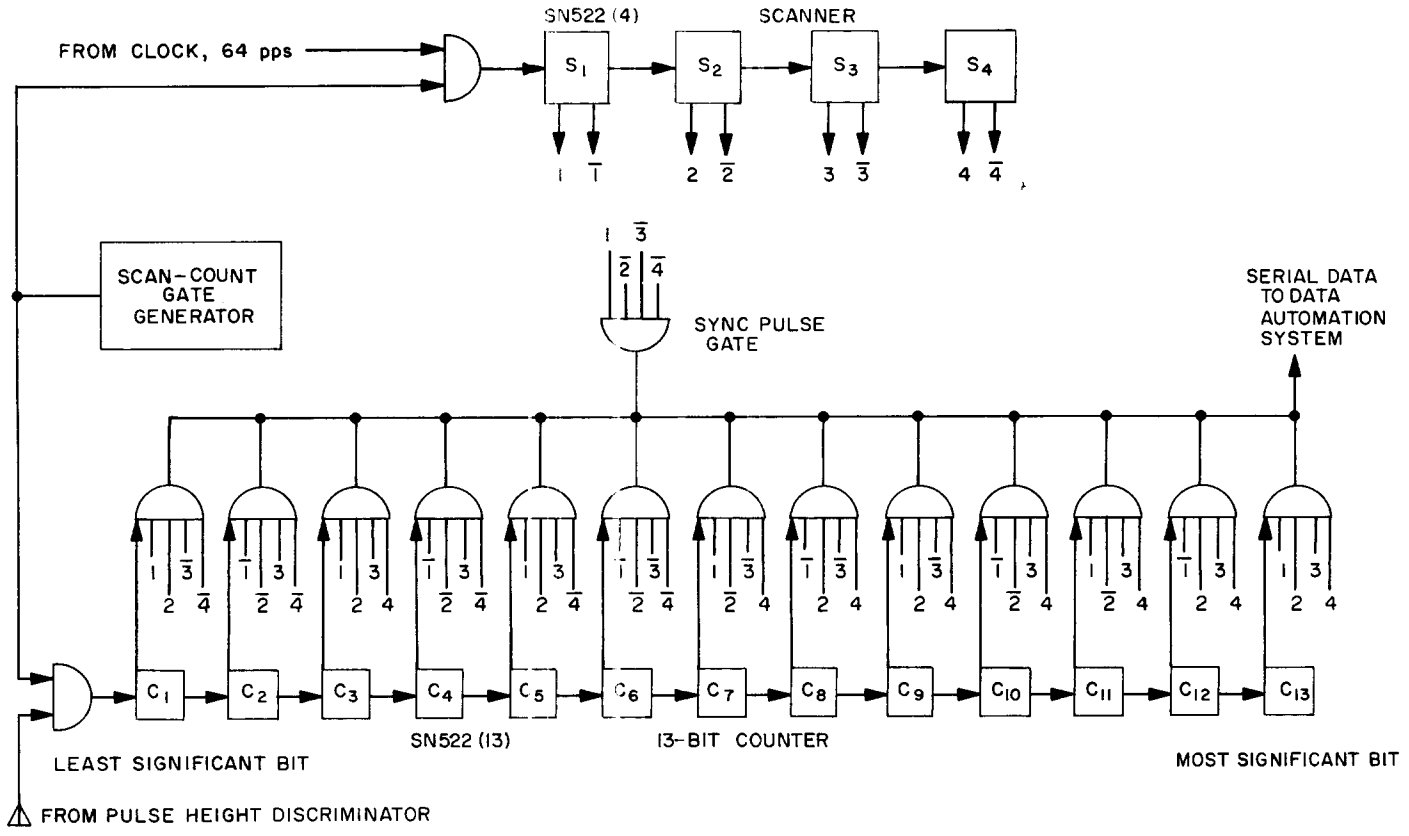

Fig. 16. Counter–scanner block diagram

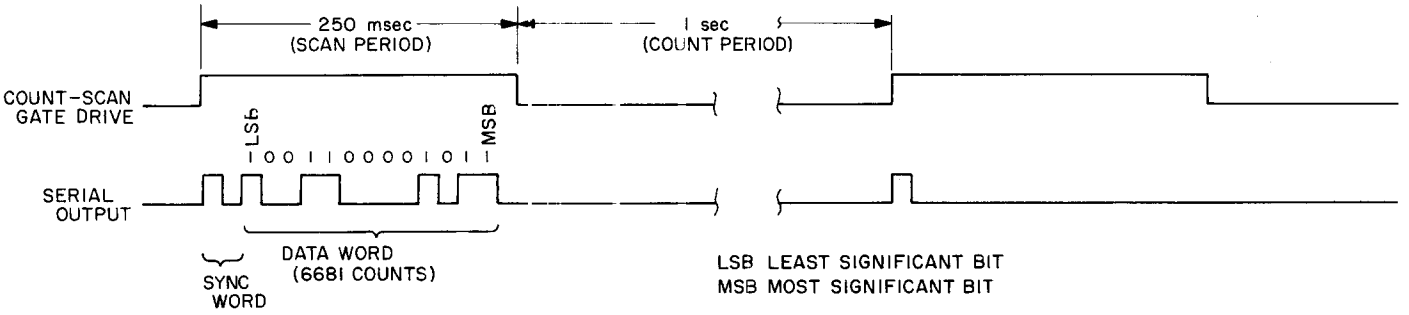

Fig. 17. Counter–scanner timing diagram

7. *Advanced Surveyor: X-Ray Diffractometer–Sampler*[4]

The design and development work is continuing on the sub-surface sampling system to be used in conjunction with the lunar X-ray diffractometer. The sampler shall accomplish the following:

(1) Cutting (including drilling and pulverizing).

(2) Acquisition or collection of sample into extractor.

(3) Extraction and vertical transport of samples.

(4) Transfer and presentation of samples to diffractometer.

A sample extractor test rig (Fig. 20) has been designed and built to demonstrate the feasibility of a principle of sample extraction and vertical transport from a hole by vibration with minimum moving parts. A cross-sectional

[4] Prepared by JPL Technical Section 322.

UNCLASSIFIED

UNCLASSIFIED
CONFIDENTIAL

view of the extractor is shown in Fig. 21. Tests are being conducted to: (1) determine and demonstrate the feasibility and effectiveness of the vibratory motion of a helical conveyor as a mode of extracting and vertically transporting samples from a lunar hole, and (2) gather data to evaluate design parameters and to indicate necessary changes in the design to produce an efficient and reliable sample extraction system.

To simulate lunar sample acquisition, these tests are being made with samples of basalt rubble, silica, sand, rutile, and mixtures of these in particle sizes ranging from 15 to 400 mesh and finer. The main parameters studied in the initial tests are:

(1) Drive speed (input rotational speed, rpm = vibration frequency, cycles/min).

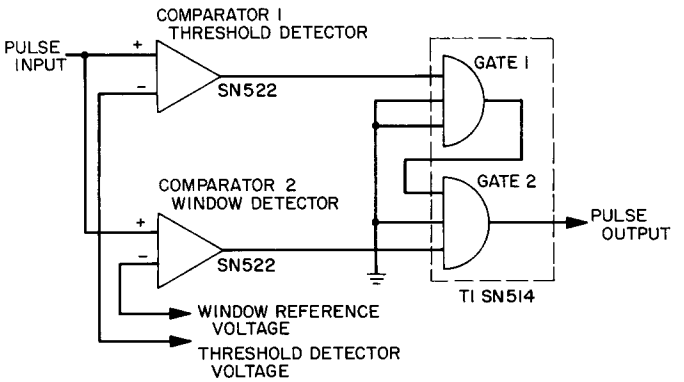

Fig. 18. Pulse-height discriminator block diagram

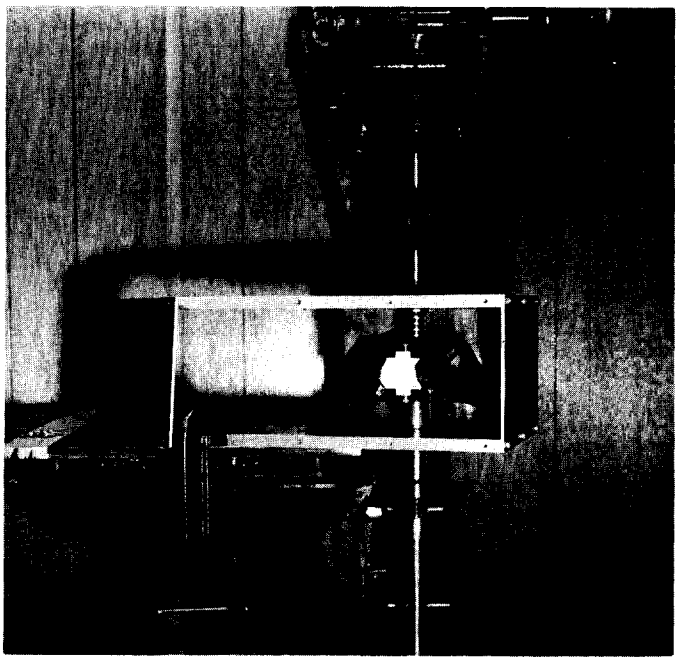

Fig. 20. Sample extractor test rig

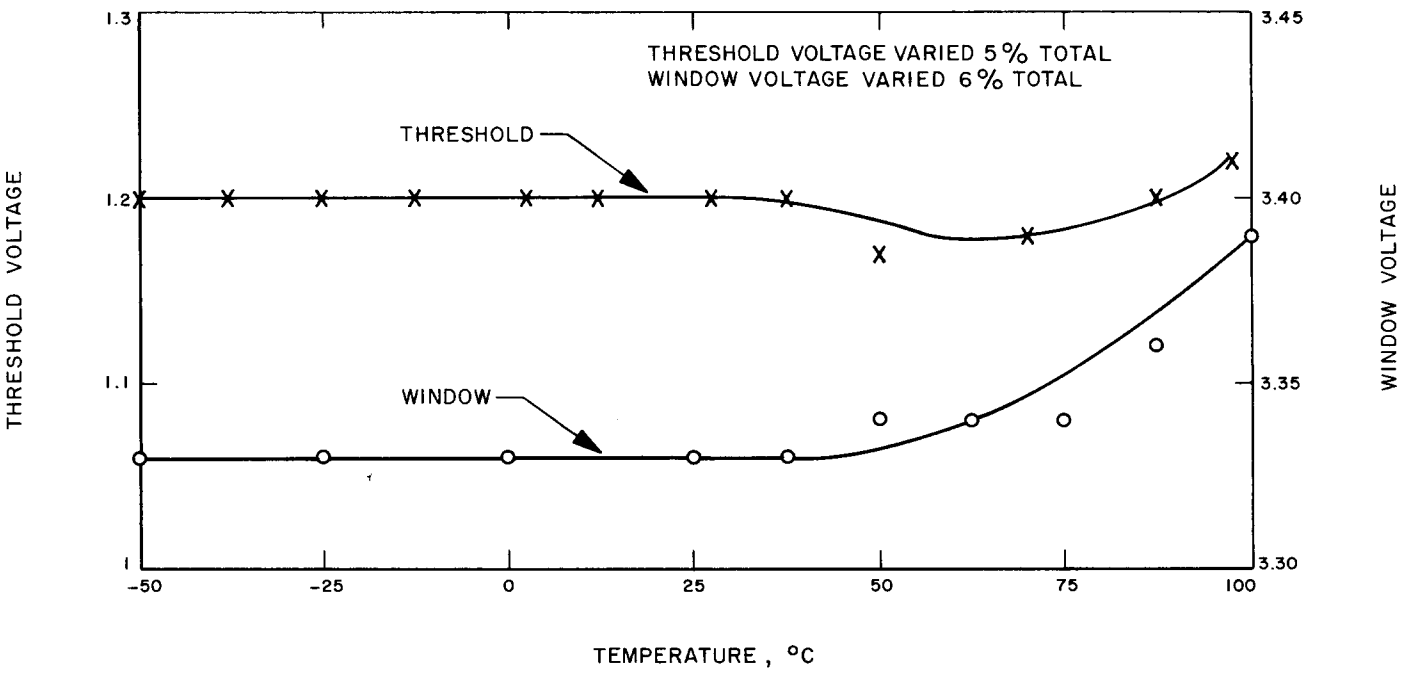

Fig. 19. Variation of threshold and window voltages with temperature

UNCLASSIFIED
CONFIDENTIAL

UNCLASSIFIED
CONFIDENTIAL

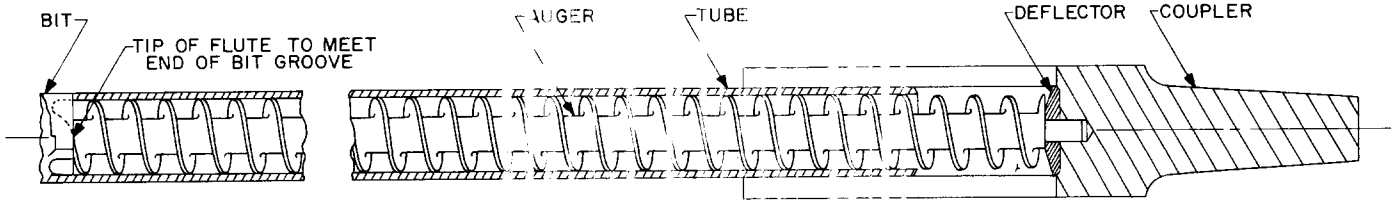

Fig. 21. Cross-sectional view of extractor

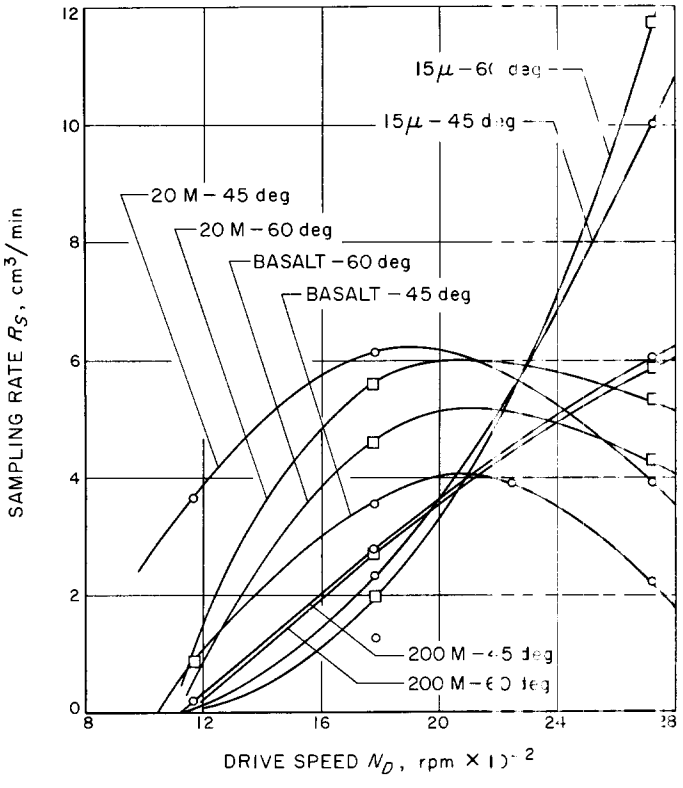

Fig. 22. Sampling rate vs drive speed

(2) Direction of drive forces (the vibratory motion of the extractor bit, which occurs in both axial (linear) and rotary (torsional) directions, causes every point on the extractor bit to trace a helical path; the effective travel of each particle on the "helical conveyor" per vibration cycle is a function of (among other items) the relative amplitudes of the linear and torsional modes).

(3) Sample particle size and density.

(4) Sampling rate (cm³ of sample/min).

(5) Fractionation (separation, if any, of particles of different densities and/or sizes from a mixture during extraction).

(6) Angle of inclination of extractor axis to the local vertical.

Fig. 22 shows curves of sampling rate versus drive speed (vibration frequency) for various particle sizes and for drive angles of 45 and 60 deg. These tests have shown that the vibratory principle is feasible and that

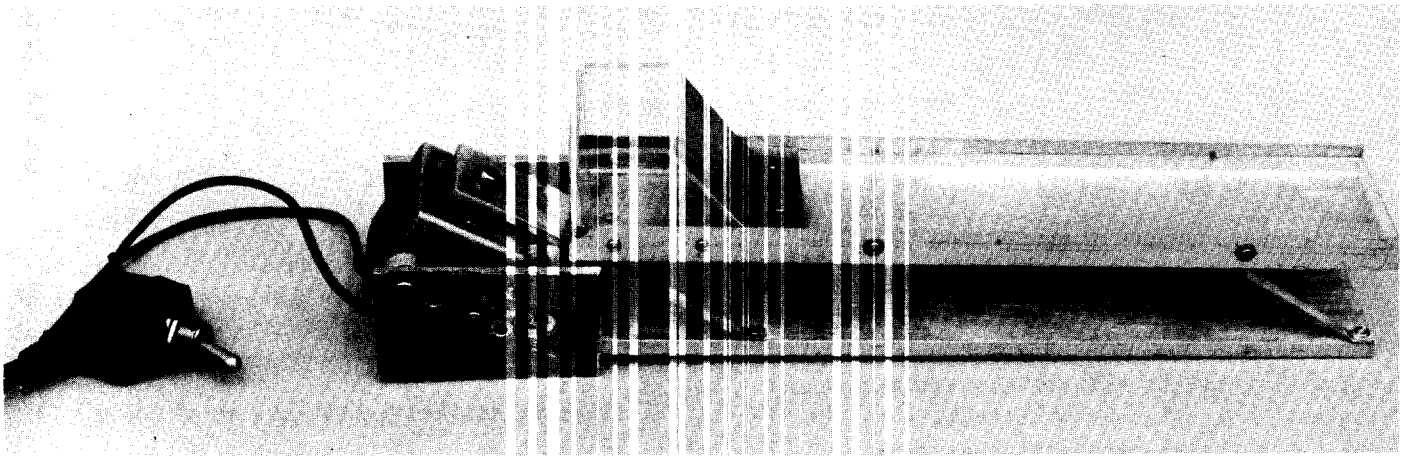

Fig. 23. Vibrating tray test rig

UNCLASSIFIED
CONFIDENTIAL

UNCLASSIFIED

the extractor mechanism functions most effectively when the vibration frequency is approximately 2100 cycles/min and the drive force angle is about 60 deg. The extractor was run at a 15-deg inclination to the local vertical to simulate spacecraft tilt, and no changes in delivery rates and effectiveness were observed.

The endurance of the test rig was simultaneously tested during these tests. It has been in operation intermittently for a total accumulated running time of approximately 75 hr at various vibratory frequency levels and drive angles. Repeated tests made on certain samples have not indicated an apparent change in results; hence, no loss in effectiveness seems to have occurred.

Additional testing and evaluation of data and parameters necessary for design optimization will be made. Also, efforts will be made to study, design, develop, and test the mechanism for the transfer phase and the presentation of collected samples to the X-ray diffractometer. A simple test rig employing the principle of particle conveyance on a vibrating tray has been assembled (Fig. 23). This rig is primarily designed to investigate: (1) the use of a simple vibrating tray for the transfer and presentation phases of the system, considering all possible spacecraft orientations relative to the local axes; and (2) the problems of fractionation and contamination between samples of a continuous flow of powdered rock. The mechanism envisioned for this system is designed to receive the powdered rock from the extractor, transfer the powder to the sample station of the X-ray diffractometer, and support the sample and permit sample rotation by the goniometer drive mechanism.

The vibrating tray principle is feasible; however, its effectiveness and reliability is yet to be determined and demonstrated. A more complete assembly embodying this principle in addition to all the other required modes has been designed and will be built in the near future. A sample presentation system using discrete samples is also being developed.

In addition, the synchronization of the extracting motion with the motions required for cutting and sample presentation will be investigated. The complete X-ray diffraction instrument system shown in Fig. 24 will be used to demonstrate the feasibility of this integrated diffractometer sampler approach. The mechanism test rig designed to study the synchronization of the drilling, cutting, sample acquisition, and extraction phases has been assembled and will soon be ready for tests. The synchronous extractor drive assembly is shown in Fig. 25.

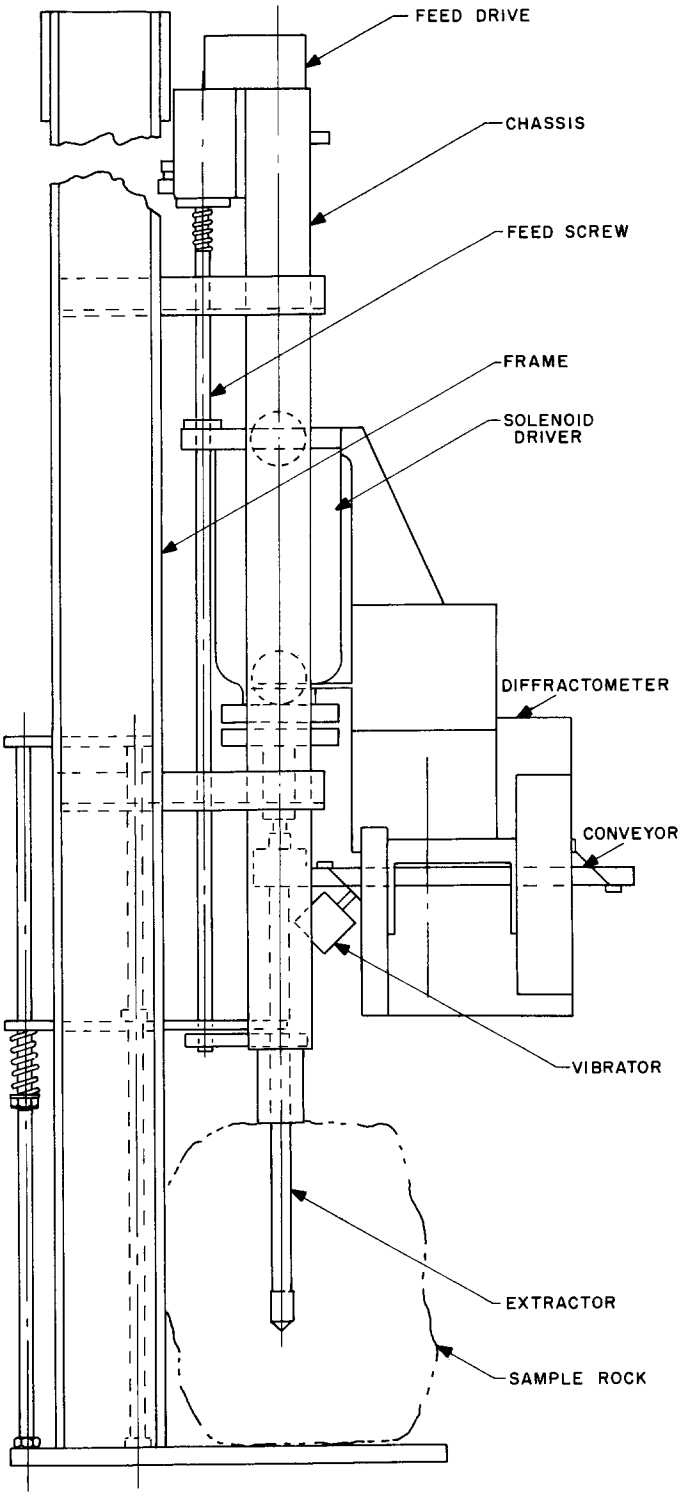

Fig. 24. X-ray diffractometer sampler system (¼ scale)

UNCLASSIFIED

UNCLASSIFIED
CONFIDENTIAL

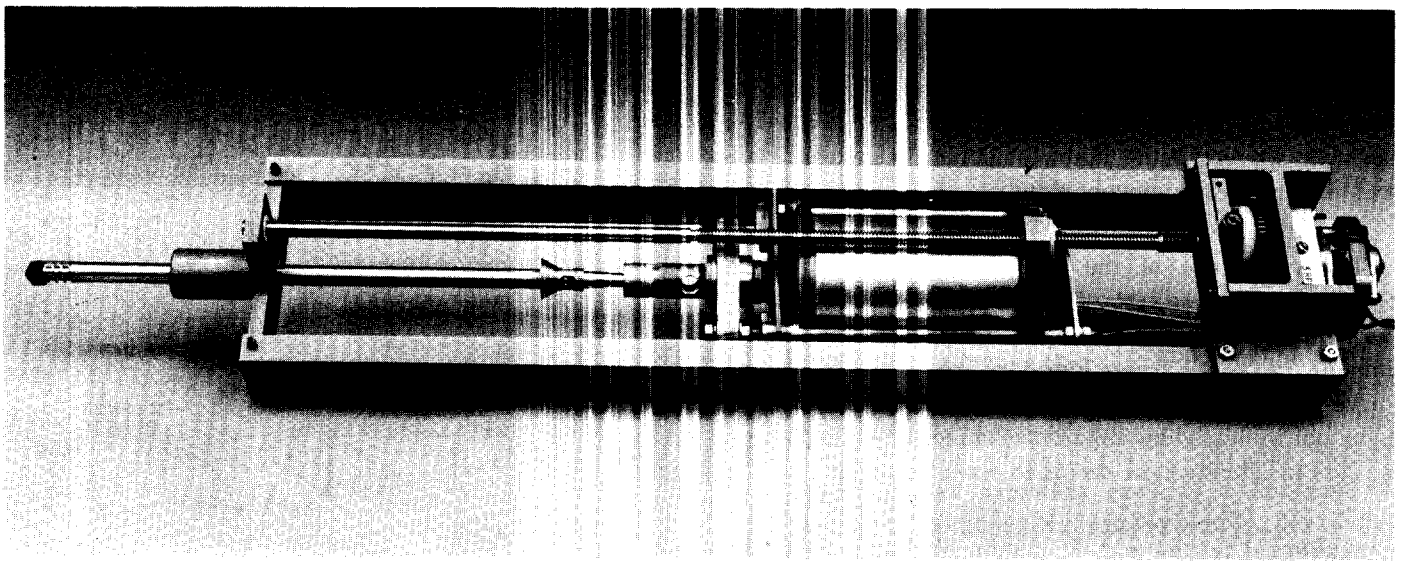

Fig. 25. Synchronous extractor drive assembly

D. Flight Control

1. Thrust Phase System Design

An analog computer study to define quantitatively the effect of vernier engine hysteresis on the flight control attitude and acceleration control loop performance was completed. A schematic diagram of the analog simulation (Fig. 26) consists of the complete three-axis attitude control system and the acceleration control system. In general, the two systems are coupled together because of vernier engine gain mismatch and the accelerometer–center-of-gravity (cg) offset effect.

The presence of hysteresis in the transfer characteristic of any or all three vernier engines produces small amplitude limit-cycle motions about the spacecraft pitch and yaw axes. The amplitudes of these motions depend on vehicle inertia, engine gain mismatch, and on hysteresis loop width. Quantitative amplitude data were obtained for each of the mission thrust phases. Table 5 presents a summary of representative data based on worst-case engine gain mismatch conditions and equal hysteresis loop width on all three engines. Although further study is required to assess fully the possible degradations to overall system performance caused by these angular motions, the following conclusions were reached during the computer study:

(1) Hysteresis-induced limit cycle modulations of vernier engines have negligible effect on midcourse correction accuracy (resulting magnitude error is less than 0.06 ft/sec).

(2) Radar noise inputs do not magnify limit cycle effects. System response from simultaneous action of radar noise and engine hysteresis appears to be roughly the superposition of responses caused by each acting separately.

Table 5. Limit cycle amplitude[a]

Configuration	Limit cycle frequency, cps	Peak angular excursion, deg	Peak angular rate, deg/sec
Midcourse	1.3	0.051	0.49
Retro-engine separation	1.6	0.054	0.43
Vernier descent	2.3	0.066	0.98

[a] Hysteresis: 1.65 lb per engine.

2. T-2 Tests

The plan for the T-2 drop test was to drop initially in the inertial hold mode with low vernier engine thrust until the "radar reliable" signal was obtained. At this time the control system would operate in the lateral velocity control mode followed by a high thrust command 5 sec after drop. During the test, the "radar reliable" signal was not generated and the vehicle remained in the inertial hold mode at low vernier engine thrust throughout the drop. The vehicle impacted at a velocity

CONFIDENTIAL
UNCLASSIFIED

UNCLASSIFIED

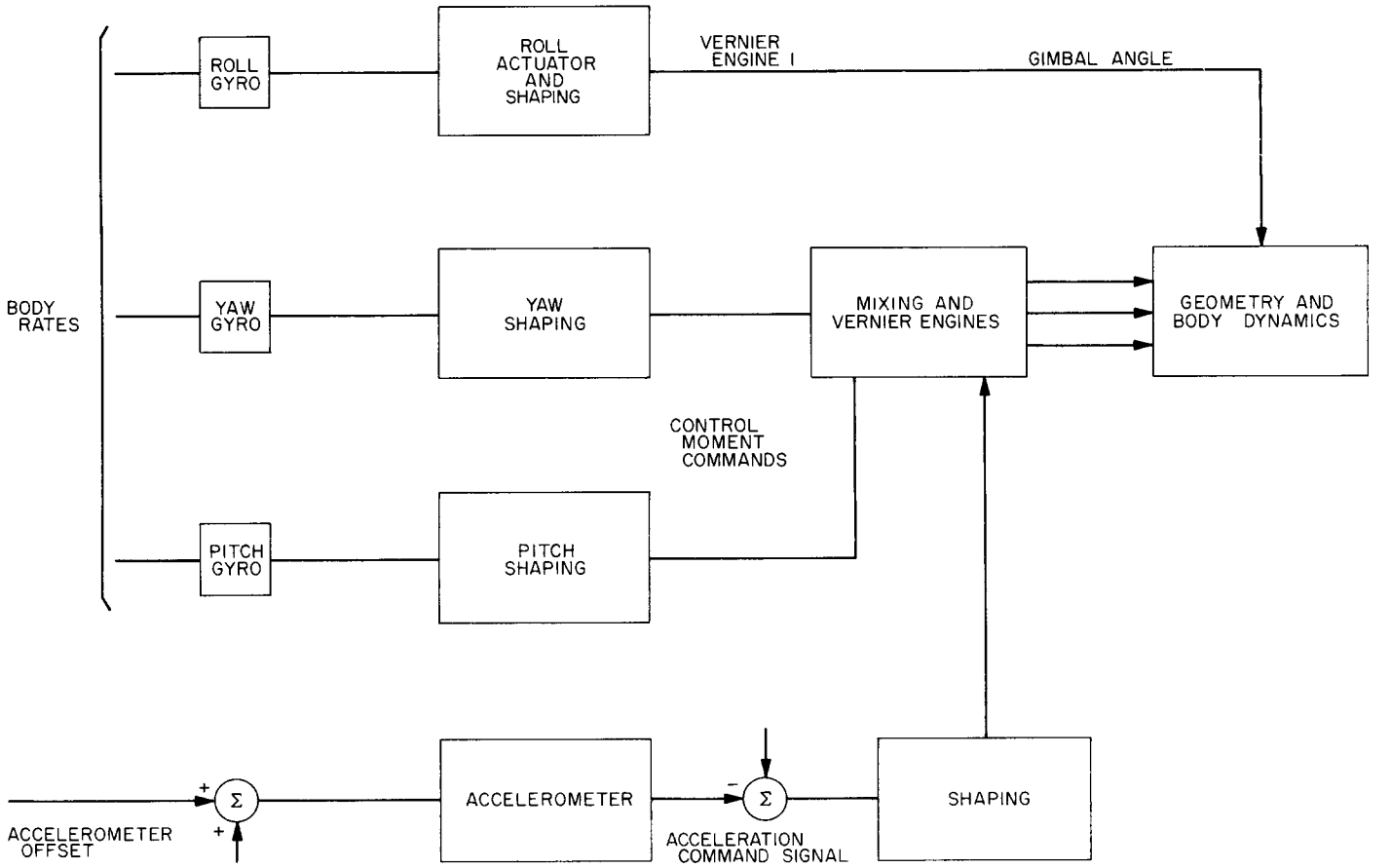

Fig. 26. Analog simulation block diagram

of approximately 61 ft/sec. Computer runs had previously predicted a terminal velocity of 66 ft/sec for this low thrust type of drop. This is within the error expected resulting from uncertainties in thrust, mass, and drag experienced during the actual drop.

During the drop, the pitch and yaw inertial hold control loops operated satisfactorily with peak angular excursions of approximately 6 deg which occurred shortly after the air bags were deployed and during ejection of the stabilizing and recovery pilot chutes. At touchdown, the telemetered pitch and yaw gyro angles were within 1 deg of the vehicle angles at which the inertial hold mode was initiated. The magnitudes of the peak pitch and yaw disturbance moments during the drop were determined to be approximately 46 and 34 ft-lb, respectively. Disturbances of these magnitudes require vernier engine thrust modulations of approximately ± 5 lb. This is well within the total thrust modulation range capability of ± 8 lb which was provided to compensate for aerodynamic disturbances, cg offset thrust axis misalignment, and engine thrust uncertainties.

At vernier engine ignition, the vehicle started a slow rolling motion which continued until impact. Subsequent analysis indicated that the roll gyro ac amplifier malfunctioned, resulting in open-loop roll control of the vehicle. The roll disturbance torques which existed during the drop were computed from optical tracking data (Fig. 27). These torques would have been within the approximately 7.6 ft-lb low thrust capability of the roll control system had it been functioning properly. Investigation of the ac amplifier malfunction disclosed that the output transistors had failed, apparently from excessively high surge currents. A review of the circuit design indicated that component safety margins were adequate. The cause of the excessive current is still under investigation.

3. *Subsystem Tests*

Flight acceptance tests on the first flight model of the sensor group were completed. The sensor group performed normally through all phases of pre-environmental and environmental tests (vibration and solar-vacuum).

UNCLASSIFIED

UNCLASSIFIED
CONFIDENTIAL

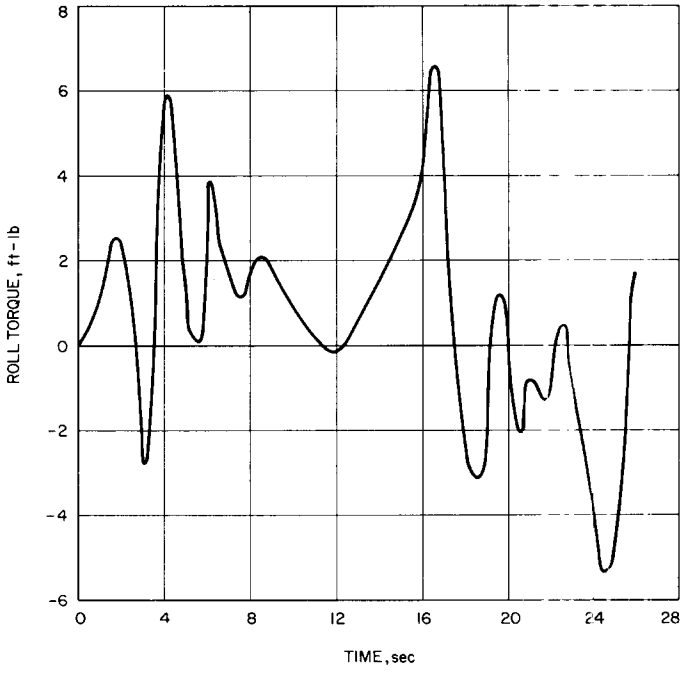

Fig. 27. T-2 roll disturbance torque

Telemetry temperature measurements made during solar-vacuum exposure indicated agreement with design values. An intermittent failure was detected in the Vernier Engine 3 control amplifier on Chassis 1A5 during post-environmental tests. The chassis was replaced and the remaining tests were completed successfully. The cause of the Chassis 1A5 failure is still under investigation.

A comparison was made of sensor group open loop operation using a normal 26-v-rms, 400-cps, three-phase sine-wave power supply, and a breadboard version of the modified square-wave power supply. Engineering models of the programmer pulse generator circuits and the square-wave ac electronics conversion unit were used in conjunction with a prototype sensor group which had been modified to represent the flight configuration as closely as possible. Evaluation of results indicated no significant differences between sine-wave and square-wave operation. Small increases in amplifier null were observed using square-wave power along with a slight decrease in pitch and yaw shaping amplifier gain. The

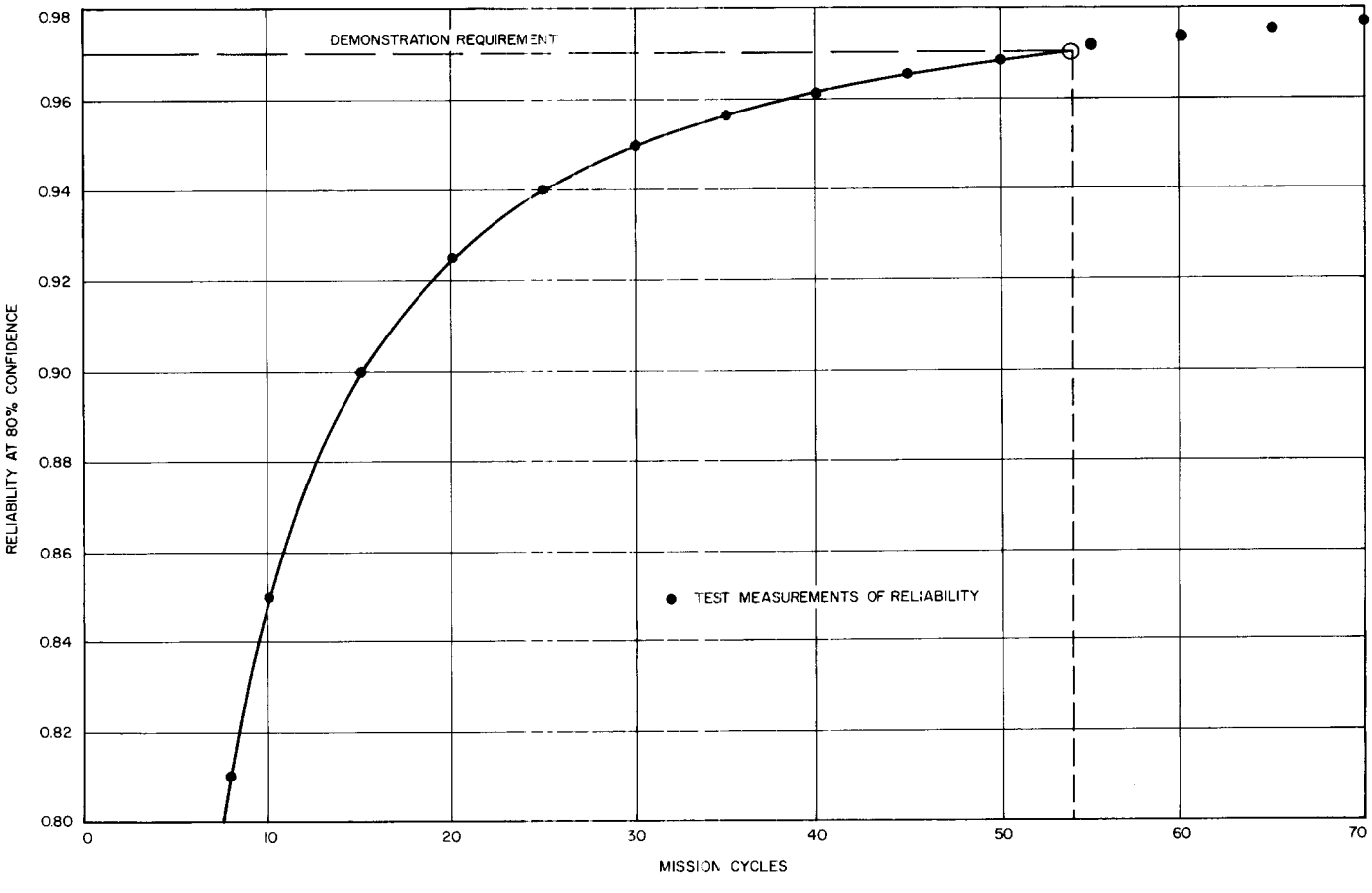

Fig. 28. Canopus sensor reliability profile

UNCLASSIFIED
CONFIDENTIAL

UNCLASSIFIED
CONFIDENTIAL

latter may be caused by the additional high-frequency noise superimposed on the 400-cps gyro signal generator output. This effect can be eliminated with minor circuit modification. The null shifts were attributed to differences in grounding.

Except for the additional high-frequency noise on the gyro signal generator output, the inertial reference unit and Canopus sensor appeared to function satisfactorily on square-wave power. Although results of this initial evaluation indicate that the sensor group performs adequately using modified square-wave power for the gyro and Canopus sensor motors, the decision to incorporate the necessary modifications in flight units will be delayed pending the results of additional tests which will be made with flight quality hardware.

4. Optical Sensors

a. Canopus sensor. Reliability demonstration tests were completed successfully on two flight model Canopus sensors (SN-3 and -9). Each unit was subjected to 250 hr of preconditioning testing to simulate conditions normally encountered prior to launch. This was followed by exposure to 27 mission cycles to reach the reliability objective of 0.97 (Fig. 28). At the beginning of the first three launch cycles each unit was subjected to expected launch vibration levels for a period of 12 min. The mission cycle consisted of continuous operation in a vacuum environment and at temperatures expected during a mission followed by functional checkout of the unit. Both units performed satisfactorily at the completion of the 27 missions.

One unit (SN-3) was then depressurized and operated in a vacuum chamber for a period of 114 hr before outgassing of the bearing gear grease contaminated the sensor window. The test was terminated at this point. During "pumping down" of the vacuum chamber, arcing within the photomultiplier tube occurred, which affected sensor operation. However, this condition disappeared and sensor performance returned to normal as soon as the vacuum transition was completed. Following disassembly, cleaning (outgassed material was removed from the window), and lubrication, the unit functional tests were completed successfully.

The minimum modified square-wave operating voltage of the Canopus sensor motor was determined in the presence of simulated boost acceleration. Three sensors were mounted on a centrifuge and subjected to 10-g acceleration along the thrust axis for 4 min and 5-g acceleration for 7 min. Half-way through each acceleration test, the motor voltage was slowly decreased until the motor stopped. Then the motor voltage was increased slowly until it started. Each sensor motor was also tested three times for stopping and starting voltages with the centrifuge not running. Results of the test indicate that the sensor motor will operate properly during launch acceleration with the proposed 21-v-rms, 400-cps, three-phase modified square-wave power supply.

b. Sun sensors. The acquisition Sun sensor sensitive plane was reoriented to coincide approximately with the spacecraft roll-pitch plane. (The center of the sensitive plane is actually offset 1.5 deg from the roll-pitch plane.) The new orientation is shown in Fig. 29. The previous roll-yaw plane configuration resulted in field-of-view interference from omnidirectional Antenna B, possible interference with the wiring harness and connector on TV Camera 2, and possible interference with the locking strut on Leg 3.

For the new configuration, the normal Sun acquisition sequence (following the 51-sec time delay after the separation and legs-down signals) will be a negative roll maneuver until one or both of the sensor cells are illuminated, followed immediately by a positive yaw maneuver

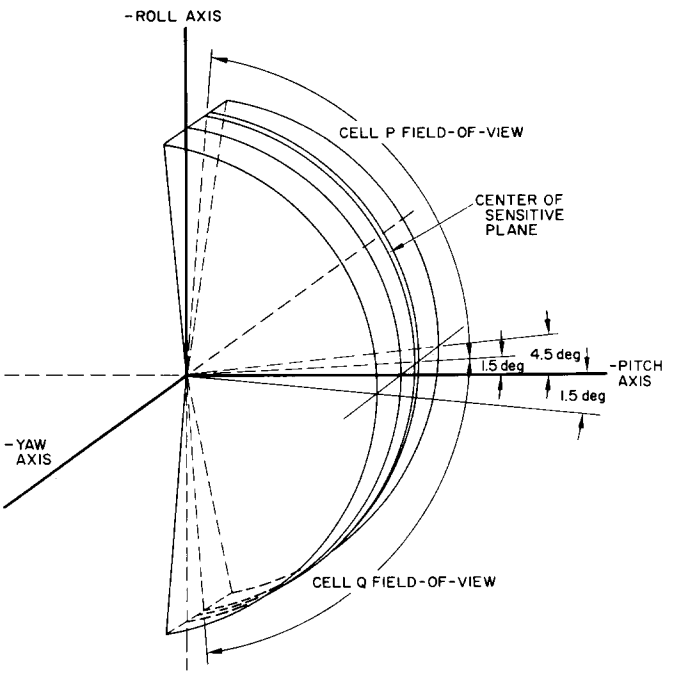

Fig. 29. Acquisition sensor field of view

CONFIDENTIAL
UNCLASSIFIED

UNCLASSIFIED
CONFIDENTIAL

until the lock-on cell of the primary Sun sensor is illuminated. Since the second rotation will always be positive yaw regardless of which cell is illuminated, some simplification of the electronic logic circuits was possible. (In the previous orientation the polarity of the second rotation depended on which cell was illuminated.) A single digital telemetry signal will be sent to indicate illumination of the slit.

Satisfactory system operation with the new acquisition sequence was verified by an analog computer study. Results of the study indicated that all transient maneuvers are well damped and the gas consumption required is essentially unchanged from that of the previous acquisition scheme. Approximately 0.054 lb of nitrogen gas is needed to acquire the Sun for any of the initial conditions considered. The gas consumption is not excessive despite having the first spacecraft precession maneuver about the roll axis where the acceleration capability is lowest. The reduced acceleration is compensated by the fact that the pitch and yaw rates do not couple into the roll axis so that less gas is used in stopping a roll maneuver and beginning a yaw maneuver than was formerly needed in stopping a yaw precession and beginning one in pitch. Because of the order of rotations chosen, the time required to acquire is longer than that needed in the previous scheme but never exceeds 18 min.

Vibration and performance tests were conducted on an engineering model of the new sensor configuration. Cell resistance versus angle to the roll-pitch plane for a test in sunlight is shown in Fig. 30.

Sensor design was completed and a detail specification prepared. Flight quality hardware is being fabricated.

5. Inertial Reference Unit

a. Gyros. Evaluation of the cleanliness of a number of disassembled gyros indicated that gyros manufactured prior to November 1963 have excessive particulate contamination in the flotation fluid, as well as generally deficient workmanship, and are not suitable for flight usage. The majority of the suspect gyros have been allocated to the T-21 and T-2 test programs. The remaining suspect gyros will be torn down and rebuilt using improved procedures and quality assurance measures. Permissible contamination levels found in gyroscope test samples will meet minimum requirements. All new gyros will be ordered according to the contamination level requirements.

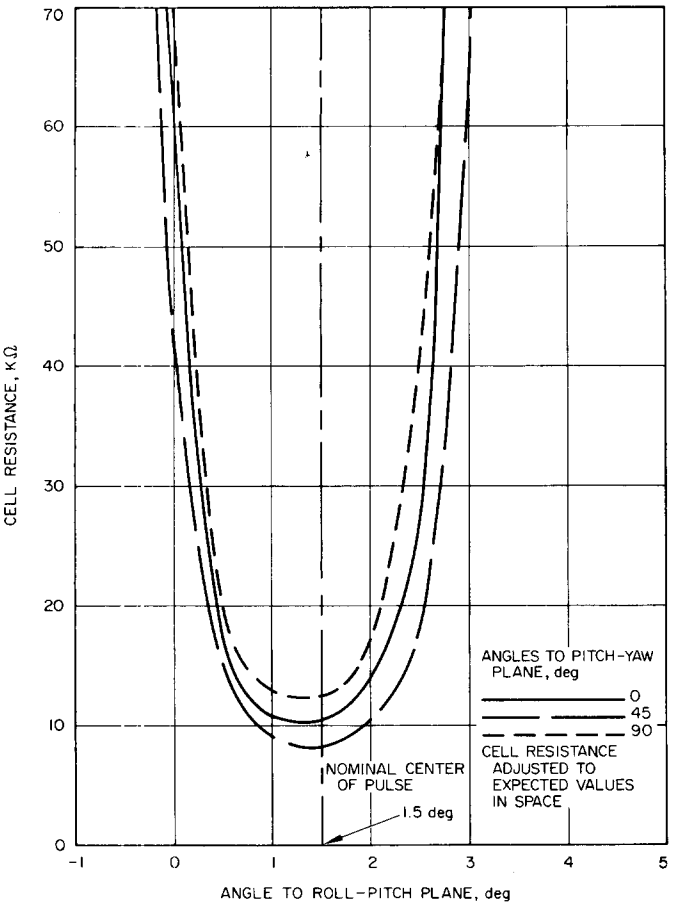

Fig. 30. Cell P resistance versus angle to the roll-pitch plane

b. Accelerometers. Additional accelerometers were ordered for the revised *Surveyor* program and to replace units expended in test. Requirements for the new accelerometers included:

(1) The range was extended from +0.01 to +0.5 g to −0.75 to +0.75 g to provide an accelerometer that is compatible with possible future changes in vernier engine thrust level, as well as to reduce signal rectification in the presence of vibration.

(2) The output signal sensitivity to changes in external load impedance was reduced by approximately a factor of 10. This change permits greater interchangeability of inertial reference units and electronics units at the sensor group level.

(3) Frequency response characteristics were specified more closely to provide greater assurance that test and computer results are representative of performance to be expected during a mission.

UNCLASSIFIED
CONFIDENTIAL

UNCLASSIFIED
CONFIDENTIAL

c. Unit tests. Tests to determine the feasibility of operating gyro motors with modified square-wave power source were completed. These tests are part of a study program to reduce the overall spacecraft power deficit by increasing the efficiency of the three-phase power generated in the flight control sensor group. A comparison was made of the performance of five gyros using 26-v-rms, 400-cps, sine wave, and the three-level delayed square wave (Fig. 31) with the 400-cps fundamental (E_p) set to 26 and 21 v rms. The effect of spin motor

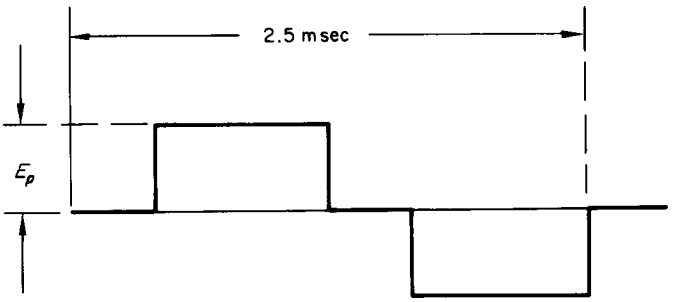

Fig. 31. Delayed square wave for gyro test

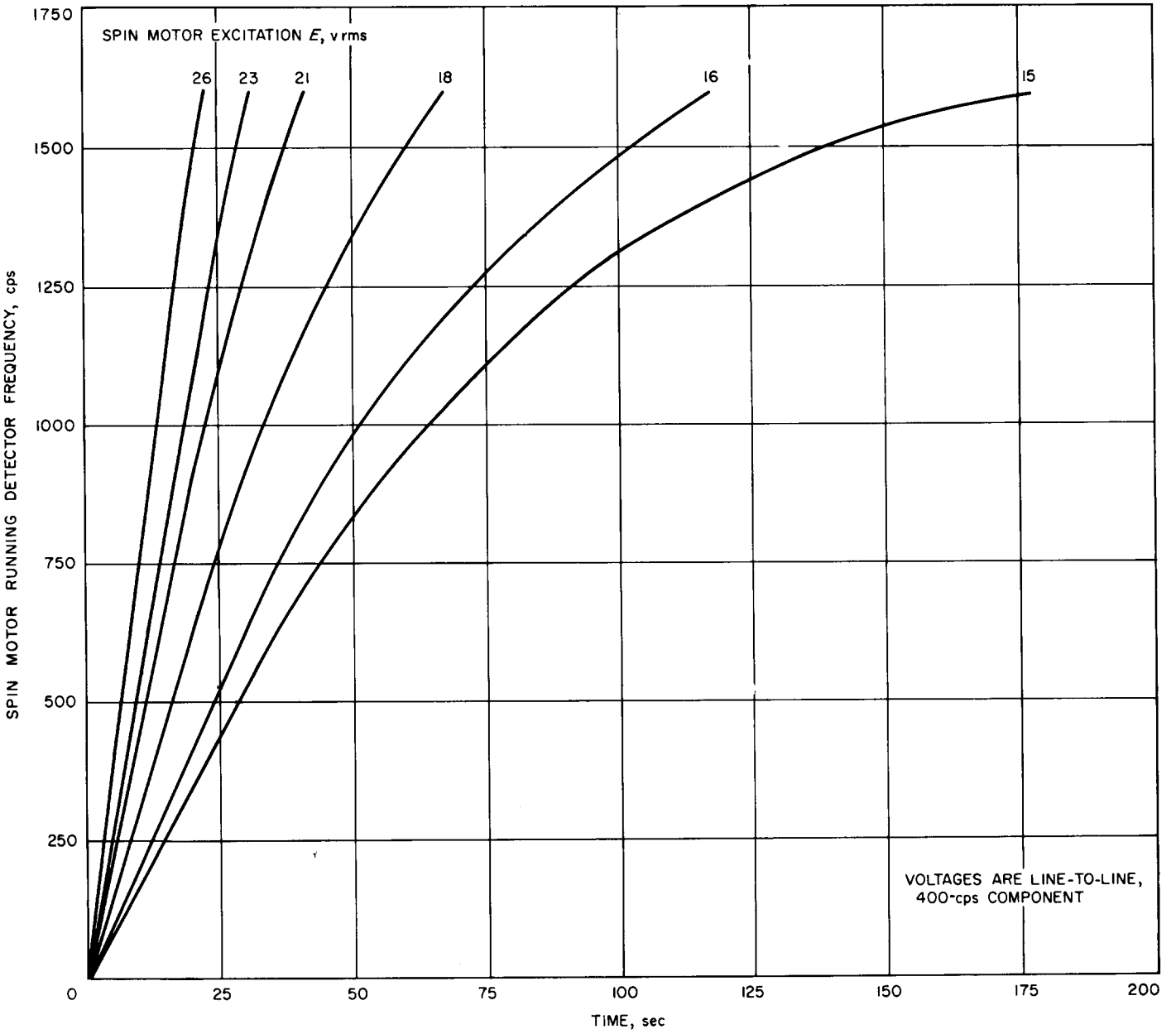

Fig. 32. Runup characteristics of Gyro SN-57

CONFIDENTIAL
UNCLASSIFIED

UNCLASSIFIED
CONFIDENTIAL

excitation on fixed drift, spin, and input axis mass unbalance was determined. Differences noted were within the test-to-test variations to be expected. Wheel synchronization and rundown times were measured with the gyros at room ambient temperature and at normal operating temperature (180°F). One gyro (SN-57) was evaluated for runup characteristics at square-wave voltage levels between 26 and 15 v rms (Fig. 32). The curves show that the torque available for acceleration of the wheel decreases rapidly at voltage levels below 21 v rms. Linearization of these curves results in the graph shown in Fig. 33, which indicates the amount of excess torque available for voltage levels between 26 and 16 v rms equivalent square wave. There is approximately a 45% reduction in excess torque when operating the gyro motor at 21 v rms.

Spikes of up to 100 mv which appeared on the output of the gyro spin motor while running and when operating on square-wave power were eliminated by placing a 0.047-μf capacitor across the standard 10,000-Ω load.

The effect of spin motor excitation levels on gyro transfer function and heater power required to maintain temperature is shown in Fig. 34. These tests indicate that the heater power requirements are increased by approximately 0.7 w at 21 v rms because the heater is compensating for the reduced spin motor power dissipation. The change in gyro transfer function results because the heat generated by the gyro spin motor is more effective than the heater in controlling the damping gap temperature. Fig. 34 shows that the gyro transfer function decreased by 1.6% when the spin motor excitation was decreased from 26 to 21 v rms. This is equivalent to a

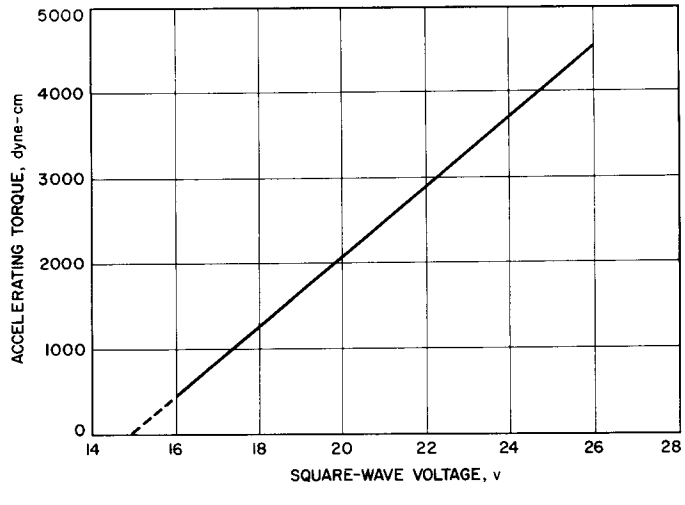

Fig. 33. Skin motor excess pull in torque for Gyro SN-57

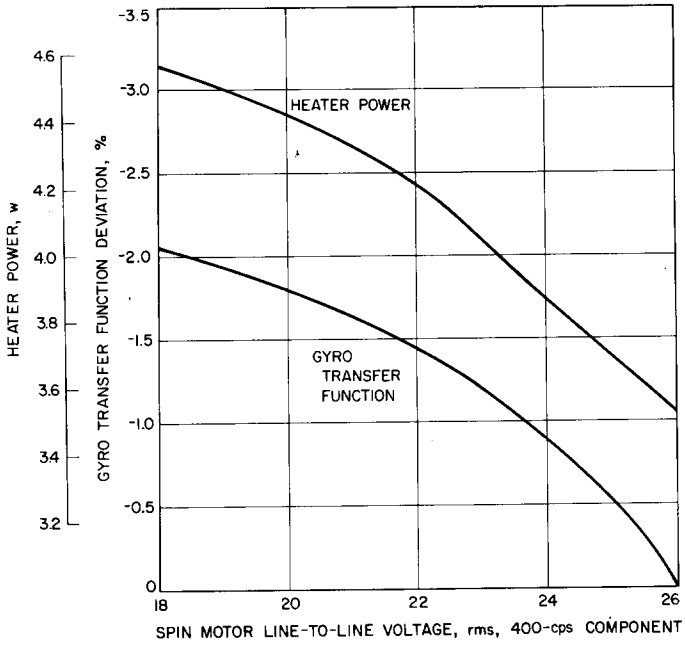

Fig. 34. Gyro transfer function deviations and heater power

decrease in damping gap temperature of approximately 0.5°F.

Based on the results of these tests and similar tests run on the Canopus sensor and the flight control sensor group, the 26-v-rms, three-phase sine-wave power will be replaced at some future period with 21-v-rms equivalent square-wave power in the flight control electronics unit.

6. Gas Jet System

a. Pressure regulator. During type-approval vibration tests along the thrust axis of the pressure regulator, an apparent resonant condition occurred in the 30- to 40-cps frequency range, which resulted in excessive regulator valve leakage. An investigation is being made to determine the cause of the failure.

b. Pressure relief valve. The pressure relief valve has completed successfully two additional 36- and 45-day storage cycle tests. The next test of approximately 45 days will end the storage tests planned for this unit.

c. Jet valves. Flight acceptance tests were completed on the fourth flight model jet valve. Tests are in progress on four additional jet valves which passed the assembly tests after having been thermally coated. All units were well within the specification requirements.

UNCLASSIFIED
CONFIDENTIAL

UNCLASSIFIED
CONFIDENTIAL

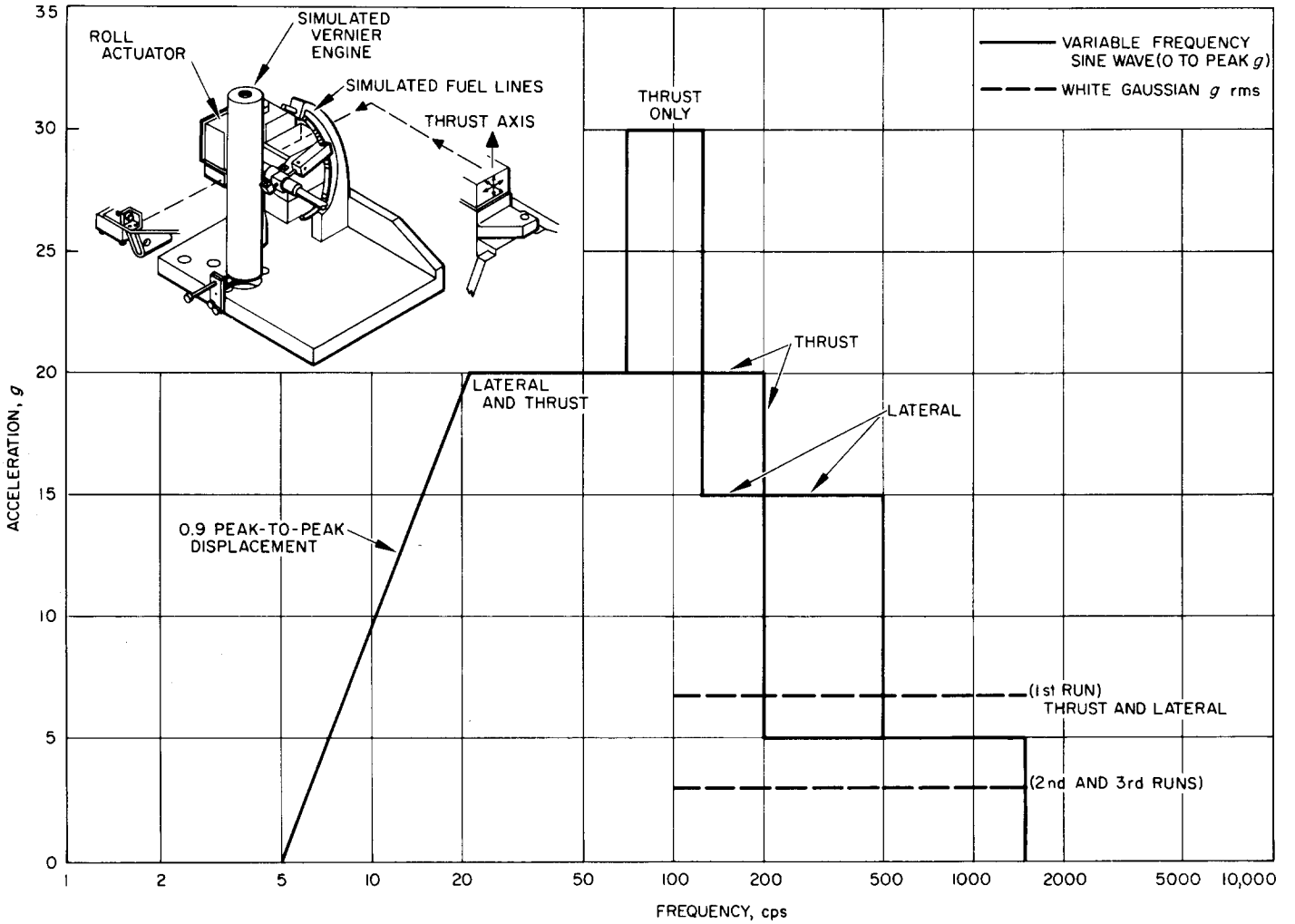

Fig. 35. Roll actuator vibration levels

7. Roll Actuator

Vibration tests were completed on an engineering model of the redesigned roll actuator. The final series of tests was conducted using revised variable frequency sine-wave inputs combined with random vibration. The sinusoidal and random levels imposed at the base of the vernier engine support bracket are shown in Fig. 35. These levels are somewhat in excess of those measured on the unit during the recent S-2A vibration tests. After completing three 2-min sweeps along the thrust axis, three 2-min sweeps along the lateral axis perpendicular to the vernier engine trunnions, and two 2-min sweeps along the lateral axis parallel to the trunnions, the mounting bracket on the test fixture broke. Since the roll actuator is not particularly susceptible to vibration applied along this axis, the tests were discontinued. Examination of the roll actuator following the test revealed no damage.

Another engineering model of the redesigned actuator is currently undergoing life tests. These tests are designed to determine the effect of preflight checkouts, launch vibration, and thermal-vacuum environments on the operation of the unit. The unit has completed a 100-hr preflight test cycle and a 36-min vibration environment.

The pin-puller presently used with the redesigned roll actuator requires a laminated shim to align the pin with the mounting bracket. Since even under normal conditions a slight misalignment can exist after assembly of the pin-puller to the mounting bracket, a test was conducted to determine if this misalignment could prevent the pin from retracting properly. To simulate worse-case conditions, a live pin-puller was mounted to a bracket in the prescribed manner, but with the shims completely removed. The misalignment that resulted for the particular pin-puller and bracket used was 0.016 in.,

UNCLASSIFIED
CONFIDENTIAL

UNCLASSIFIED
CONFIDENTIAL

which exceeds the expected maximum misalignment. The squib in the pin-puller was fired and the pin retracted completely as required.

8. Electronics Unit

Redesign of the ac electronics control unit (ECU) and programmer was initiated to provide the 21-v-rms, 400-cps, three-phase modified square-wave power supply. Tests on an engineering model of the supply indicated an operating efficiency of approximately 60% into a 10-w load. The spacecraft power deficit can be reduced by approximately 600 w-hr by replacing the sine-wave supply with the modified square-wave supply. Redesign of the ac ECU involves the electronics unit wiring harness, modification of Chassis 1A7, and addition of a new Chassis 1A6. Modification of the advanced flight control programmer includes changing the tuning fork, redesign of the 400-cps output amplifiers, and addition of a delay circuit to provide a −90-deg phase signal.

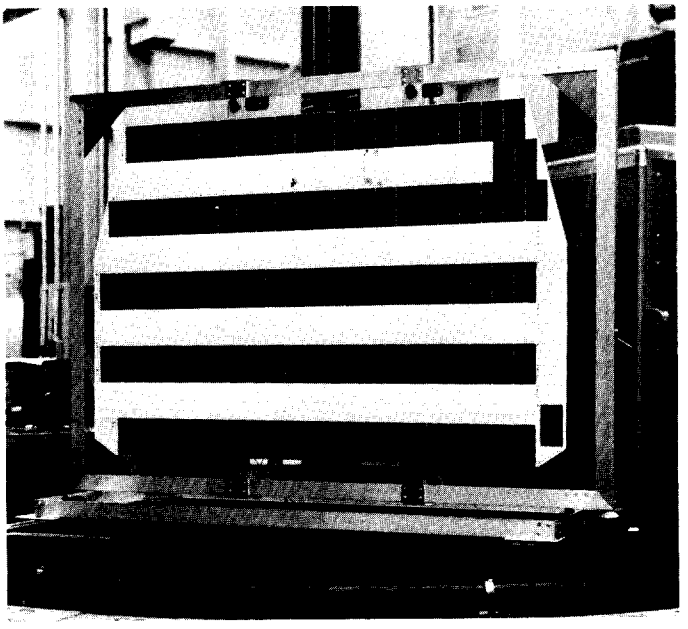

Fig. 36. Reliability assurance test panel installation in thermal chamber

E. Electrical Power Supply

1. Solar Panels

a. Reliability assurance test solar panel. Flight acceptance testing of the reliability solar panel has been completed, including preenvironmental sunlight performance, vibration, post-vibration sunlight electrical performance, thermal-vacuum, and post thermal-vacuum sunlight electrical performance. Fig. 36 shows the reliability panel mounted on a handling stand prior to the thermal-vacuum exposure. Results of electrical performance tests are summarized in Table 6. Throughout the test program performance of the panel was acceptable, with an electrical performance margin of 6% above the minimum requirement. A dummy Sun sensor was installed on the reliability panel and final inspection was completed.

b. Thermal control model solar panel. Fabrication of a thermal control model (TCM) solar panel was initiated. The TCM panel has flight-rated thermal characteristics, but is electrically nonfunctional. The TCM modules are low-efficiency modules and have thermal characteristics identical to flight modules. Since electrical functioning was not required for the TCM solar panel, it was possible to eliminate the negative wire-tab connection from the modules.

c. Elevated-temperature sunlight electrical performance testing. Experience with performance testing of the *Surveyor* solar panels showed a tendency for cracked solar cells to exhibit failure only at temperatures above ambient. Consequently, a test plan was prepared for elevated-temperature testing of solar panels with test temperatures ranging from ambient to maximum lunar day solar panel temperatures (110 to 120°C).

Preliminary tests were conducted on solar cell modules to evaluate any effects of heating at the proposed temperatures. Results of the preliminary tests verified the

Table 6. Reliability solar panel flight acceptance performance tests at Table Mountain

Item	Power output, w (at 100 mw/cm², 25°C)			
	Specification requirement	After fabrication	After vibration	After thermal-vacuum
Total panel	44.0	46.72	46.10	47.27
Subgroup[a]				
V-1	8.8	9.43	9.50	9.63
V-3	8.8	9.41	9.52	9.85
V-5	8.8	9.36	9.46	9.75
V-7	8.8	9.28	9.25	9.52
V-9	8.8	9.30	9.24	9.46

[a]The reliability panel has 5 subgroups compared to 9 subgroups on a flight panel.

UNCLASSIFIED
CONFIDENTIAL

UNCLASSIFIED
CONFIDENTIAL

planned test approach and design of the elevated temperature test equipment was begun. Test equipment consists of an insulated flight acceptance test container to which has been added a plastic sheet window, hot air ducting and temperature instrumentation, and a separate heater and fan unit with associated control and instrumentation equipment.

d. Balloon flights. As previously reported, two sets of *Surveyor* solar cells (2 per set) were tested at an altitude of 80,000 ft. The data has been reduced by JPL and has been supplied to Hughes Aircraft Company together with the flight specimens. Fixtures are being designed to mount the calibrated cells. After the cells are mounted to the fixture they will be used to calibrate secondary standards for use on *Surveyor* solar panel test programs.

e. Solar cell modules. Flight acceptance testing of all solar cell module lots (1 through 27) has been completed. The third solar cell module type-approval test (TA-3A) was completed. Table 7 shows the comparison of the results from TA-1, TA-2A, and TA-3A. The major cause of power degradation continues to be the high-temperature vacuum test. The average degradation caused by this exposure for the three type-approval tests was 3.19 mw. The TA-3A test indicated a large degradation in power after ultraviolet radiation exposure, but this was found to be caused by an oil deposit on the cover glass. The power output of the solar cells returned to its pre-ultraviolet value after the removal of the oil film. The total degradation after the TA-1 test was approximately 6 mw as compared to 2.6 mw in TA-2A and 3.5 mw in TA-3A. The larger degradation in TA-1 can be accounted for by errors in test technique, which were corrected.

f. Investigation of infrared test techniques. A feasibility study was conducted to evaluate the applicability of infrared radiation measurements for solar array performance analysis. The test is performed by utilizing a high level current bias to produce internal heat generation which raises the average solar cell temperature to a few degrees above ambient. A scanning infrared camera is then used to obtain a "thermal photograph" of the array. It was anticipated that damaged cells would exhibit an abnormal heat dissipation and, therefore, could be detected.

Table 7. Comparison of solar cell module type-approval tests

Test	Mean power, mw			Mean degradation, mw			Standard deviation, mw		
	TA-1	TA-2A	TA-3A	TA-1	TA-2A	TA-3A	TA-1	TA-2A	TA-3A
At start	113.9	116.8	121.6	—	—	—	—	—	—
Post-beam	113.8	116.8	121.4	0.95	−0.12	0.25	0.05	0.88	0.37
Post-high temperature sterilization	113.6	—	—	0.19	—	—	1.06	—	—
Post-ethylene oxide	113.1	—	—	0.57	—	—	0.54	—	—
Post-storage temperature	113.2	116.4	121.6	−0.16	0.72	−0.23	0.64	1.16	0.48
Post-ultraviolet	112.3	117.0	119.5	0.93	−0.56	2.06	0.96	0.93	1.11
Post-temperature cycle	112.3	117.3	121.2	0.04	−0.32	−1.67	1.21	0.75	0.78
At start (TA-2A only)[a]	—	118.4	—	—	—	—	—	—	—
Post-high temperature vacuum	108.5	115.8	118.3	3.72	2.60	3.24	1.30	2.34	1.78
Post-low temperature soak	107.9	115.8	118.1	0.60	0.00	0.21	1.29	0.41	0.55
Post-series	107.9	115.8	118.1	5.99	2.60	3.50	2.67	2.29	2.18

[a]The second type-approval test program had to be started twice due to a faulty test procedure in the original test run.

UNCLASSIFIED
CONFIDENTIAL

UNCLASSIFIED
CONFIDENTIAL

Tests were conducted using two different scanning infrared cameras: a special-purpose infrared camera manufactured by Barnes Engineering Company, and a scanning thermal plotter manufactured by Philco Corporation. A typical photograph using the Philco equipment is shown in Fig. 37. An ordinary optical photograph of the test array is shown in Fig. 38. A complete raster was scanned every 5 sec with a resolution of approximately 35 lines/in. The highest temperature (brightest area) indicated by the photograph is approximately 35°C. The three modules having the lowest temperatures were cracked, resulting in gross failures. A cracked corner of one module (Fig. 37) is discernible.

Results to date indicate that the infrared test technique can be used advantageously for rapid laboratory tests to detect gross failure, i.e., near open-circuit condition. Further testing is required to fully evaluate the potentials of the technique.

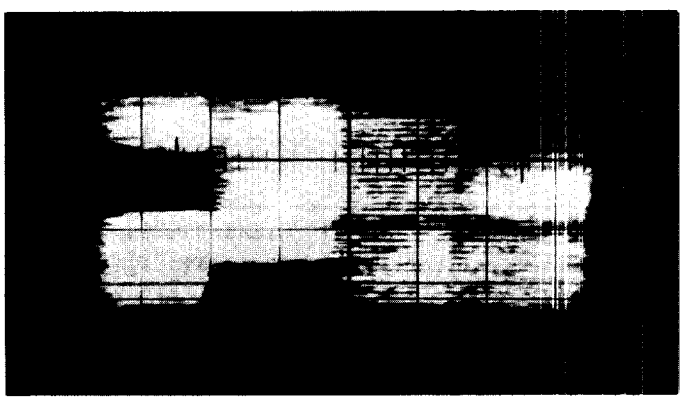

Fig. 37. Typical photograph of the test array using Philco scanning thermal plotter

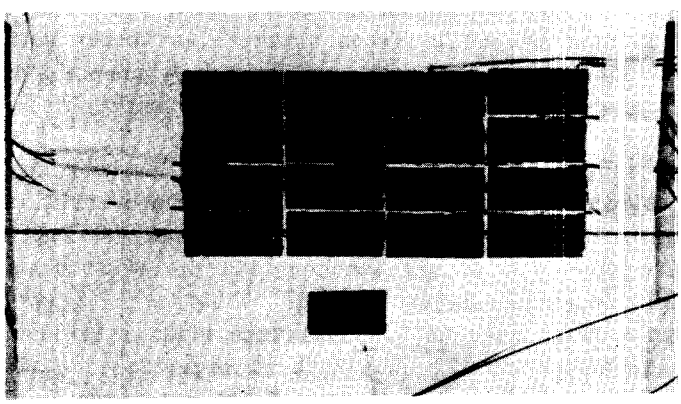

Fig. 38. Optical photograph of the test array

2. *Batteries*

a. Main battery. Five reliability model main batteries of flight quality, SN-R4 through -R8, were subjected to type-approval level vibration tests at Melpar, Incorporated. Each battery underwent a total of 12 min of combined sinusoidal-random vibration in each of three orthogonal axes, one of which was parallel to the spacecraft thrust axis. Battery degradation in voltage was observed during post-vibration high-rate battery discharge. Each battery indicated internal cell damage in the outer row of cells (farthest from the battery mounting surface).

Since five prototype main batteries, SN X-37, X-38, X-39, X-40, and X-43, were qualified under type-approval test levels of vibration at Hughes Aircraft Company, survey tests were run to determine test differences between the Melpar and Hughes vibration setups. Among the differences was overhang of the Melpar fixture, which does not occur in the Hughes fixture. This may have resulted in abnormal loads within the batteries tested at Melpar.

Battery SN-4 was subjected to type-approval level vibration using the six 2-min increasing frequency sweeps at Melpar. During the first 2-min sweep in the thrust axis, cell voltage degradation was observed at approximately 110 cps. However, at the conclusion of the sweep, the battery voltage was above specification limits under an 85-amp discharge. At the start of the second sweep, the battery indicated damage and the test was discontinued at 19 cps.

Battery SN-7 was subjected to type-approval level vibration at Hughes Aircraft Company. The test was performed using the six 2-min increasing frequency sweeps per axis of vibration with no degradation. The battery was then tested by repeating 2-min sweeps in the thrust direction (the most critical direction of vibration). Ten additional 2-min sweeps were successfully completed. Electrical measurements showed that the battery did not experience any damage during vibration.

Inspection of manufacturing processes and quality indicated no difference between the type-approval and the reliability batteries.

The following tasks are being considered or are underway: (1) further examination and comparison of the Hughes and Melpar fixtures, (2) vibration of a battery at Hughes using the Melpar fixture, and (3) vibration of a

UNCLASSIFIED
CONFIDENTIAL

UNCLASSIFIED

battery at Hughes with the same overhang as the Melpar fixture.

3. Main Power Switch

The operation of the main power switch (described in *SPS 37-30*, Vol. I) is controlled by applying power to the motor terminals through the spacecraft harness. The motor drives a gear train that raises and lowers, by cam action, the platform on which a shorting bar is mounted. When power is supplied to the proper motor terminals, the platform moves to the other end of the cam travel and the motor current self-interrupts. No further switch action takes place until power is supplied to the other motor terminal, which at that time is in contact with the motor coil through the self-interrupting contacts.

4. Power System Integration Testing

An upgrade in the power system integration test setup was accomplished. Power carrying leads, previously unshielded, were shielded and lengthened to simulate the spacecraft wiring harness. Spurious signals generated by the unshielded leads hampered accurate measurement of certain critical system voltages. One unnoticed signal was a large current spike being drawn (probably by the boost regulator) from the battery at a 10-kc repetition rate. The boost regulator circuit used in the breadboard tests, however, is not identical to the latest circuitry; thus the current spike problem may not exist in the present configuration. The problem is being investigated.

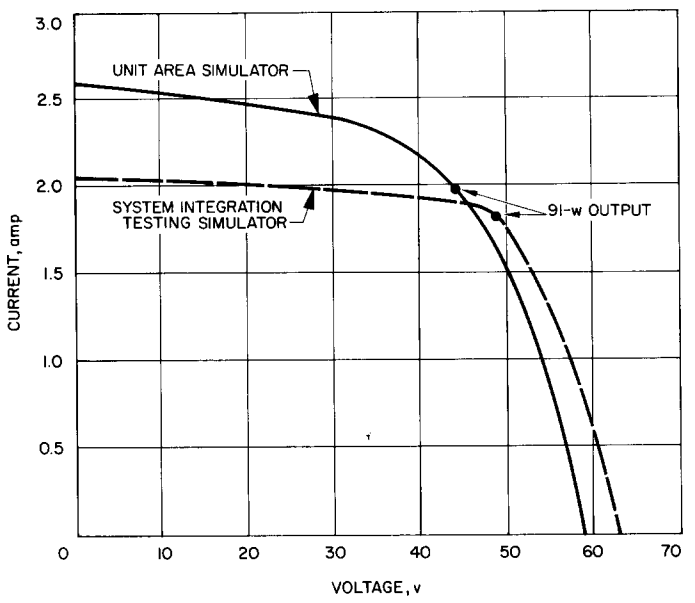

Fig. 39. Comparison of system integration testing simulator and unit area simulator

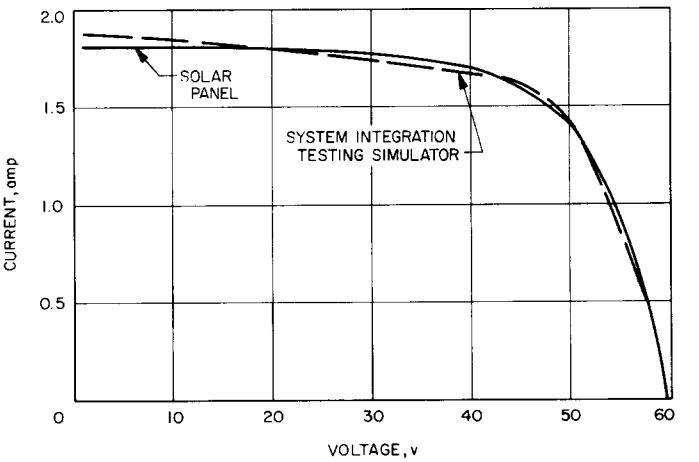

Fig. 40. Comparison of system integration testing simulator and *Surveyor* solar panel electrical characteristics

Simulation of the solar panel is critical in unit testing. It was found that the solar panel simulator used in unit test did not closely approximate the solar panel curve. A comparison of the solar panel simulator used in integration testing and the one used in unit test is shown in Fig. 39. Both solar panel simulators were set for 91-w output. The maximum power point on the solar panel simulator used for unit testing is much broader than that on the solar panel simulator used for integration testing. The broad curve causes an error in testing. The solar panel simulator used in the unit test area will be modified. In Fig. 40 the electrical characteristics of the system integration solar panel simulator are compared with those of the solar panel.

F. Engineering Mechanics

1. Landing Dynamics

a. Ground clearance. A minimum ground clearance of 4.2 in. (to the bottom of the square tube) for a 20-ft/sec vertical velocity and an estimated minimum ground clearance of 5–5½ in. for a 15-ft/sec vertical velocity have been established as criteria for the present A-21 *Surveyor* spacecraft based on a 3-σ flight control dispersion

UNCLASSIFIED
CONFIDENTIAL

UNCLASSIFIED CONFIDENTIAL

ellipse relating lateral velocity and incidence at touchdown.

An investigation was completed to evaluate the practicability of improving *Surveyor* ground clearance during touchdown. The investigation was made on the basis of simple changes to the landing gear geometry. The corresponding effect of these changes on stability and loads was also assessed or estimated.

The simplest changes that can be made to the landing gear design to improve ground clearance are: (1) increase foot height, (2) increase leg length, and (3) increase leg inclination to the vehicle x-y plane.

Of these changes, the one most easily achieved is the foot height increase, since this only involves a redesigning of the footpad. With everything else unchanged, a foot height increase of 3 in. (from 6.5 to 9.5 in.) is possible with the present shroud envelope limitations.

An increase in leg length would likely require a change in shock absorber attachments to the leg, although the shock absorber itself would not require redesign. It is possible with the present envelope constraints (keeping the footpad height at 6.5 in.) to increase the leg length from 40.5 to 50 in.

Increase in leg inclination to the vertical could be accomplished by increasing the length of the telescoping lock strut. This would necessitate an adjustment to the A-frame, but an incidence change of 5 deg could be accomplished without major difficulty.

The changes could be incorporated into the vehicle singly or in any of several combinations if the envelope limitations with respect to the *Centaur* shroud were not violated.

The clearance investigation was carried out at 20 ft/sec on a 15-deg slope with the single leg oriented downhill. Ground clearance was assessed using the combination of landing gear parameters shown in Fig. 41. The results are summarized in Table 8; Column 1 lists nominal conditions for current A-21 spacecraft design.

The investigation showed that the effect of increasing the foot height h_f by 3 in. (Column 2) is to increase minimum clearance by approximately 1 in. Increasing leg inclination to the x-y plane, α, by 5 deg (Column 3) increases minimum clearance by approximately 1½ in.

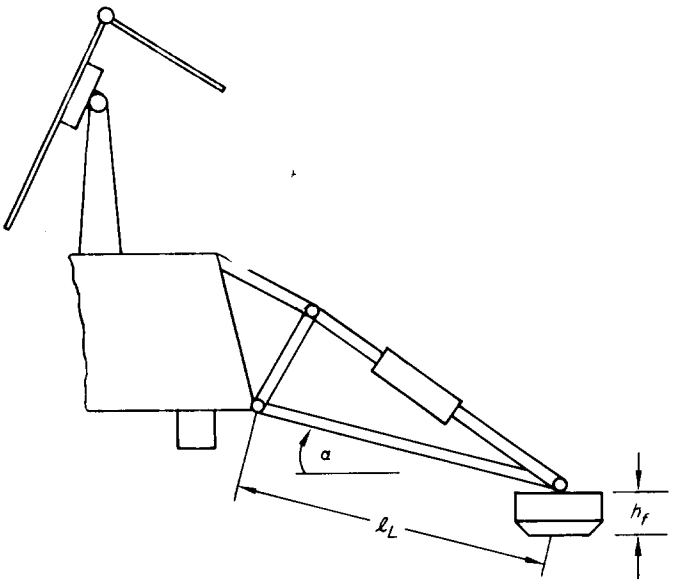

Fig. 41. Landing gear ground clearance study parameters

These effects were shown to be cumulative; thus, increasing h_f by 3 in. and α by 5 deg at the same time (Column 4) resulted in a minimum clearance increase of 2½ in.

Increasing leg length ℓ_L by 9½ in. at the same time as α is increased by 5 deg (Column 5) resulted in a minimum clearance increase of only ¾ in. This implies that a 9½-in. leg length increase actually reduces ground clearance by ¾ in.

No increase in crushable block height has accompanied any increases in the above parameters. If in each case the block height is correspondingly increased to maintain the same clearance between the block and ground (before deflections are permitted), simple geometric considerations show that: (1) 3-in. h_f increase yields a 3-in.

Table 8. A-21 spacecraft ground clearance assessment

Parameter	Investigation				
	1	2	3	4	5
Foot height h_f, in.	6.5	9.5	6.5	9.5	6.5
Leg length ℓ_L, in.	40.5	40.5	40.5	40.5	50.0
Leg inclination to the x-y plane, α, deg	18.0	18.0	23.0	23.0	23.0
Increases to minimal ground clearance, in.	—	1.0	1.5	2.5	0.75

UNCLASSIFIED CONFIDENTIAL

UNCLASSIFIED

clearance increase, (2) 5-deg α increase yields a 7.05-in. clearance increase, and (3) 9.5-in. ℓ_L increase yields a 2.95-in. clearance increase.

Thus, it appears that increases in ground clearance can be best achieved by increases in α and h_f, since increase of these quantities by the amounts considered does not deteriorate stability when no corresponding increase is made in crushable block height. When the crushable blocks are lengthened, however, it may be necessary to lengthen the legs to maintain acceptable stability characteristics. Increase in length-to-diameter ratio of the blocks may also be a problem, due to side loads. Load levels would be expected to increase 15% for the α change but should not be appreciably affected by an increase in h_f.

The investigation indicated that a 3½-in. increase in h_f with an appropriate increase in block height should yield a clearance increase of about 2 in. with no load or stability penalties. These changes could be achieved simply and may therefore be worthwhile. Further, clearance increases may be affected by α increases, although a more detailed analysis of this problem would be required. Changes in footpad and crushable block size or position must be evaluated carefully with respect to rocket exhaust heating and changes in radar performance.

b. S-2A spacecraft drop test analysis. A study has been conducted using the IBM forced response program to determine the feasibility of simulating lunar landing loads with Earth gravity and zero horizontal velocity as the landing conditions for forthcoming drop tests of the S-2A spacecraft. The procedure for arriving at maximum-load landing conditions was carried out in two steps.

The first step was to determine lunar landing conditions that produce the most severe structural and component loads. The landing situations examined encompassed lateral velocities up to 7 ft/sec, with corresponding vehicle incidences, for friction coefficients ranging from zero to unity. On all lunar cases the vehicle landed on a 15-deg slope with the single leg downhill, at a vertical velocity of 20 ft/sec.

For each simulated landing, the three components of acceleration were examined at nine selected points on the vehicle, in addition to two components of bending moment at two places on the mast. These 31 responses (27 accelerations and 4 bending moments) were compared on 59 separate IBM simulated landings, and from these, four sets of landing conditions were selected as being most severe from a structural standpoint (Table 9).

Table 9. Most severe conditions for lunar landings ($\mu = 1.0$)

Longitudinal velocity, ft/sec	Lateral velocity, ft/sec	Initial incidence, deg	Site slope, deg
−20	2	2	−15
−20	−6	0	−15
−20	6	−9	−15
−20	0	0	0

The second step was to duplicate, insofar as possible, each of these sets of responses with regard to both magnitude and time correlation. This was done by analytically dropping the vehicle under landing conditions which are readily attainable during an actual test program, i.e., Earth gravity, zero horizontal velocity, and friction coefficient less than 0.8. By using a trial and error approach, test site landing conditions were obtained which yielded vehicle structural responses in very close agreement with those selected from the lunar landings, thereby demonstrating the feasibility of establishing the S-2A spacecraft drop test conditions which should produce the most severe structural loads (Table 10).

Table 10. S-2 spacecraft drop test landings to reproduce loads in Table 9 ($\mu = 0.75$)

Vertical velocity, ft/sec	Horizontal velocity, ft/sec	Initial incidence, deg	Site slope, deg
−18	0	0	−15
−19	0	16	0
−20	0	−10	−15
−20	0	0	0

The study utilized a mathematical model based on the modal data corresponding to the S-2 vehicle (i.e., the mast was at Station $x = +6.0$ in., $y = 0$ in.). Calculations are being carried out to analytically alter this model to correspond to the S-2A vehicle configuration. On completion of this alteration, the study outlined above will be conducted to determine actual S-2A vehicle maximum-load drop test conditions. Still another model using data from the forthcoming T-2A spacecraft modal survey will be used for analysis of the drop test data.

2. Dynamic Analyses

The theoretical elastic properties of the antenna/solar panel positioner (A/SPP) mast and the upper and lower tripod supports were determined for use in dynamic analyses of the A/SPP. The elastic properties of the

UNCLASSIFIED
CONFIDENTIAL

UNCLASSIFIED
CONFIDENTIAL

Table 11. Elastic properties of A/SPP in boost configuration

Mast stiffness	
Top of mast (z = 128.5)	4.55×10^6 in.^{2}-lb
Upper support	15.20×10^6 in.^{2}-lb
Lower support	4.85×10^6 in.^{2}-lb
Springs of upper tripod support of mast	
Lateral translational spring	115,000 lb/in.
Rotational spring	4160 in.-lb/deg
Spring of lower tripod support of mast	
Lateral translational spring	42,100 lb/in.
Rotational spring between mast and planar array	1730 in.-lb/deg

mast and tripod supports are listed in Table 11 for the model of the A/SPP for vibration normal to the centerline of Leg 3. The elastic properties of the mast and tripod supports result in influence coefficients at the top of the mast ($z = 128.5$) given by the matrix equation:

$$\begin{bmatrix} \delta \\ \alpha \end{bmatrix} = 10^{-6} \begin{bmatrix} 1581 & 69 \\ 69 & 4.26 \end{bmatrix} \begin{bmatrix} P \\ M \end{bmatrix}$$

where:

P = lateral force at top of mast, lb

M = moment at top of mast, in.-lb

δ = displacement at top of mast, in.

α = rotation at top of mast, rad

The above influence coefficients for the mast are applicable to landing configurations of the A/SPP as well as to the boost configuration shown in Fig. 42.

The model of the A/SPP shown in Fig. 42 applies to the S-2A vibration test which resulted in the failure of the elevation motor housing. As reported previously in *SPS 37-30*, Vol. I, the failure occurred at a frequency of 9.6 cps at which time the planar array and the solar panel were acting as a single rigid body. Test data taken previous to the failure determined the rotational spring between the top of the mast and the planar array (Table 11).

The model shown in Fig. 42 provides data for a dynamic analysis of the A/SPP with three degrees of freedom:

ξ_1 = lateral translation of planar array and solar panel, inches

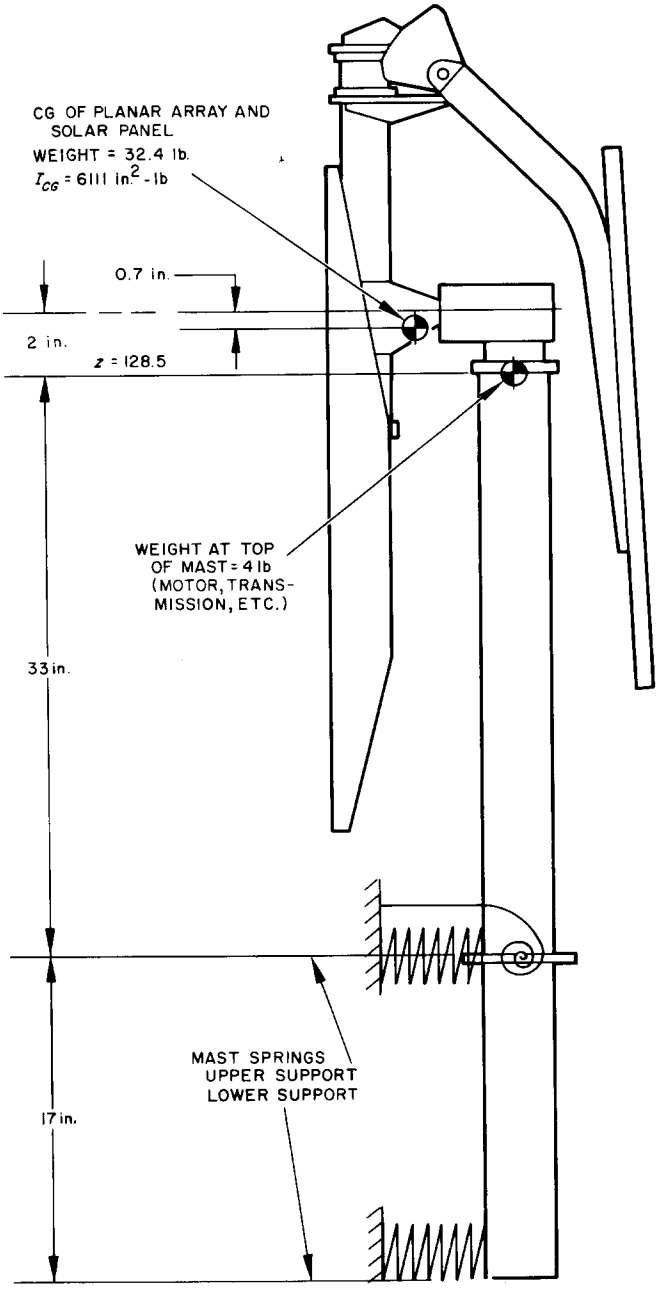

Fig. 42. Mass properties of A/SPP in boost configuration

ξ_2 = rotation of planar array and solar panel, radians

ξ_3 = lateral translation of mass at top (z = 128.5) of mast, inches

For these three degrees of freedom, the influence coefficient matrix obtained from the data of Fig. 42 is:

$$C = \begin{bmatrix} 1765 & 67 & 1667 \\ 67 & 14 & 69 \\ 1667 & 69 & 1581 \end{bmatrix} \times 10^{-6}$$

UNCLASSIFIED
CONFIDENTIAL

UNCLASSIFIED
CONFIDENTIAL

where the influence coefficient matrix is for the three coordinates in the order ξ_1, ξ_2, ξ_3.

The influence coefficient matrix together with the mass properties of Fig. 42 result in the fundamental frequency of 9.5 cps, which agrees with the frequency at which the elevation motor housing failed in the vibration test. The theoretically-obtained mode shape compares well with the mode shape observed in the vibration test and shows that the translation and the rotation of the A/SPP are "in phase" (translational and rotational displacements in the direction resulting from a lateral force acting at the solar panel positioner). The second resonant frequency obtained from the model is at 16 cps and for this resonance the translation and rotation of the A/SPP are "out of phase."

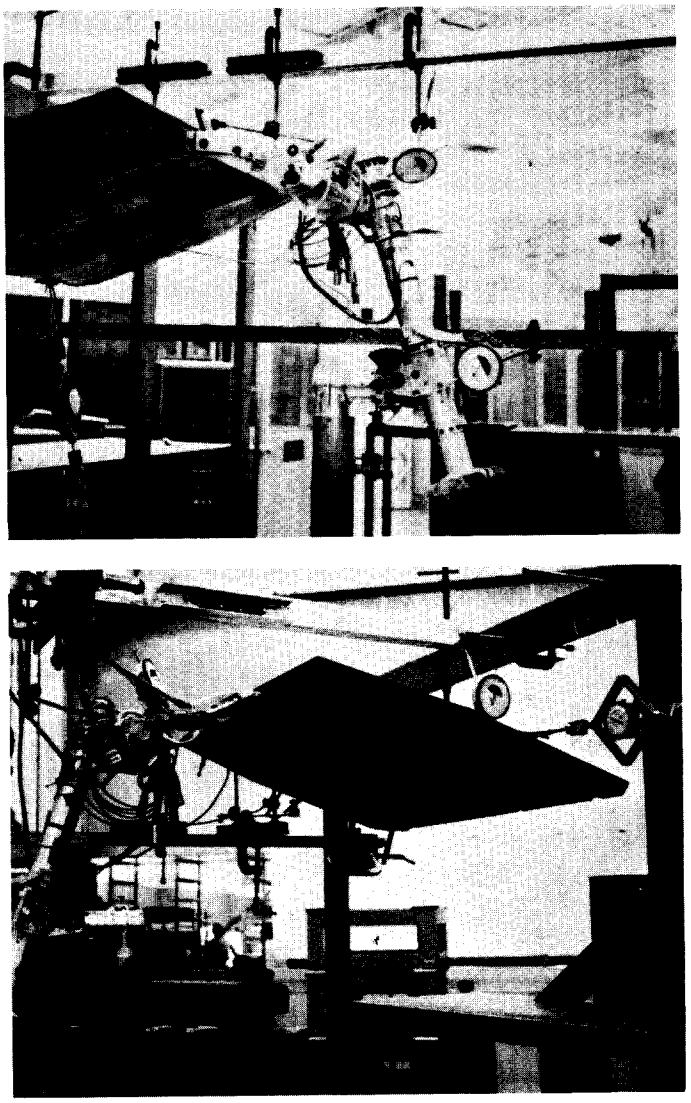

Fig. 43. Test setup for measuring A/SPP displacements (loading Conditions 3 and 4)

Static tests were made to determine the elastic properties of the A/SPP in an extreme position of the landing configuration. In this extreme position, the mast is vertical, the solar panel is 18-deg down from horizontal, and the planar array post is at 18-deg to the mast. Four loading conditions were used: (1) load at top of planar array post, normal to plane of planar array, (2) load at top of planar array post, parallel to plane of planar array, (3) load on solar panel, normal to panel, and (4) lateral load on solar panel, in plane of panel.

Displacements of the A/SPP were measured by nine dial gages (1-in. stroke). Loads were applied in ten increments up and ten increments down and good linearity was exhibited. Fig. 43 shows the test setup for loading Conditions 3 and 4, in which the planar array is removed for accessibility.

Springs for the A/SPP model obtained by data reduction together with theoretical analyses are listed in Table 12. These data have been used in a dynamic model of the A/SPP which results in a low frequency solar panel mode (motion parallel to the plane of the panel) of 6 cps.

Table 12. Elastic properties of A/SPP in landing configuration

Mast torsional spring	3930 in.-lb/deg
Motor housing torsional spring	1295 in.-lb/deg
Motor housing bending spring[a] (bending about horizontal neutral axis)	1425 in.-lb/deg
Torsional spring of planar array post	2400 in.-lb/deg
Bending spring at yoke attachment to solar panel positioner (for bending due to lateral force acting in plane of solar panel)	3620 in.-lb/deg
Lateral translational spring of solar panel arms (due to Vierendeel action of arms caused by lateral force acting in plane of solar panel)	298 lb/in.
Bending spring of solar panel arms for force acting normal to plane of panel	1260 in.-lb/deg

[a]Motor housing bending spring is for the relative rotation between the top of the mast and the planar array and includes the effects of the elevation mechanism (gear tooth bending, etc.). It is evident that this spring may be affected by the elevation of the planar array. The spring of 1425 in.-lb/deg was obtained by static test in the landing configuration. Table 11 shows the spring of 1730 in.-lb/deg determined by data obtained from the vibration test in the boost configuration.

CONFIDENTIAL
UNCLASSIFIED

UNCLASSIFIED
CONFIDENTIAL

This dynamic model is "base-fixed" at the upper three corners of the spaceframe. For the A/SPP on the "free-free" test vehicle the resonant frequency will be slightly greater than 6 cps, and it is expected that this low frequency mode will be of prime importance in a lunar landing with the centerline of Leg 1 downhill.

The data of Table 12 will be incorporated in a free-free model of the spacecraft for a study of the dynamics of lunar landing conditions. This study will arrive at test conditions to be used in the S-2A spacecraft drop test.

3. Dynamic Tests

a. S-2A spacecraft A/SPP motion attenuation study. Following the failure of the A/SPP elevator motor housing during type-approval testing, a series of vibration tests was conducted to evaluate various devices designed to restrict the motion of the A/SPP in the 9- to 11-cps frequency range.

Initially, damping strips (aluminum strips clamped between teflon sleeves), were evaluated at ¼- and ½-*g* input levels using various clamping pressures. This configuration yielded a maximum reduction in solar panel motion of 34%. The mast dampers were then wrapped with Mylar tape. The reduction of the panel motion attributed to the tape wrapping was negligible. A small impact damper (steel ball in tube) was then attached to the solar panel. This device also proved ineffective as a motion attenuator.

A second series of A/SPP motion limiting tests was performed at ¼-, ½-, ⅞-, and 1¼-*g* input with braces on the solar panel and the planar array. This configuration was evaluated, with varying clearances between braces and panels, and with rubber impact pads of 40 and 70 durometer hardness. The maximum solar panel motion reduction resulting from the panel braces was 91%.

The third series of A/SPP motion limiting tests was conducted with a ½-*g* input parallel to Leg 3 with the solar panel braced snugly against the rubber support pads, and the planar array braces removed. These test results showed an 83% motion reduction.

Finally, the solar panel brace and pods were removed and replaced with an aluminum tube wrapped around the mast with the ends protruding into the solar panel. This device gave a motion reduction of 89% for ½-*g* inputs parallel to Leg 3. Tests conducted normal to the Leg-3 axis with a ¾-*g* input showed negligible solar panel displacement and a maximum bending stress on the motor housing (original design) of 35K psi.

It was concluded that adequate restriction of the A/SPP motion can be achieved by using a modification of the motion limiting rods used in the final test. The flight design to satisfy this concept as used during structural approval testing is shown in Fig. 44.

b. S-2A spacecraft structural approval testing. Prior to conducting a low-frequency dynamic clearance investigation at B levels and structural approval tests at C levels, the following changes were made to the spacecraft: (1) installation of the redesigned A/SPP elevation axis motor housing, (2) addition of active solar cells (6 cells high × 4 cells wide) to the solar panel in the areas of impacting by motion limiting rods, (3) installation of teflon-tipped motion limiting rods and tip sockets, (4) installation of stray energy monitoring devices at A/SPP pin pullers, and (5) addition of electrical contacting monitoring circuits on thermal switches.

Table 13 summarized the type-approval tests in the order in which they were performed. Extensive mast and A/SPP instrumentation was recorded for Tests 18

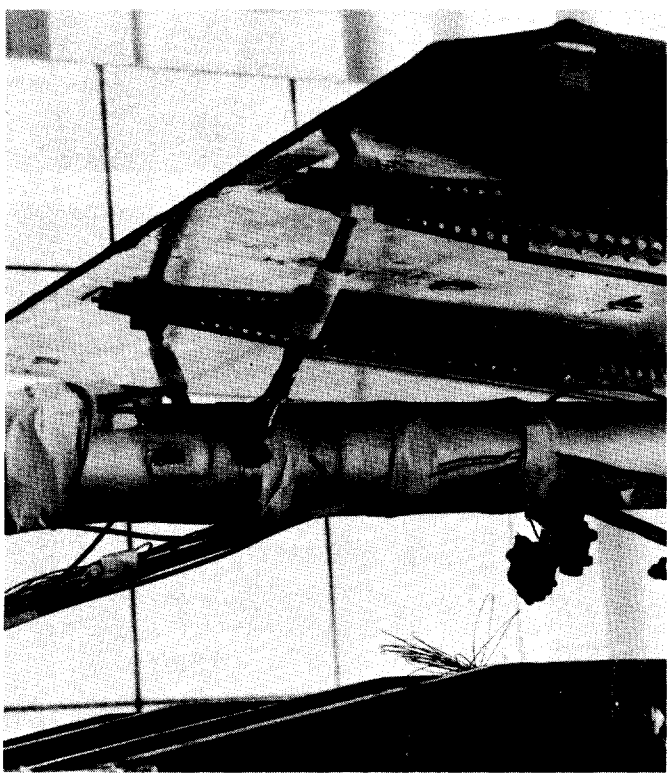

Fig. 44. A/SPP motion limiting rod flight design

CONFIDENTIAL
UNCLASSIFIED

UNCLASSIFIED
CONFIDENTIAL

Table 13. S-2A spacecraft type-approval test summary

Test no.	Test level[a]	Frequency range, cps	Remarks
18	B	5 to 15	Lateral input parallel to panels; maximum solar panel motion is less than 1-in. double amplitude
19	C	5 to 1500	Lateral input parallel to panels; test interrupted due to a 300% over-test at 26 cps resulting in failure of retrorocket support brackets; test resumed at 24 cps after replacing brackets
20	B	5 to 15	Lateral input perpendicular to panels; maximum solar panel motion is less than 1 in.
21	C	5 to 1500	Lateral input perpendicular to panels
22	B	5 to 50	Longitudinal input along roll axis
23	C	5 to 1500	Longitudinal input along roll axis

[a]Reference Revision 1 to JPL Specification 30240 D.

through 23. Complete instrumentation for Compartments A and B were recorded for Tests 22 and 23. During Test 18 the maximum excursion of the solar panel was less than 1 in. The maximum allowable movement of the panel in the direction of test is 1.2 in.

Lateral vibration Tests 18 through 21 were successfully completed with 6 lb of preload on each solar panel motion limiting rod. During Test 22, however, both rods disengaged from the tip sockets and the test was interrupted at 42 cps. The preloads were increased to 20 lb on each rod and the B-level acceleration again applied, sweeping from 50 to 42 cps.

During Test 23 the rods again disengaged in the 40-cps region. It was discovered that the strap that attaches the rods to the mast had loosened, permitting rotation of the complete assembly about the mast. After tightening the strap the C-level testing was continued, first sweeping from 50 to 100 cps, then from 50 to 40 cps. No further malfunctions were noted. The completion of Test 23 concludes the structural approval testing of the S-2A spacecraft.

c. Retrorocket vibration measurements. An analysis was made of the dynamic force components of two of the retro-engines fired at Arnold Engineering Development Center (AEDC), Tullahoma, Tennessee.

Results of the analyses for the A-21-17 and A-21-24 engines will be published shortly and will include: (1) power spectral density plots (PSD) of the quiet portions of the firings for comparison with PSD's of the prior-to-firing condition, (2) probability densities of the existing random forces, and (3) shock spectrum analyses of the observed transient phenomena.

As originally suspected, the levels of the sustained random forces are negligible (Fig. 45). The peaks shown at approximately 40 and 120 cps can be attributed to AEDC test stand frequencies, while the remaining peaks have little contained energy due to their narrow bandwidths. Conservatively assuming that the two peaks at 72 and 86 cps are in reality one peak (broader resonance) and that the half-power points are located at 0.10 lb^2/cps, the total rms force is $\leq$ 2 lb.

Fig. 46 shows a shock spectrum analysis of one of the typical force transients recorded during the A-21-24 engine firing. The test stand frequencies of approximately 36 to 40 cps and 120 to 130 cps are clearly evident. The energies contained in frequencies other than these are

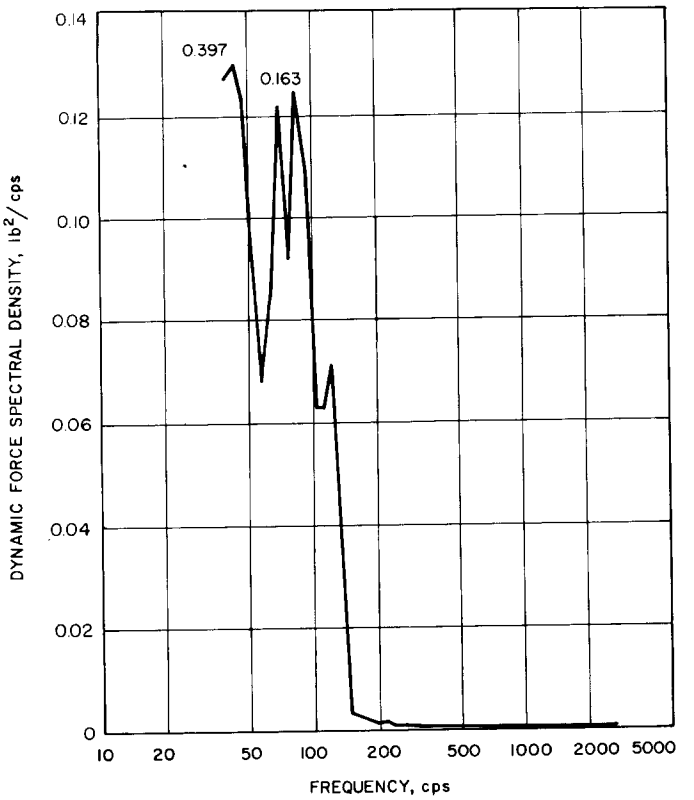

Fig. 45. Sustained random force levels in A-21-17 engine firing

CONFIDENTIAL
UNCLASSIFIED

UNCLASSIFIED
CONFIDENTIAL

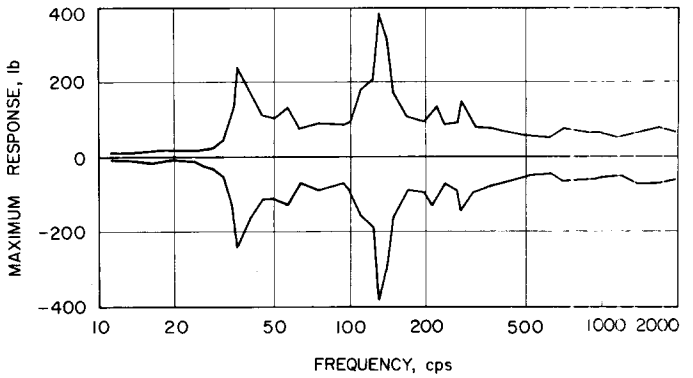

Fig. 46. A-21-24 firing shock spectrum analysis

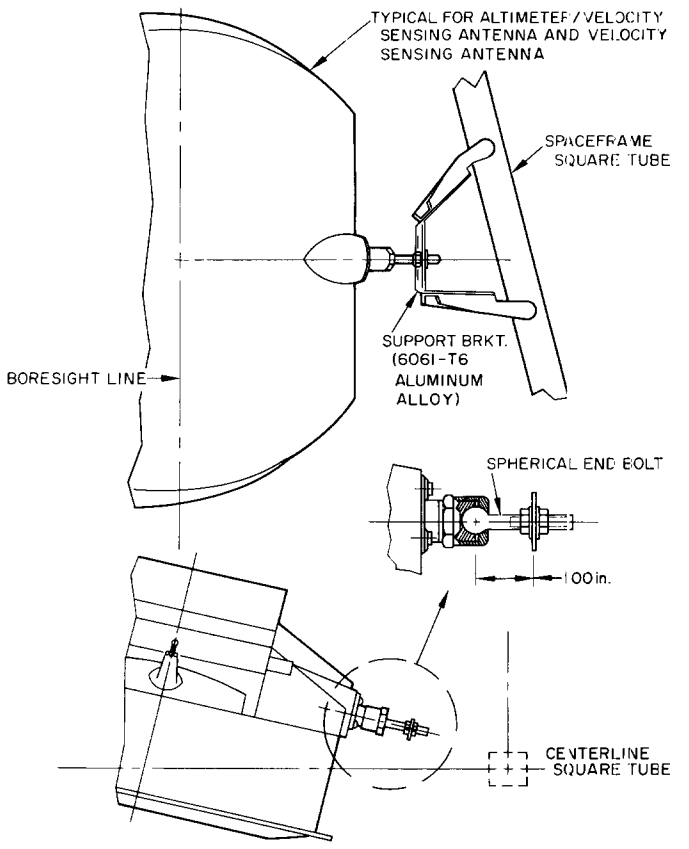

Fig. 47. RADVS antennas inboard support

considered negligible from a structural standpoint when compared to the random force spectrum applied during flight acceptance or type-approval vibration levels related to *Atlas–Centaur* powered flight. A check on functional performance may be required, however, when the spacecraft is subjected to these transients.

A series of tests is being conducted on the S-2A spacecraft to determine the response of the structure to these transient forces. The spacecraft is mounted on the longitudinal vibration fixture via the three piezo-electric force gages through which the retro-engines at AEDC were fired. The AEDC force responses as recorded on tape are being used to excite the electrodynamic vibrator, which in turn pulses the spacecraft. The responses at "critical" locations, such as omnidirectional antennas, radar altimeter and doppler velocity sensor, flight control sensor group and planar array, are being monitored to determine the severity of the effect. In addition, modified tapes (AEDC data minus the test stand frequencies) and special taped pulses (half sinusoids and triangular functions) are being used to excite the spacecraft so that a comprehensive range of pulse shapes may be used.

The intent here is not to duplicate the environment at AEDC, but to examine the responses to each of the pulses for comparison with each other and with the results of other tests: e.g., powered flight vibration, drop tests, etc. If necessary, the results will be used in an attempt to analyze the free-free behavior of the spacecraft/retro-engine to such force transients. Further data reduction is being performed on "twang" tests conducted on the firing stand at AEDC and on the side force and turning moment effects of the force transients.

4. Structural Analysis

a. Proof test of frangible RADVS spaceframe attachment. The lowest point of both of the radar altimeter and doppler velocity sensor (RADVS) antennas falls below the lower edge of the lower spaceframe square tube by the amounts shown in Fig. 47. These low points, which are in the vicinity of the inboard structural supports for both antennas, also fall within the envelope of a 10-cm protuberance when the maximum landing gear deflections occur.

To minimize damage during landing to the lower surfaces of Compartments A and B (which are located directly above the altimeter and velocity antennas), an elastic support structure was incorporated at the inboard edge of each antenna. The design of this support is based on the requirement that the supports remain rigid during boost and retro deceleration loading conditions, but allow large vertical deflections without suffering catastrophic failure if the antenna strikes the lunar surface during landing (Fig. 47).

The ball socket joint shown is designed to break static friction at a 75 in.-lb applied moment. After rotation of the ball joint begins, the center section of the support

CONFIDENTIAL
UNCLASSIFIED

CONFIDENTIAL
UNCLASSIFIED

bracket will undergo elastic torsional deformation and finally large bending deformations as the antenna rotates upward about the axis of the two outboard supports.

Static loads were applied to three test specimens (see test arrangement shown in Fig. 48). The test specimens were assembled with production hardware and the ball joints were torqued to the required value. Loads were applied in three directions to evaluate possible directional characteristics. A dial gage was employed to indicate the threshold of joint slip. The test results gave a maximum range of breakaway load magnitude varying from 60 to 80 lb. These values are considered to be satisfactorily close to the design requirement. However, additional tests are planned which will include temperature extremes.

b. Proof test of upper cluster (T-2SS spaceframe). Extensive redesign has been incorporated in the T-2SS spaceframe and parachute harness as a result of changes in the parachute deployment mechanism and a need for weight reduction. Since the early drop tests of the T-2 vehicle, including actual parachute deployments, the vehicle weight has increased from 165 to approximately 210 lb. After considering these two facts, structural verification tests of the upper main spaceframe cluster and parachute attachment were performed for the increased load magnitude.

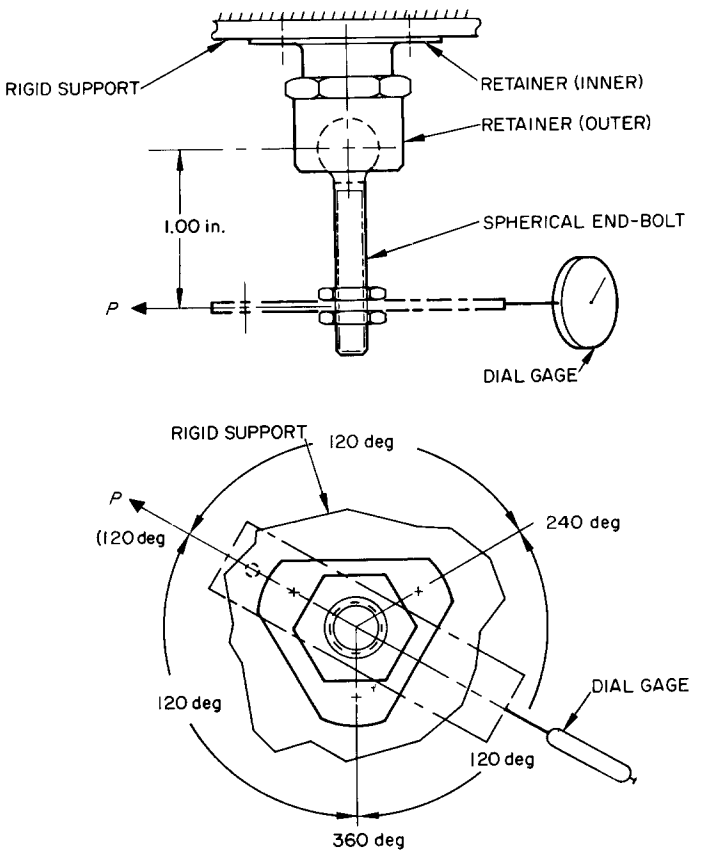

Fig. 48. RADVS antennas support bracket test arrangement

Loads were applied to the test specimen in three directions (Fig. 49). The test specimen was rigidly attached at the base to laboratory structure and impact loads were applied to the end of the parachute cord (Fig. 50). The rate of loading shown in Fig. 51 was based on accelerometer data obtained during actual parachute deployment drop tests of model T-2. The design requirement was the application of 2000-lb peak load as a half sine wave in a time of 0.10 sec.

The desired rate of loading during the tests was obtained experimentally by adjusting the drop weight and height and by monitoring the load cell mounted in series (Fig. 50). The peak load magnitude and number of load repetitions applied in each loading direction are outlined in Table 14. The rate of loading curve shown in Fig. 51 is a trace of the load cell reading taken during a typical test. The 2000-lb peak load corresponds to an acceleration of approximately 9 *g* (ultimate) acting on the vehicle at the time of parachute deployment.

Table 14. Parachute cord dynamic load schedule

Load direction (Fig. 49)	Load magnitude P, lb	Repetitions
Position 1	2000	30
Position 2	2000	30
Position 3	2000	30
Position 1	2500	1
Position 2	2500	1

All metal parts were inspected for permanent damage following each test phase and found to be satisfactory. The parachute cords became frayed and four cords failed during the repeated load tests. A cord with a rating of 3000 lb was used to complete the impact tests. However, since the peak load used is the maximum (ultimate load) predicted for the spaceframe and is far too severe for the actual cord, no design change was made. An inspection should be performed after each T-2SS drop test for evidence of cord fraying.

CONFIDENTIAL
UNCLASSIFIED

UNCLASSIFIED
CONFIDENTIAL

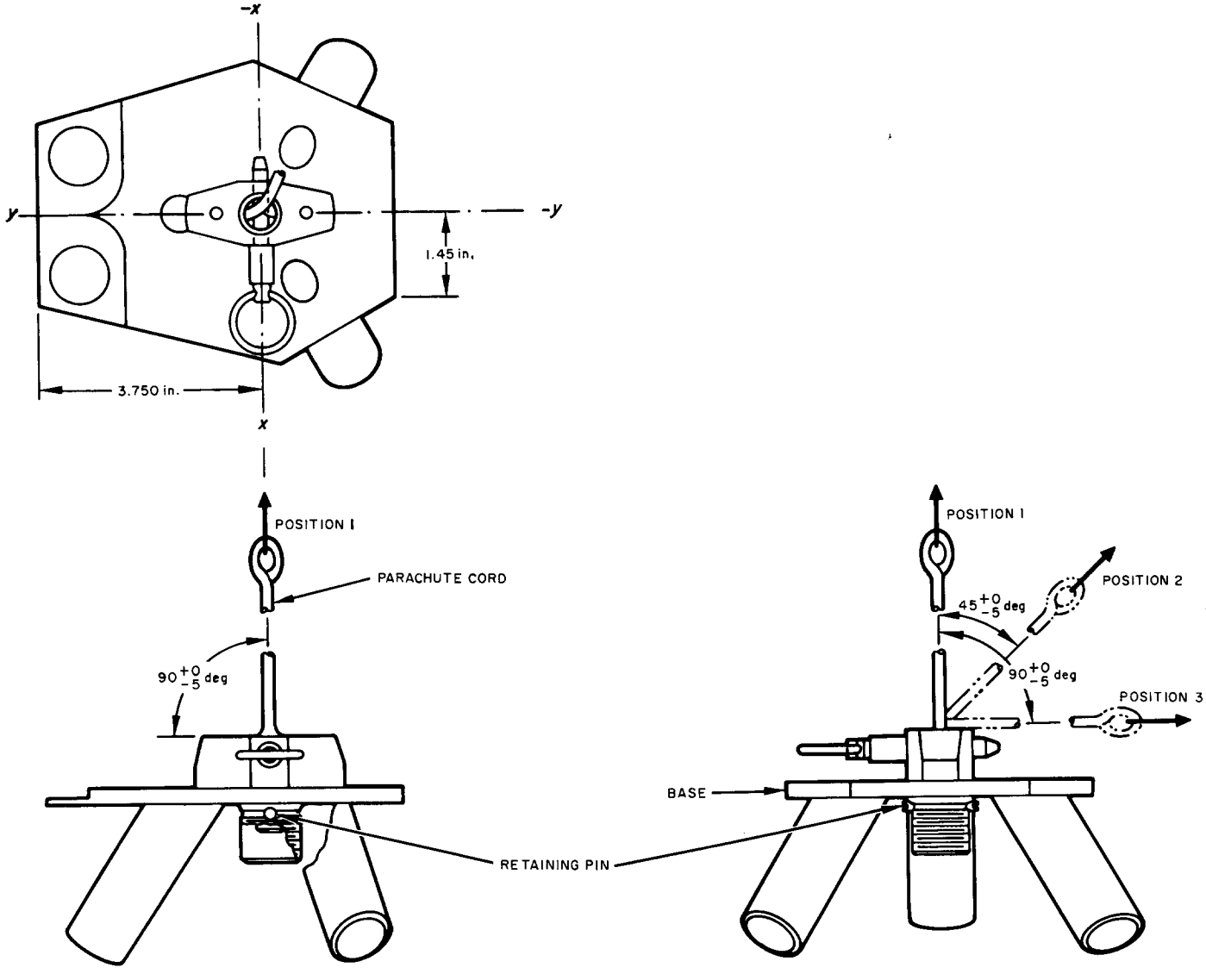

Fig. 49. Upper main spaceframe cluster and parachute attachment test arrangement

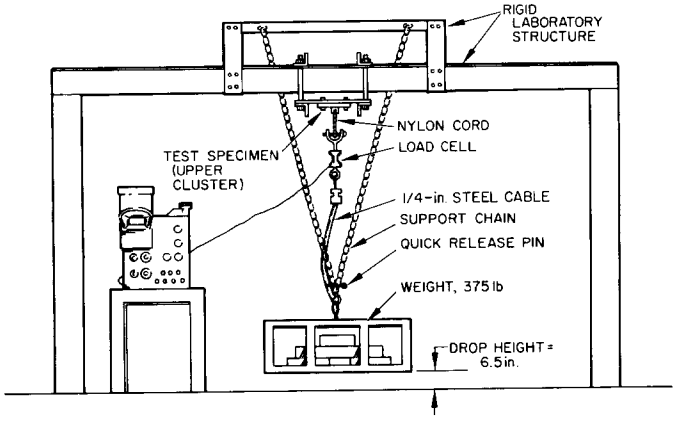

Fig. 50. Method of application of dynamic loads (Position 1)

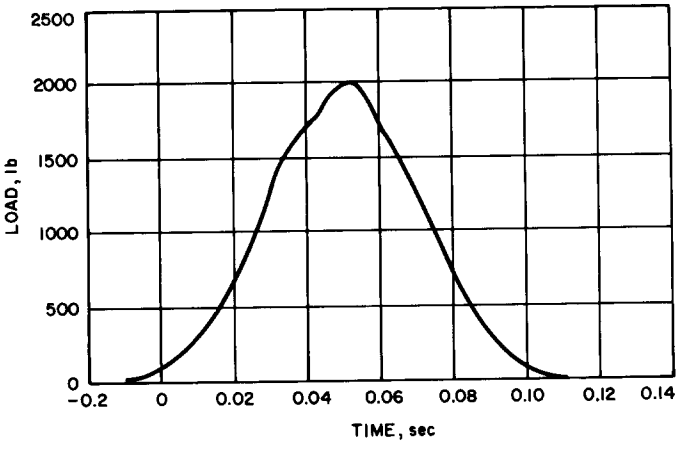

Fig. 51. Parachute cord rate of loading

CONFIDENTIAL
UNCLASSIFIED

UNCLASSIFIED

Additional repetitive static load tests at limit load are currently being performed to ascertain if fraying and breakage of the parachute cord under repeated loading is a problem.

G. Propulsion

1. Main Retrorocket Engine

a. Quality-assurance test program. The final ballistic and thrust vector excursion data have been received from the Arnold Engineering Development Center for the four quality-assurance engines tested there. Thrust, side force, and thrust vector excursion angle data for these engines are presented in Fig. 52. An error analysis for the test series has also been completed. Further analysis of the data, including simulation of the instantaneous side force data for the analog flight control model, correlation with the vibration data obtained at the engine attachments, and a statistical analysis of the vector excursion data will be completed. The data analysis performed to date indicates that the retrorocket engine meets all of the system performance parameters.

b. Vibration testing. Because an attachment fitting failure occurred during previous vibration testing of Engine A21-19, the attachment fittings were modified to eliminate the notch effect of the uncontrolled radius and the roll pin was replaced with a solid hinge pin. The attachment modification was thoroughly evaluated by subjecting inert Engine A21-F to additional vibration tests. Engine A21-F was first subjected to the quality-assurance vibration test levels, where the maximum response of the engine center-of-gravity was limited to 5 *g*. A safety margin test was then performed with the response limitation removed and the full specification input applied, corresponding to the level initially imposed on Engine A21-19. Vibration testing of quality-assurance Engines A21-19 and A21-22 was initiated. Following the vibration testing, the engines will be subjected to humidity and drop testing prior to firing at the Elkton Division of Thiokol Chemical Corporation. The attachment fittings of inert Engine A21-B failed during vibration testing of the S-2 vehicle at Hughes Aircraft Company (HAC) due to excessive input levels used during the test. After being repaired, the engine successfully completed the S-2 vibration test program.

c. Safe-and-arm assembly. Quality-assurance testing at the component level was completed on the safe-and-arm assembly. Hi-Shear Corporation delivered all flight units of the PC-37 squib after the successful completion of the squib test program. Assembly of flight safe-and-arm assembly units has begun at the Thiokol Bristol Division. Further quality-assurance testing of the safe-and-arm assembly will be conducted during the remaining rocket engine tests.

d. Performance prediction. To demonstrate compliance with the spacecraft requirement for prediction of the engine operating time to within $\pm 1\%$, Hughes Aircraft Company (HAC) and Thiokol Elkton Division developed an empirical prediction technique based on the ballistic parameters measured during the development and qualification test programs. The empirical relationship has been used to predict t_{3500} (time from ignition signal to 3500 lb of thrust during tailoff) for Engines A21-11, -12, -17, -18, -23, and -24 at a constant temperature of 50°F, and for Engines A21-7, -8, and -14 at the thermal gradient condition. The results are given in Table 15. The probability is at least 0.914 that future predictions made on an identical population will be within 1% of the actual value to a 90% confidence level.

Table 15. Comparison of predicted and measured t_{3500} values

Engine	Test condition	t_{3500}, sec		Error sec
		Predicted	Measured	
A21-11	Constant 50°F	38.17	38.22	−0.05
A21-12	Constant 50°F	38.38	38.37	0.01
A21-17	Constant 50°F	38.84	38.78	0.06
A21-18	Constant 50°F	39.08	38.88	0.20
A21-23	Constant 50°F	39.30	39.39	−0.09
A21-24	Constant 50°F	38.72	38.61	0.11
A21-7	Thermal gradient	39.99	40.25	−0.26
A21-8	Thermal gradient	39.09	39.15	−0.06
A21-14	Thermal gradient	39.82	39.80	0.02

2. Vernier Propulsion System

a. System development. The first S-6 expulsion unbalance test, S-6-1, using actual propellants was conducted at the Air Force Missile Development Center (AFMDC).

UNCLASSIFIED

UNCLASSIFIED
CONFIDENTIAL

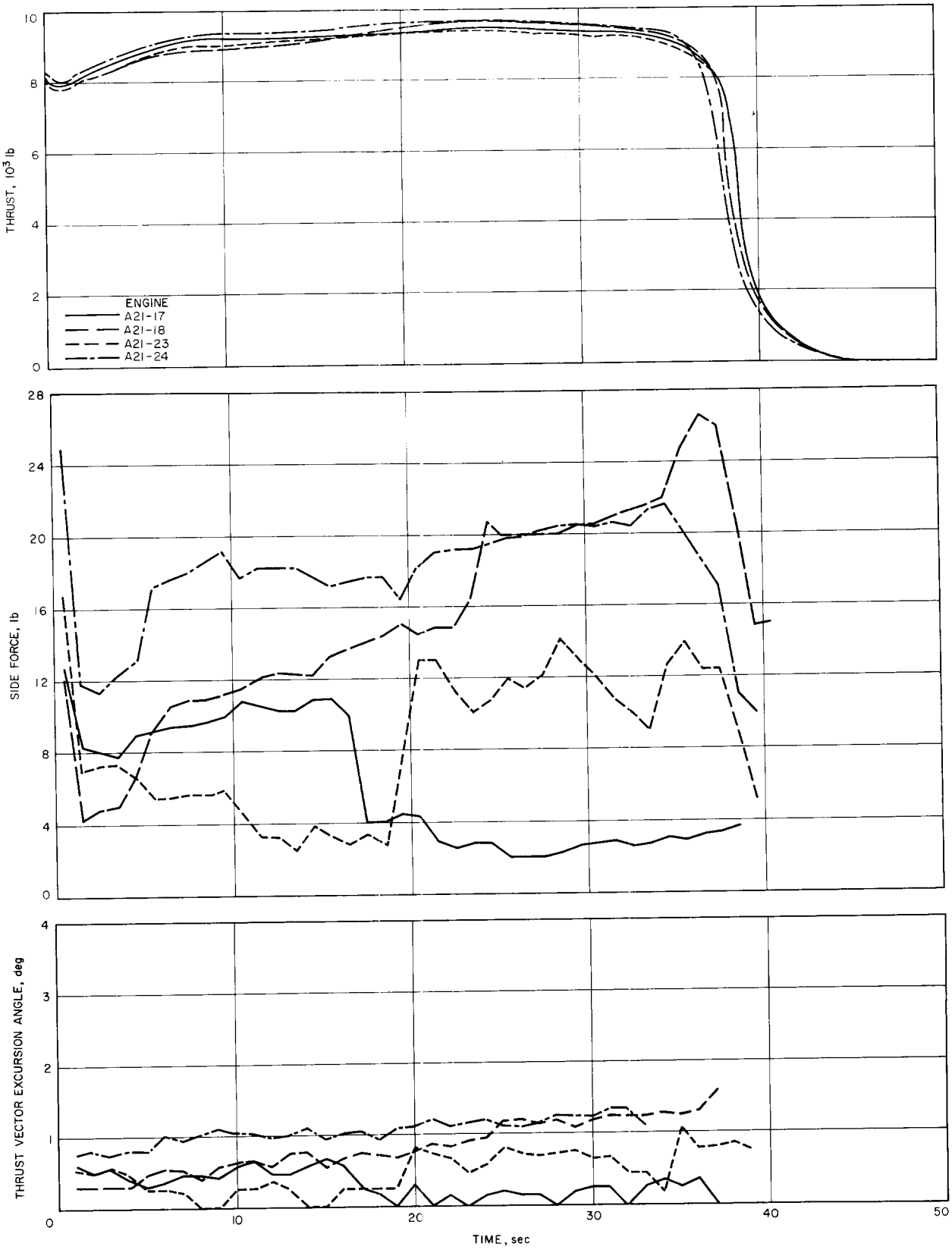

Fig. 52. Thrust, side force, and thrust vector excursion angle as functions of time

UNCLASSIFIED
CONFIDENTIAL

UNCLASSIFIED
CONFIDENTIAL

This test was a measure of the propellant unbalance resulting from equal engine demands with all vehicle legs at ambient temperature conditions. The second test, S-6-2, was conducted with unequal engine demands and with all vehicle legs at ambient temperature. Following this test, all propellant tanks were removed from the vehicle, and tanks modified by the removal of the interior bead on the girth weld were installed.

The data from Test S-6-2, from Tests S-6-X, S-6-XB, and S-6-1 (conducted during previous reporting periods), and from special static loading tests were reviewed. It was concluded that no valid unbalance data were obtained due to inadequacies in the suspension system and load cells. After an evaluation of the existing load cells, it was decided to obtain new cells from the Baldwin-Lima-Hamilton Corporation. The S-6 suspension system was replaced with one of a different design. The main features of the new design are low linear deflection under tensile load and compliance to nontension loads.

The S-7 storage test was initiated. Propellant loading was normal in all respects, with the exception of an oxidizer tank bleed quick-disconnect which hung open during loading. The decision was made to rely on the quick-disconnect cap secondary seal and proceed with the test. Tank ullage samples were taken periodically over the next 30 hr. These samples, analyzed at the AFMDC chemical laboratory, indicated a transfer of propellant vapor into the gas ullages of both propellant systems.

Some external leaks were experienced during the early portion of the test, as evidenced by a slight (5 to 10 psi/hr) pressure decay in both the oxidizer and fuel ullages. This problem was corrected by the addition of helium K-bottles to increase the ullage volumes and decrease the pressure decay rate.

The first firing of the S-7 system was normal in all respects, but moderate unprogrammed thrust changes were experienced during the second and third firings. After the first and second firings, the engines were found to leak at the oxidizer inboard bellows seal and were returned to HAC to be rebuilt. On the completion of the third firing, the vehicle was defueled, decontaminated, and returned to HAC. The unprogrammed thrust changes encountered in the last two firings are under investigation.

On arrival at HAC, the propulsion hardware was inspected, and no major effects of propellant storage were observed. Some minor residue traces were found and removed for analysis. The S-7 vehicle is currently being upgraded.

The gas entrapment device was used successfully in the last T-2 and S-6 tests at AFMDC. The gas entrapment was very small, indicating satisfactory filling of the systems.

b. Component development

Relief valve. Two relief valves utilizing an elastomeric piston seal were fabricated by the vendor and subjected to functional tests at ambient conditions, as well as at 65°F. At ambient conditions using air as the test fluid, the valve functioned within specification limits and had a differential pressure between crack and reseat of 10 psi. At the low-temperature conditions, the differential pressure range between crack and reseat was 50 to 80 psi; the specification requirement on differential pressure spread is 40 psi maximum. The factors which contributed to this increased spread are as follows: (1) greater seal compression because the difference in thermal coefficients of the stainless-steel piston and the aluminum valve body results in a higher frictional drag force; and (2) increased viscosity of the seal lubricant causing a higher frictional drag force.

Recent HAC experience demonstrates that the seal compound deteriorates rapidly in the presence of NO_2 oxidizer vapors. The vendor was requested to conduct development tests utilizing Teflon U-cup-type seals. The piston of one of the development relief valves was modified to accept the Teflon seals, and functional tests were conducted at ambient conditions with Teflon seals manufactured by three different companies, again using air as the test fluid. Because of excessive differential pressure spread at ambient conditions, two of the three types of seals were eliminated from testing at low temperature. The third type exhibited excessive leakage at the low-temperature conditions, but examination of the parts after disassembly revealed scoring of the piston bore. Efforts are now being directed toward developing the optimum seal groove and piston bore configuration to permit usage of the Teflon seal to eliminate the propellant vapor compatibility problem and the need for a seal lubricant.

Pressure regulator. Fabrication of the test hardware to investigate various seal configurations was completed. High- and low-temperature tests with varying compressive loadings were begun.

CONFIDENTIAL
UNCLASSIFIED

UNCLASSIFIED
CONFIDENTIAL

Review and analysis of the data obtained during regulator testing indicated that 90% of the units tested do not meet specification requirements for regulated pressure over the range of flow rates and inlet pressures experienced by the assembly. A composite of the test data acquired by HAC during the regulator testing is shown in Fig. 53. To rectify this problem, a program has been instituted to improve the regulator droop characteristics by increasing the sensing area and modifying the spring characteristics.

Quick disconnect. A coupler assembly utilizing an omniseal was subjected to cycling tests after propellant exposure testing. The unit that had been cycled 200 times prior to propellant testing completed an additional 500 cycles without evidence of leakage.

Helium squib valve. During low-temperature type-approval testing of the helium release–dump valve, the Phase II (dump) squib failed to ignite after the Phase I (release) squib function. Investigation of the failure disclosed that the ceramic cup had broken its bond and moved a distance sufficient to break the bridge wires. The following corrective modifications were incorporated: (1) increase of the bonding surface on the cup, (2) swaging of an aluminum ring onto the cup to provide a positive mechanical retainment, and (3) shortening of

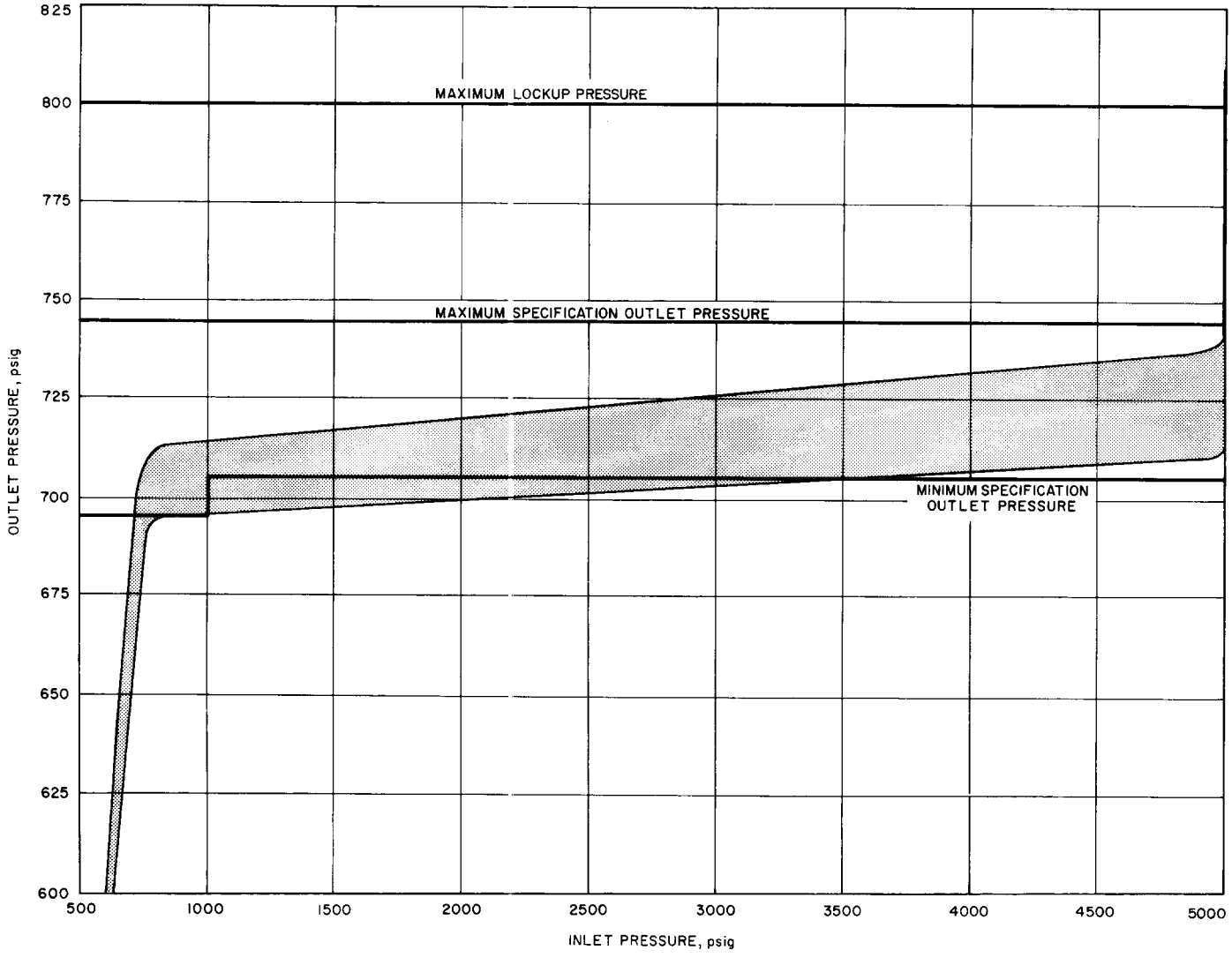

Fig. 53. Pressure regulator performance envelope

UNCLASSIFIED
CONFIDENTIAL

UNCLASSIFIED
CONFIDENTIAL

the release piston length in the valve to reduce the shock of the piston striking the valve body. Verification tests were performed to determine the level of shock produced by the release squib and the adequacy of the modifications. Fabrication of a new lot of squibs of the modified design is in process, and preparations are being made to repeat the type-approval tests.

Material tests. A test is in progress at the Placerita Canyon, California, Test Site to determine the effects of helium pressure on the permeability of Teflon propellant bladder material to MON-10 oxidizer[5]. Preliminary results of runs carried out with helium pressures between 100 and 400 psi indicate that a permeation rate of about 0.2 mg MON-10/hr/cm^2 of bladder material is obtained with a helium pressure of 200 psi. This value is comparable to the value of 1.22 mg N_2O_4/hr/in.^{2} obtained for a similar Teflon material at JPL.

Further tests of Parker Viton A O-rings exposed to liquid MON-10, a Freon TF flush, and vacuum drying showed that the temperature at which vacuum drying is carried out has little effect on the degree of permanent set experienced by the Viton O-rings. It is, therefore, tentatively concluded that the exposure of the O-rings to MON-10 is responsible for the observed deformation of the oxidizer O-rings and that the flushing and vacuum drying procedures presently employed for cleanup of hardware exposed to MON-10 are satisfactory.

An exposure of aluminum tubing samples with various surface treatments to the vernier propellants was completed. Samples of 5052-0 aluminum tubing were prepared with chromate coatings, sulfuric-acid anodized coatings, electroless nickel coatings, and bare passivated aluminum surfaces. The results of this test indicate that electroless nickel is the only coating tested which effectively resists the action of dry propellants; however, some pitting occurs in the nickel coating in moist propellants. The chromate and sulfuric-acid anodized coatings frequently showed considerable degradation. None of the coatings tested appear to offer any significant advantage over bare passivated aluminum for surfaces exposed to MON-10, monomethylhydrazine, or monomethylhydrazine hydrate.

c. Tank development

Propellant tanks. The 6 Al–4 V titanium propellant tank program, subcontracted to Airtek Dynamics, Inc., is progressing satisfactorily. The porosity problem has been solved, and tank deliveries should be completed in the near future. All required type-approval testing has been successfully completed.

In accordance with HAC specifications, bulk yield and burst tests are performed on an initial three tanks and an additional tank selected at random from each production lot of ten. The two tanks selected burst at 1400 and 1370 psig, respectively—well above the acceptable limit.

Helium tank. The 6 Al–4 V titanium helium tank program, subcontracted to Airtek Dynamics, Inc., is also progressing satisfactorily. All forgings are available and completely machined. Several tanks have been welded with no evidence of porosity. Initial bulk yield and burst tests have been successfully completed.

3. Thrust Chamber Assemblies[6]

a. RMD thrust chamber assembly. The *Surveyor* thrust chamber assemblies (TCAs) are being provided to Hughes Aircraft Company (HAC) by JPL. Since the last report (*SPS, 37-29*, Vol. I), the Reaction Motors Division (RMD) of the Thiokol Chemical Corporation was placed under contract by JPL for the development of the *Surveyor* TCA, including prequalification testing. RMD was also authorized to release material procurement and subcontracting in support of hardware procurement for qualification testing and for the first four *Surveyor* flights. Contract negotiations are in progress for the remainder of the program, including deliveries of flight engines for the four flights.

A design review of the RMD *Surveyor* TCA, designated TD-339, was conducted by JPL at the RMD Denville, New Jersey, facility, with HAC personnel in attendance. The review coincided with the initiation of drawing change control. The overall conclusion reached by the design review board was that, although a number of problems existed in the TCA, all of the problems which were investigated, with the possible exception of the inability of the TCA to meet the shutdown requirements, are either solvable with reasonable effort or can be circumvented by relatively minor relaxation of the requirements imposed on the TCA (with corresponding changes being required in other spacecraft interface areas). All

[5]MON = mixed oxides of nitrogen.

[6]Prepared by JPL Section 273.

UNCLASSIFIED
CONFIDENTIAL

UNCLASSIFIED
CONFIDENTIAL

problems enumerated by the review board have been taken under consideration, and some have already been solved. Some progress has been made in solving the shutdown problem.

b. Alternate TCA. When the RMD TCA was reinstated as the *Surveyor* engine, it was decided to conduct a prequalification test program with the MIRA 150A TCA to qualify the design with minimal effort. This prequalification test effort was successfully completed increasing confidence that a qualification program could be successfully conducted if it were to be implemented. The data from the testing are being reduced and prepared for inclusion in a final report.

Development of the MIRA 150A TCA was described in previous issues[7] of the *Space Programs Summary*, Vol. I.

H. Thermal Control

1. Subsystem Thermal Analysis and Design

a. Compartments. The spacecraft prelaunch operational sequence was reviewed to assure compatibility with Compartments A and B prelaunch temperature requirements. To reserve adequate thermal capacity for the high-power acquisition mode required immediately following launch, the thermal tray prelaunch temperature is limited to 110°F. The existing prelaunch sequence will cause thermal tray temperatures in excess of 110°F; therefore, action was initiated to revise the prelaunch sequence. Prelaunch thermal dissipation capability was established at 20 and 14 w for Compartments A and B, respectively; the prelaunch sequence of events must be revised to keep the average thermal dissipations of Compartments A and B within these limits.

b. Attitude control. The current nitrogen tank thermal design was reviewed as a result of the tank material change and the tank installation redesign. The study indicates that redefinition of the nitrogen tank surface treatment is necessary. The spaceframe-mounted nitrogen line surface treatment was modified to optimize the transit temperatures. The new treatment has polished aluminum on the section shadowed by the deployed solar panel (normal transit attitude) and white paint on the remainder of the surface. A transit temperature range of −180 to 90°F will exist with this surface treatment.

c. Vernier engine. A detailed parametric study to define the optimum thermal design parameters for Vernier Engine 2 was completed. The study indicated that it is advisable to retain the head end paint pattern while reducing both the size and thickness of the integral solar collector. Fig. 54 shows the dimensions of the new solar collector, while Fig. 55 shows the resultant Vernier Engine 2 temperature distribution.

Redirection to substitute gold for vacuum-deposited aluminum (VDA) as the basic thermal control coating for vernier engines will require a complete thermal reanalysis on the vernier engines. Although gold has an infrared emittance approximately equal to that of VDA, its solar absorption is between 2 and 3 times greater than that of VDA. This increased solar absorption will require that a more stringent account of reflections, especially side loading on the engines, be taken into account.

Recent interpretation of the thrust chamber assembly (TCA) interface specification raises the allowable upper temperature limits (including contained propellants) to 125°F. This change will allow the TCA's present nominal transit coast phase temperature range of 30 to 80°F to be raised to approximately 50 to 100°F and thus allow for the increase in temperature tolerances that are expected from the use of gold instead of VDA on the engines.

d. Radar altimeter and doppler velocity sensor (RADVS). Both T-21 and flight spacecraft temperature predictions were completed for the current T-21 passive thermal design. The predicted in-flight performance is reported in Table 16. The predictions for the klystron power supply modulator (KPSM) without the doppler velocity sensor (DVS) klystron tube assembly and for the signal data converter (SDC) are based on a comprehensive analysis utilizing reasonably predictable parameters. In contrast, the predictions for the receiver transmitter antennas and doppler velocity sensor klystron tube assembly are estimates since the dominant thermal parameters of the hardware are less definitive.

Comparing allowable temperatures with the predicted in-flight values at the start of RADVS warmup for a

[7] *SPS 37-22*, pp. 77–79; *SPS 37-23*, pp. 51, 52; *SPS 37-24*, pp. 36–38; *SPS 37-26*, pp. 48–51; and *SPS 37-29*, pp. 62, 63.

CONFIDENTIAL
UNCLASSIFIED

UNCLASSIFIED
CONFIDENTIAL

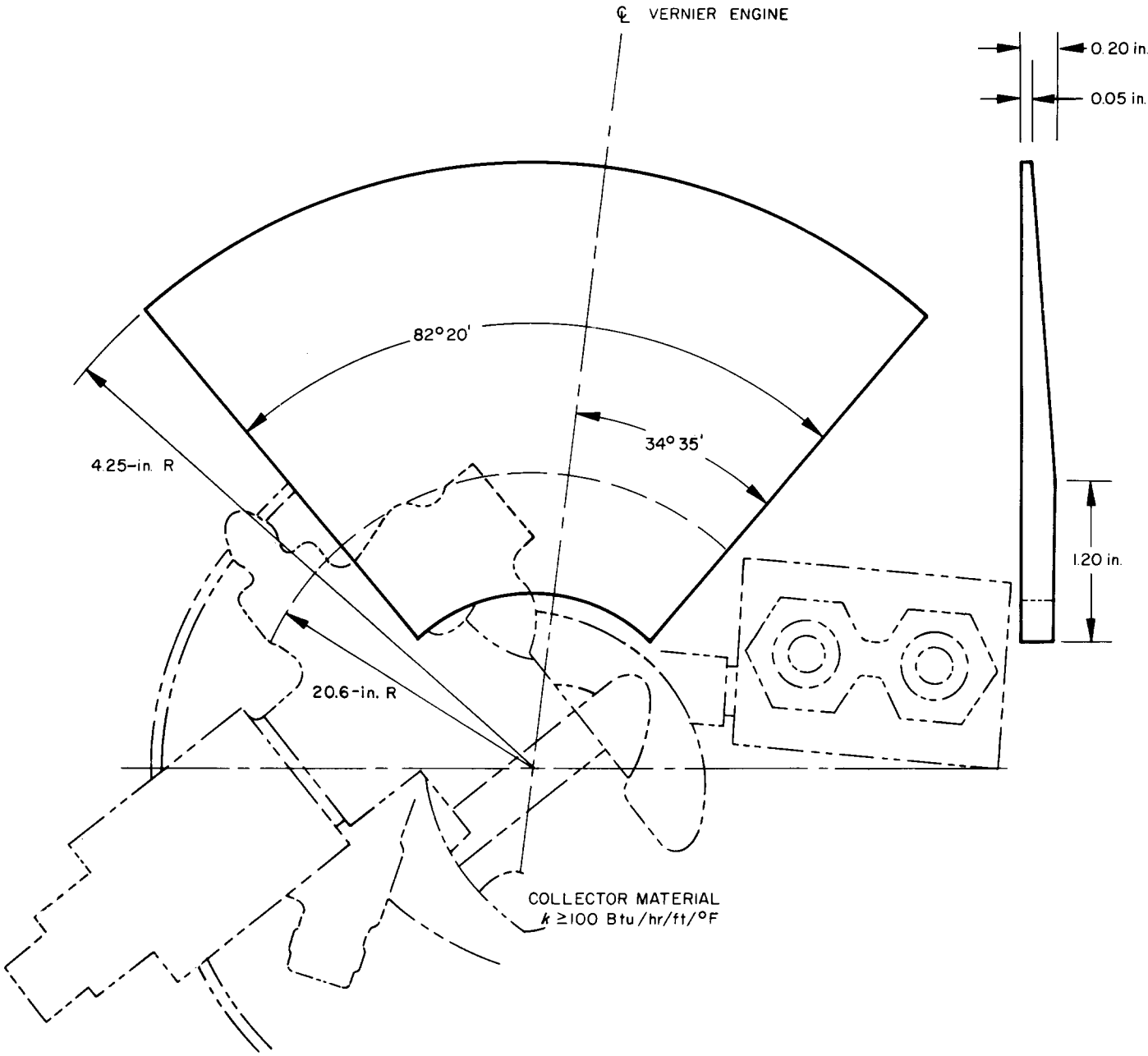

Fig. 54. Redesigned solar collector

4-min mission, the following conclusions regarding RADVS thermal control problems are apparent:

(1) *Klystron power supply modulator.* Assuring verification of the predicted temperatures with T-21 test data, the KPSM unit can operate within flight operational limits by raising the unit temperature approximately 12°F by adjusting the thermal finish design.

(2) *Signal data converter.* The optimized passive thermal design for the SDC (with thermal blanket) will not provide a predictable temperature range that satisfies the allowable start temperature range (e.g., approximately 100°F predicted versus 75°F allowable ranges) for the 4-min mission. This incompatibility can be resolved by: (1) relaxing allowable start temperatures to coincide with the present

UNCLASSIFIED
CONFIDENTIAL

UNCLASSIFIED
CONFIDENTIAL

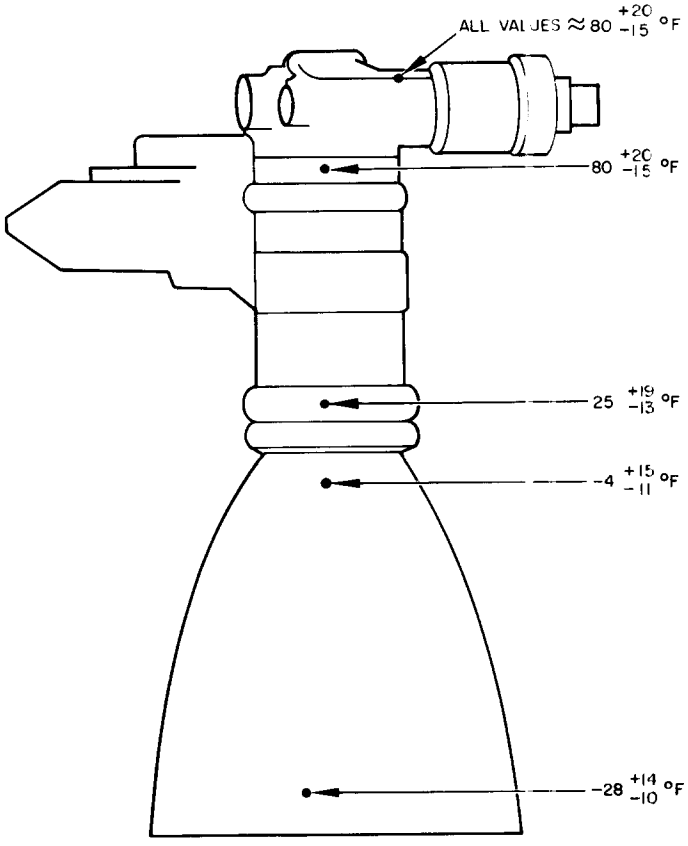

Fig. 55. Vernier Engine 2 temperature profile

thermal capability, or (2) employing an active thermal control system using electrical heaters.

(3) *Receiver–transmitter antennas.* Present estimates show that the predicted preamplifier start temperature range exceeds the allowable temperatures. However, this incompatibility is not considered serious based on the necessarily conservative temperature predictions of the entire receiver–transmitter assembly. Current plans are to use information from T-21 thermal-vacuum testing (thermal control phase) to determine if a problem exists, since the test results are considered to be the only valid indicator of important antenna thermal characteristics such as temperature gradients, nominal temperatures, and cooling during eclipse.

e. Solar panel. The maximum rate of temperature change experienced by the solar panel when entering and leaving a solar eclipse condition was reviewed. Temperature profiles were prepared for cooling during a solar eclipse and for heating after leaving the eclipse. Assuming a conservative initial temperature of 145°F, the maximum rate of change during the first minute of the cooling phase is 34°F/min. The maximum rate of change during the first minute of the heating cycle was found to be 31°F/min (based on a −200°F initial temperature corresponding to a 1-hr eclipse).

The temperature profiles were based on the assumption that the solar panel is isothermal throughout the cooling and heating modes. The thermal characteristics of the solar panel were analyzed to determine the validity of the isothermal assumption. The value of the Biot number, the ratio of internal resistance to external resistance, is an indicator for determining whether the panel will be isothermal. The external resistance is formulated from the emissive power of the solar panel and the internal resistance is simply the thermal resistance between the cell side and back side of the panel. When the Biot number is equal to or less than 0.1, the maximum error in temperature of any given time will be less than 5%. Since the thermal characteristics of the solar panel result in a Biot number of 0.025, the solar panel can be considered isothermal without introducing significant errors.

2. T-21 System Test Support

a. Emergency shutdown. The emergency shutdown procedure ensures that the vehicle will not be damaged by excessive cooling in the event of a complete facility and vehicle power failure. Spacecraft thermal response requires that all chamber wall shrouds be warmed from −310 to 0°F within 1 hr. The requirement is based on vehicle cooldown rates observed during eclipse conditions in the MT-1 sector thermal tests. Three trial emergency shutdowns of the chamber thermal system (without the T-21 vehicle installed) were evaluated. Two shutdowns lasted for 1 hr. The third lasted for 2½ hr as it became obvious that data would be required for extended time periods.

The warmup is performed by circulating pressurized hot gas through the chamber shrouds. The chamber thermal shroud system consists of three circumferential wall shrouds each covering a 120-deg segment and a fourth shroud for the floor. The experimental emergency warmups indicated that the temperature of the floor and two sidewall shrouds could be raised to 0°F within 1 hr. The third sidewall shroud (Shroud C) remained cold (≈ −100° to −150°F) at the end of 1 hr, but had warmed to −30°F in 1¾ hr. Despite the failure of one of

UNCLASSIFIED
CONFIDENTIAL

UNCLASSIFIED

Table 16. Predicted thermal performance of T-21 RADVS for flight conditions

RADVS units	Temperature predictions for transit phase						Allowable temperature at start of RADVS warmup of 4 min-mission, °F	
	Coast phase		Thermal descent phase temperature variances		Unit temperature at start of RADVS warmup, °F			
	Bulk nominal and prediction uncertainty, °F	Estimated temperature spread about nominal, °F	Maximum heating mode, °F	Maximum cooling mode, °F	Minimum	Maximum	Minimum	Maximum
KPSM								
Without DVS klystron tube assembly	15±25	±13	+10	−15	−38	63	−26	116
DVS klystron tube assembly	20±40	—	+30	−25	−45	90	−49	100
SDC								
Motherboard assemblies	50±30	±11	+5	−5	4	96	30	95
Low voltage power supply	50±30	±8	+10	−20	−8	98	25	104
Receiver–transmitter antennas								
Altimeter velocity antenna								
Dish and skirts	(−160 to 110)±45	—	+70	−40	−245	225	Unknown	Unknown
Septum	(−105 to 5)±45	—	+70	−40	−190	120	Unknown	Unknown
Feedhorn	(−16 to 4)±35	—	+35	−40	−91	74	Unknown	Unknown
Preamplifier	34±35	±10	+45	−30	−41	124	−40	100
Velocity sensor antenna								
Dish and skirts	(−160 to 110)±45	—	+70	−40	−245	225	Unknown	Unknown
Septum	(−105 to 5)±45	—	+70	−40	−190	120	Unknown	Unknown
Feedhorn	(−24 to −4)±35	—	+35	−40	−99	66	Unknown	Unknown
Preamplifier	26±35	±10	+45	−30	−49	116	−40	100

the chamber sidewall shrouds to meet the 1-hr warmup requirement, preliminary review of the data indicated the emergency warmup would be satisfactory for the protection of the vehicle with the possible exception of four units adjacent to the cold wall shroud. These units, Vernier Engine 2, vernier propellant lines in Sector 1, the KPSM, and the altimeter velocity preamplifier, required a more extensive review to determine their cooldown rates in the chamber emergency warmup environment.

This review indicated that the temperatures of Vernier Engine 2, the propellant lines, and the KPSM will always remain above the lower limit in an emergency shutdown. The altimeter velocity preamplifier is the only unit in danger of excessive cooling. However, the part of the preamplifier, the crystal holders, which would be damaged by an excessive cooldown would be relatively easy to replace. It was recommended that no additional emergency chamber warmup capability be provided at this time.

If a power failure were to occur during a programmed eclipse when many units would have already experienced a severe cooldown, lower temperature limits would be exceeded on many subsystems. Since approximately 3% of T-21 test time will be spent in an eclipse environment, the probability of a power failure during the condition is small. However, a backup power supply will be required for any thermal-vacuum testing in which a lunar night test is performed. Many subsystems that are designed functionally and thermally for transit will be controlled near their lower temperature limit with protective heaters. The time for these units to cool below their lower temperature limits during a power failure would be too short for an emergency chamber shroud warmup to be successful.

b. Pretest temperature predictions. Pretest temperature predictions were prepared for use in real-time monitoring of data during the T-21 tests. In general, most T-21 systems will operate at temperatures which are

UNCLASSIFIED

UNCLASSIFIED

higher than those anticipated on an A-21 spacecraft. Spectral mismatch between the solar simulation and the actual Sun would cause thermal finishes to exhibit a higher solar absorptance in test than in space. Some systems have a higher incident solar intensity in test than in space because of a chamber variation in intensity in the vertical direction. The RADVS preamplifier level is the test plane where an intensity of one solar constant is set; units above this plane will receive an excess of solar energy.

Compartments. Typical temperature profiles of the upper thermal trays in Compartments A and B are shown in Fig. 56. The compartment system is one of the few exceptions to the trend of higher temperatures on the T-21 vehicle as compared to the A-21 spacecraft in transit. Despite the fact that the solar intensity is 105% of a solar constant at the compartment radiators, this difference occurs because the infrared energy from the removed solar panel/planar array is not present. These differences, while not large, are expected to result in a temperature difference of approximately 5°F. The same magnitude of temperature difference that exists on the compartment thermal trays in the T-21 and A-21 vehicles will exist on the contained electronic units.

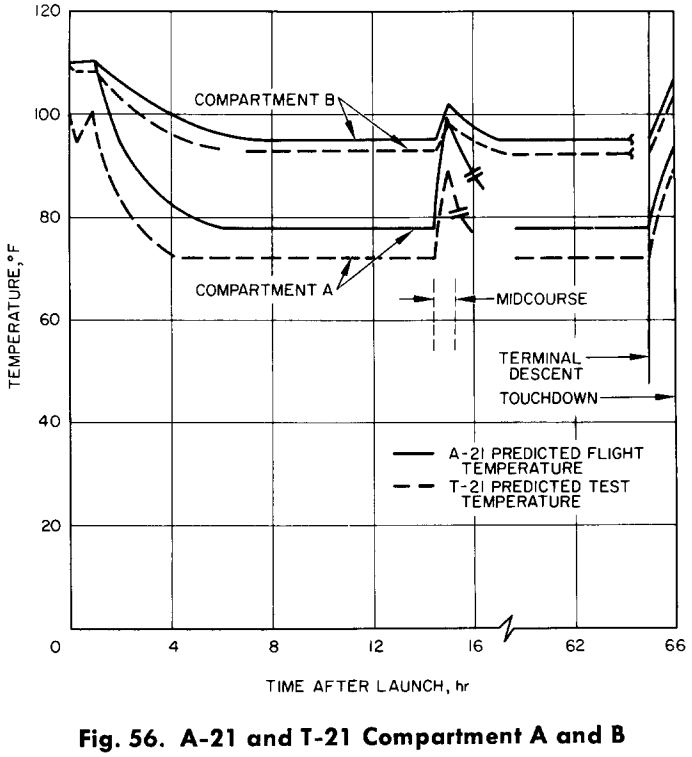

Fig. 56. A-21 and T-21 Compartment A and B temperature profiles

RADVS. RADVS preamplifier temperatures are shown in Fig. 57. Temperatures for the most part are 5°F higher on the T-21 test vehicle than on the A-21 spacecraft in flight. Differences in temperature levels can be attributed to the difference between the chamber environment and the space environment, such as the infrared energy input from the chamber walls, solar reflections from the chamber floor, differences in the temperature of the adjacent spacecraft surroundings, and the higher solar absorptance of the inorganic white paint when exposed to the S4-A solar simulator. The SDC is predicted to be 18°F higher in test than in flight because of the higher simulated solar intensity at this plane during test.

Vernier engines. Predicted vernier engine temperatures are shown in Fig. 58. A number of anomalies exist in the vernier system which should be identified. The design of the system has undergone changes which will be flown on an A-21 spacecraft, but have not been incorporated in the T-21 vehicle prior to thermal-vacuum testing. Therefore, the thermal testing of this system can only be considered developmental in nature. Examples of these differences are titanium propellant tanks on the A-21 spacecraft and aluminum tanks on the T-21 vehicle, a thicker tank wall on the A-21 helium tank as compared to the T-21 vehicle, and a difference in the engine attachment bracketry.

Differences in the operational aspects also exist. Inert liquid propellant with thermal properties differing from the actual propellant will be substituted. Additionally, the A-21 thermal analysis takes into account a midcourse propellant expenditure whereas the volume of fluid remains constant during T-21 tests. The helium tank will contain no gas during the T-21 test program. Temperature gradients occur in the engines which are not reflected in Fig. 58. Temperatures at specified points corresponding to a test thermocouple of flight sensor location are provided to demonstrate trends.

c. Solar mapping of shadow shrouds. The mapping data of the shadow lines of the shadow shrouds obtained in the fit and function environmental phase was analyzed. These shrouds simulate the shadow cast by the solar panel on a flight vehicle (Fig. 59). Fig. 60 shows mapping data for two typical locations, one at the Compartment A radiators and the other at the Vernier Engine 2 solar collector expressed as the length of the solar intensity decay–buildup region. As a comparison, corresponding values are shown for the shadow zone from the solar panel on a flight vehicle in space and for

UNCLASSIFIED

UNCLASSIFIED

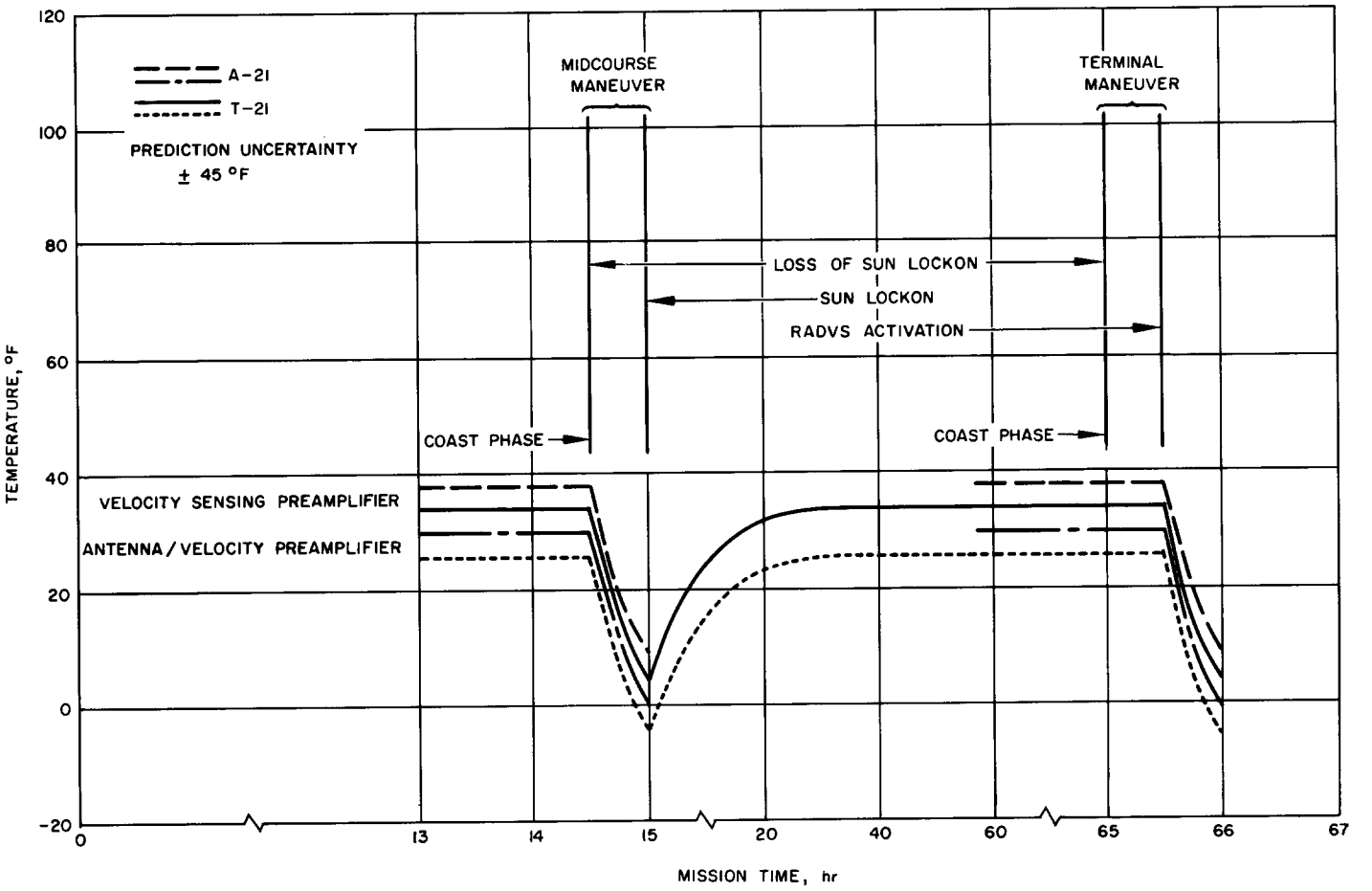

Fig. 57. A-21 and T-21 RADVS preamplifier temperature profiles

the shadow region on the T-21 vehicle in test if the solar panel had been used instead of the shadow shrouds.

The width of the decay region in space and in test are similar but the width of the intensity buildup region on the compartment radiators during the test is double the flight value. This performance is acceptable and will result in a satisfactory environment for solar-thermal-vacuum testing. In contrast, the zone of varying intensity on the Compartment A radiators would have been 17 in. wide if the solar panel were used instead of the shadow cold shrouds. This 17-in. zone is almost the width of a row of thermal switch radiators and valid thermal testing would not have been possible.

3. *Thermal Finishes*

The study of the potassium content in the silicate paint was concluded. The spread in data was caused by normal inaccuracies in the spectrographic analysis. The final analysis, after 5 weeks storage, showed 7.7% potassium. An extensive chemical analysis program would be required to identify the degradable species in the paint other than the pigment.

The study on vacuum-deposited aluminum (VDA) was completed and indicates that the use of VDA on epoxy laminate structures should be restricted to areas where temperatures no higher than 250°F are expected. These results are based on 100-hr exposure at the desired temperature and in a vacuum of 10^{-6} torr. Short-term thermal exposure may allow much higher temperatures to be used. The main difference between the epoxy laminate VDA and the aluminum VDA is in the substrate. Gross substrate change begins at 300°F for the epoxy and catastrophic failure occurs at 500°F. The aluminum substrate is useful to 500°F but some change in reflectance and appearance occurs at 500°F.

UNCLASSIFIED

UNCLASSIFIED

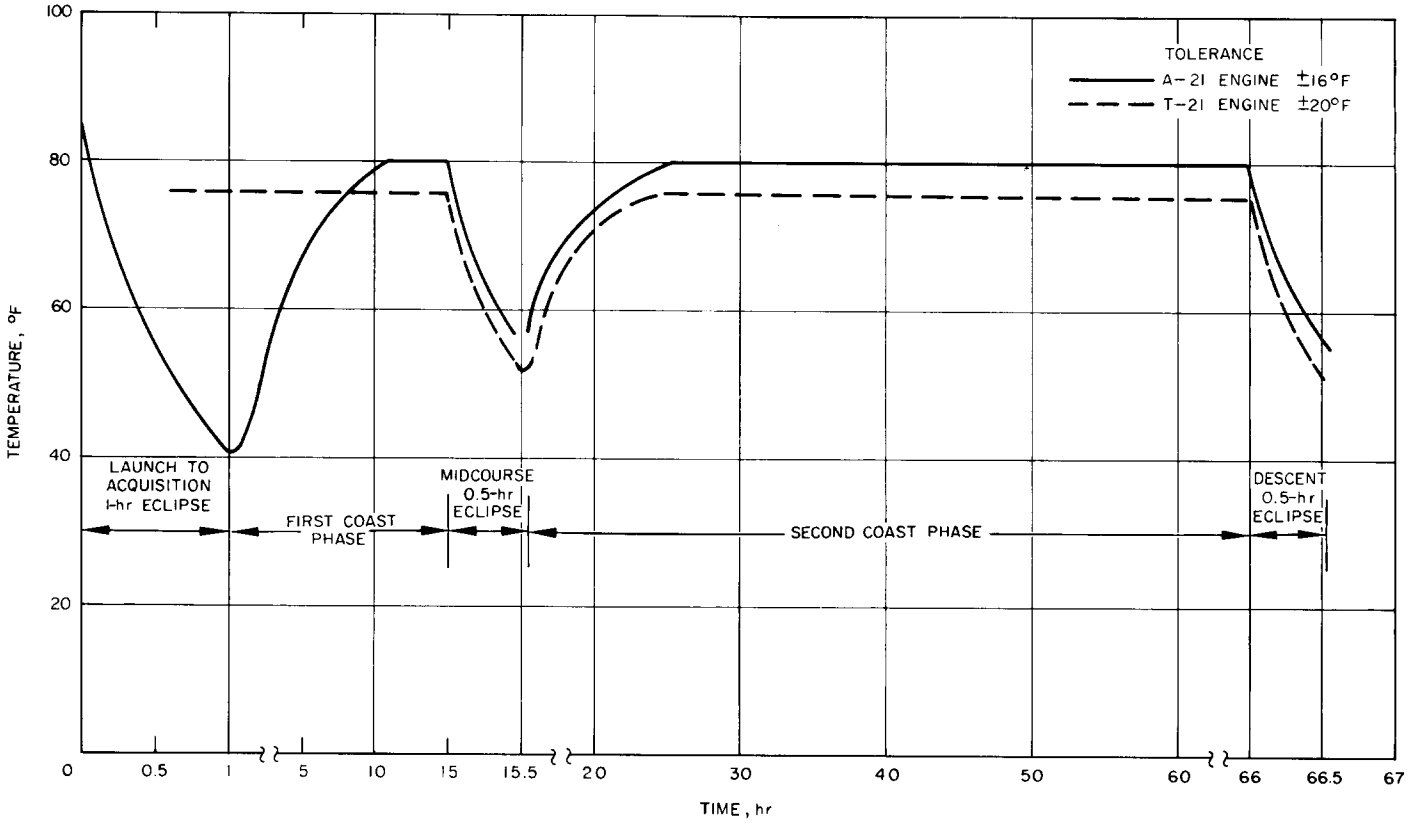

Fig. 58. A-21 and T-21 vernier engine temperature profiles

4. *Retro Plume–Spacecraft Radiation Heating*

The thermal problems attributed to particle radiation from the main retro plume are being examined by semi-empirical analysis. The radiosity of the particle plume was determined experimentally from radiometric measurements taken during retro-engine firing tests conducted at Arnold Engineering Development Center. The particle plume is assumed to have a conical configuration with a constant radiosity; the conical half angle was synthesized from particle mass distributions available in the literature.

The particle plume radiosity was measured in the region within a few exit diameters downstream of the nozzle exit plane. The experimental radiosity used for design purposes is $(\epsilon\ \sigma\ T^4)_{plume} = 6.5$ Btu/sec-ft^2. This radiosity is independent of the assumed plume shape because it represents an integrated value obtained from a volumetrically distributed source viewed in a solid angle by a radiometer with a 60-deg conical field angle. The calorimeter data, based on a hemispherical field of view, are consistent with the radiometer data but depend on the geometry of the particle and the diffuser duct into which the rocket plume is directed. It is recognized that the experimentally determined value is conservative since the measurements were taken at the hottest portion of the plume, i.e., just outside the nozzle exit plane. Various regions of the spacecraft will "see" a particle plume of nonuniform radiosity with the maximum value occurring adjacent to the exit plane and decreasing to zero at hundreds of exit diameters downstream of the exit plane.

The particle plume shape is based on a mean distribution of particle mass at a station 5 exit diameters downstream from the exit plane. The distribution of particle sizes was taken from analytically derived data. These data yielded a mass distribution corresponding to a cone with a 13-deg semivertex angle. Additional particle distribution data yielded a conical half-angle of 3.3 deg. The 13-deg cone is being used for design purposes because it is more conservative.

The design equation used to determine the direct radiant energy absorbed at any surface A_i is

$$q_i = 6.5\ \alpha_i\ F_{i\text{-}plume}\ \text{Btu/sec-ft}^2$$

UNCLASSIFIED

UNCLASSIFIED

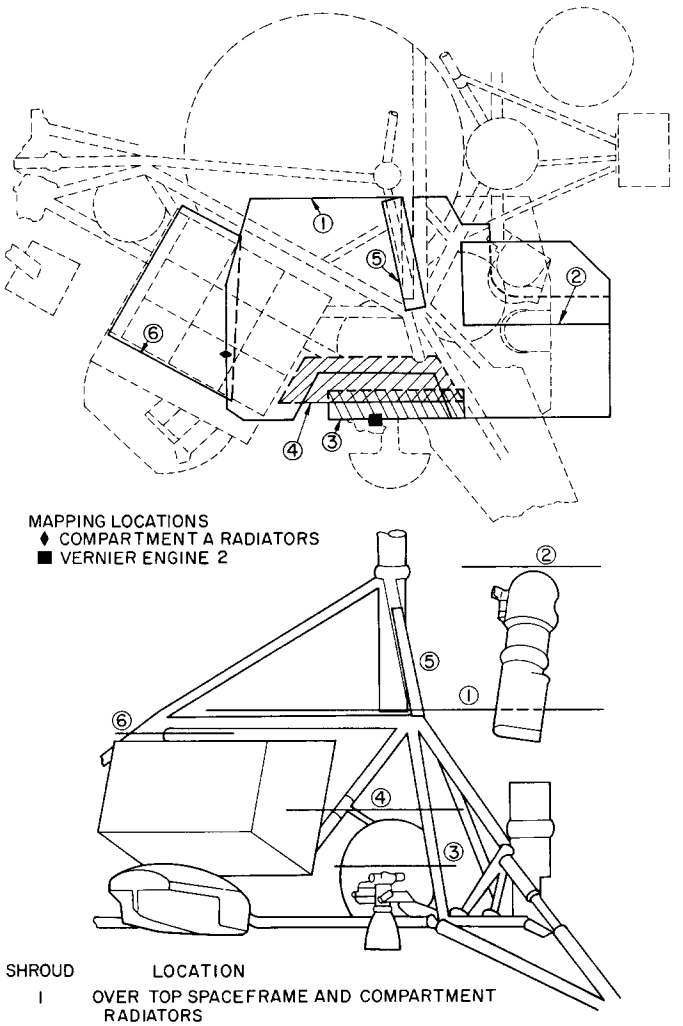

SHROUD	LOCATION
1	OVER TOP SPACEFRAME AND COMPARTMENT RADIATORS
2	OVER TV 3
3	OVER VERNIER ENGINE 2
4	OVER FUEL TANK 2
5	OVER MAST SUPPORT TUBE
6	OVER COMPARTMENT RADIATORS FOR COMPLETE SHADOWING

Fig. 59. Shadow simulation for T-21 transit tests

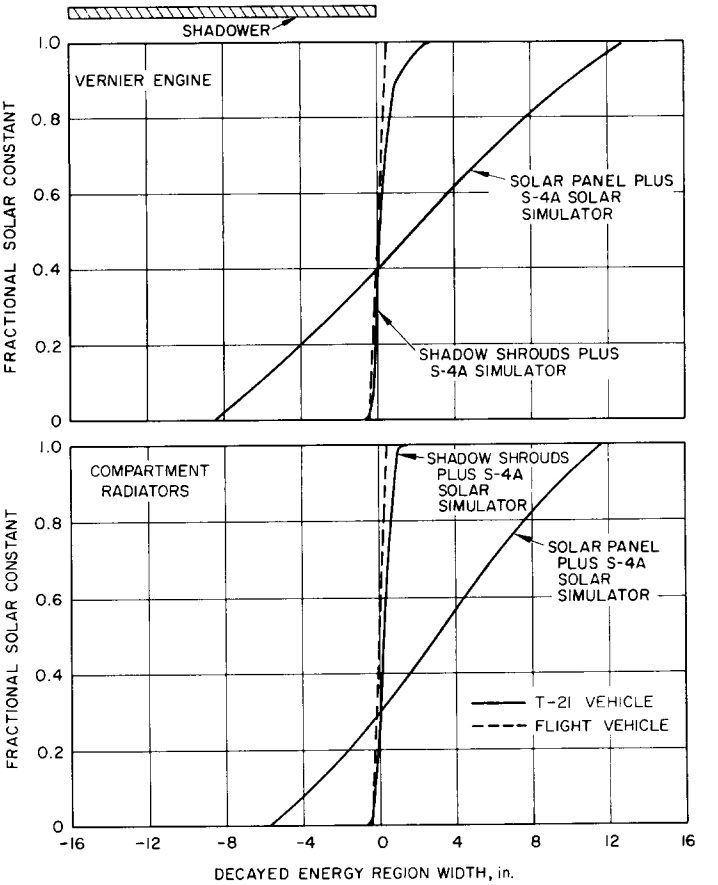

Fig. 60. Shadow line distortion in T-21 test compared to flight

where α is the long-wave absorptance appropriate to the plume as a source, and $F_{i-plume}$ is the shape factor from A_i to the 13-deg conical plume.

The spacecraft–plume radiation heating problem was reappraised to make maximum use of the reduction of the exhaust particle plume shape. Radiation view factors from items on the lower region of the spacecraft to the 13-deg semivertex angle cone were remeasured using a scale model of the spacecraft and a paper model of the particle plume cone. The resultant heat fluxes ranged from approximately 0.5 to 0.9 Btu/sec-ft^2, approximately half of that previously reported. The magnitude of spacecraft radiation heating was recalculated, incorporating the reduced heat flux values into a screening process utilizing analytical procedures and including more detail than previously available. The critical problem area group was restudied to determine the realistic values of spacecraft maximum temperatures which could be expected at the end of retro burning, including effects such as one-dimensional conduction heat transfer through wall sections, lunar surface heating during terminal descent, and surface reradiation. The results are summarized in Table 17, where the problem area items are now the two RADVS antennas.

The two temperature-sensitive portions of RADVS antennas are the interior surface of the parabolic dish and the microwave absorber-lined inner surfaces of the skirts. Calculated maximum temperatures of the downward facing parabolic dish surfaces ranged from approximately 325 to 395°F, depending on the presence or absence of descent-phase lunar surface heating; the top

UNCLASSIFIED

UNCLASSIFIED
CONFIDENTIAL

Table 17. Problem area group

Item	Thermal mode during terminal descent prior to start of retrorocket burning	Estimated maximum temperature, °F	Maximum allowable temperature, °F
RADVS antennas			
Interior surface of parabolic dish[a]	Maximum heating mode during descent	395	257
	Minimum heating during descent	325	257
Interior surface of skirt; i.e., surface of microwave absorber[b]	Maximum heating mode during descent	625	257
	Minimum heating during descent	555	257

[a]Maximum temperatures are calculated for the following conditions:
(1) Total incident flux = 1.0 Btu/sec-ft² for 40 sec.
(2) $\alpha_{dish} = 0.10$ for 4140°R source.
(3) No reradiation ($\varepsilon_{dish} = 0$); one-dimensional conduction through thickness of dish.
(4) Initial temperature at start of retrorocket burning for maximum heating mode = 225°F; initial temperature at start of retrorocket burning for minimum heating mode = 155°F.

[b]Maximum temperatures are calculated for the following conditions:
(1) Incident direct flux = 0.6 Btu/sec-ft² for 40 sec.
(2) α_{skirt} 0.6 for 4140°R source; $\varepsilon_{skirt} = 0.4$.
(3) Reradiation considered; one-dimensional conduction through thickness of dish.
(4) Initial temperature at start of retrorocket burning for maximum heating mode = 225°F; initial temperature at start of retrorocket burning for minimum heating mode = 155°F.

surfaces of the dish have corresponding maximum temperatures approximately 70°F cooler by virtue of conduction through the fiberglass/aluminum honeycomb section. The significant parameter was the total incident heat flux and was assumed to be 50% greater than the direct input; the added increment is assumed to be attributable to surface interreflections. The specified maximum allowable temperature of 257°F has received attention from a materials-high temperature limitation viewpoint. Findings indicate that the materials can withstand short duration exposure to at least 350°F. The microwave absorber-lined areas of the skirt are similarly expected to heat to 550 to 625°F, depending again on the presence of lunar surface heating. Examination of the thermal-physical properties of the microwave absorber material reveals that a rapid temperature rise will result because of both a high surface absorptance ($\alpha \sim 0.6$) and low effective heat capacity. The urethane foam portion of the microwave absorber has a very low thermal conductivity ($k \sim 0.018$ Btu/hr ft°F), thereby limiting conduction heat transfer to the inner fiberglass-honeycomb sections. Material-temperature incompatibilities are numerous; the DTA epoxy-curing agent loses considerable strength above 257°F; the microwave impedance sensitive aluminum loaded fiberglass loses considerable strength above 400°F; at approximately 600°F, charring produces impedance mismatching. Although differential incident flux and lateral conduction effects have yet to be included, the overheating situation appears to be critical.

Restudy of the susceptibility of the remaining items to plume radiation heating showed that the crushable blocks and foot pads could be classed in the nonproblem group because of the conduction heat transfer through the aluminum honeycomb sections. The maximum expected temperatures of 190°F on the crushable blocks and 140°F on the foot pads are considerably below the 250°F maximum allowable. Several items previously listed in the "Further Study Required" group, such as the KPSM, omnidirectional antenna booms, antennas, and auxiliary battery compartment, have been relegated to nonproblem status. A solution to the RADVS antenna overheating problem combines a continued examination of antenna thermal transient characteristics with protection system preliminary designs utilizing nodal network thermal analysis techniques.

I. Spacecraft Vehicle and Mechanisms for Basic Bus

1. Spacecraft Vehicle

a. Vehicle status.

T-21 system type-approval test vehicle: thermal finish on the vernier propulsion system has been updated and is acceptable for thermal-vacuum and solar simulation testing.

T-1 separation type-approval test vehicle: has been revised for retrorocket separation development tests (Fig. 61). Fabricated parts required for tests are being manufactured. Instrumentation for measuring horizontal and vertical positions of the retrorocket as it is dropped at 1 Earth g has been completed and calibrated (Fig. 62). The squib firing system control box has also been completed and checked out.

UNCLASSIFIED
CONFIDENTIAL

UNCLASSIFIED
CONFIDENTIAL

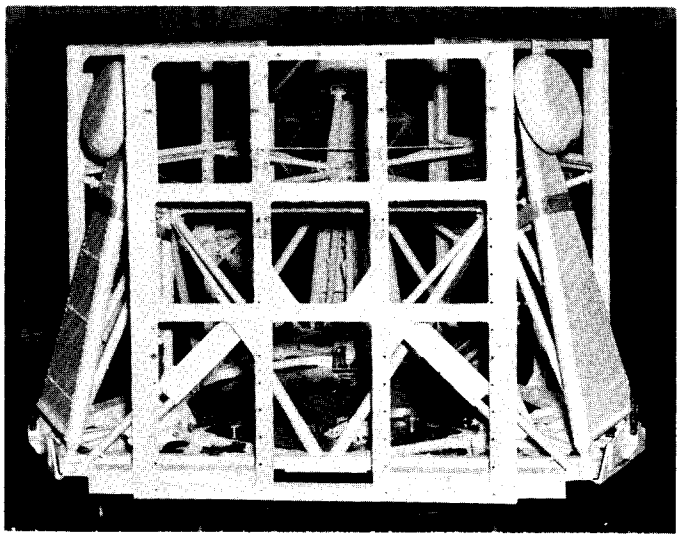

Fig. 61. T-1 vehicle upgraded for retrorocket separation tests

T-2SS backup vehicle for T-2 drop tests (Fig. 63): has been completed and is awaiting a possible revision resulting from difficulties experienced in the T-2S program.

T-2S drop test vehicle: has been returned for repairs. It will be used to test an updated recovery system to be incorporated on T-2SS.

S-2A structural test vehicle: has completed vibration tests.

S-6 vernier propulsion system qualification vehicle: design work was completed for updating the vehicle to reflect the current vernier propulsion system.

S-7 vernier propulsion system qualification vehicle: was upgraded for full-load vibration testing with a current vernier propulsion system.

S-8 tether test vehicle: tests of the radar altimeter and doppler velocity sensor noise interaction with the vernier engine system have been completed. The vehicle has been returned to the final assembly area for revisions prior to tethered buzz tests at AFMDC.

Thermal control model (TCM): engineering has been completed; fabrication is in progress.

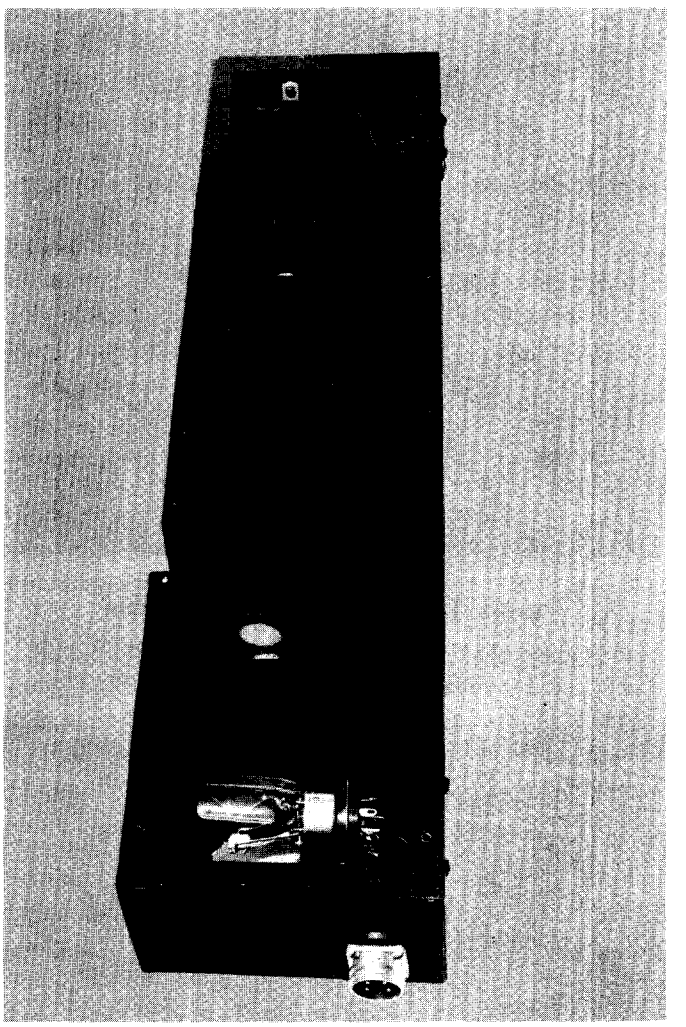

Fig. 62. Translation device for retrorocket separation tests

SC-1 first-flight spacecraft: was returned from systems test for changes in vernier propulsion system, nitrogen gas system, and wiring harness.

SC-2 proof test model: was scheduled for delivery to systems test (Fig. 64).

b. Wiring harness. Engineering has been completed for the S-8 buzz test harness. The TCM vehicle will use a flight-type harness plus an instrumentation harness.

c. TV resolution charts. A series of development-type charts has been prepared for the M-13 spacecraft model and for other test purposes (Fig. 65).

CONFIDENTIAL
UNCLASSIFIED

UNCLASSIFIED
CONFIDENTIAL

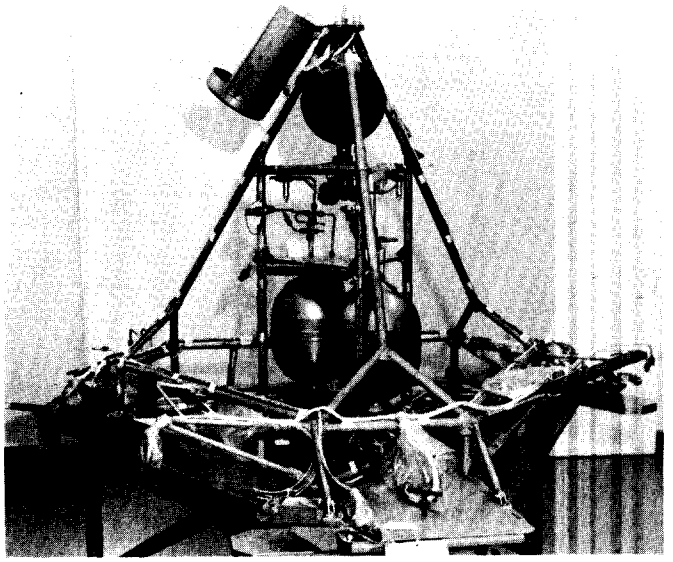

Fig. 63. T-2SS soft landing test vehicle

2. Mechanisms for Basic Bus

a. Omnidirectional antenna mechanisms. The two omnidirectional antenna mechanisms (designated A and B) use tapered, fiberglass cloth tubes bonded to aluminum hinge bracket assemblies. They deploy and lock the antennas into operating position prior to separation from *Centaur*.

Structural qualification of the A and B mechanisms is continuing on the S-2A vehicle. Type-approval vibration in the vehicle x- and y-axes has been completed successfully.

b. Antenna-solar panel positioner. The positioner provides mounting, positioning, position indicators, and launch and landing locks for the planar array antenna and solar panel. The antenna support structure has three controllable axes; the solar panel is mounted to the antenna support structure by a single controllable axis.

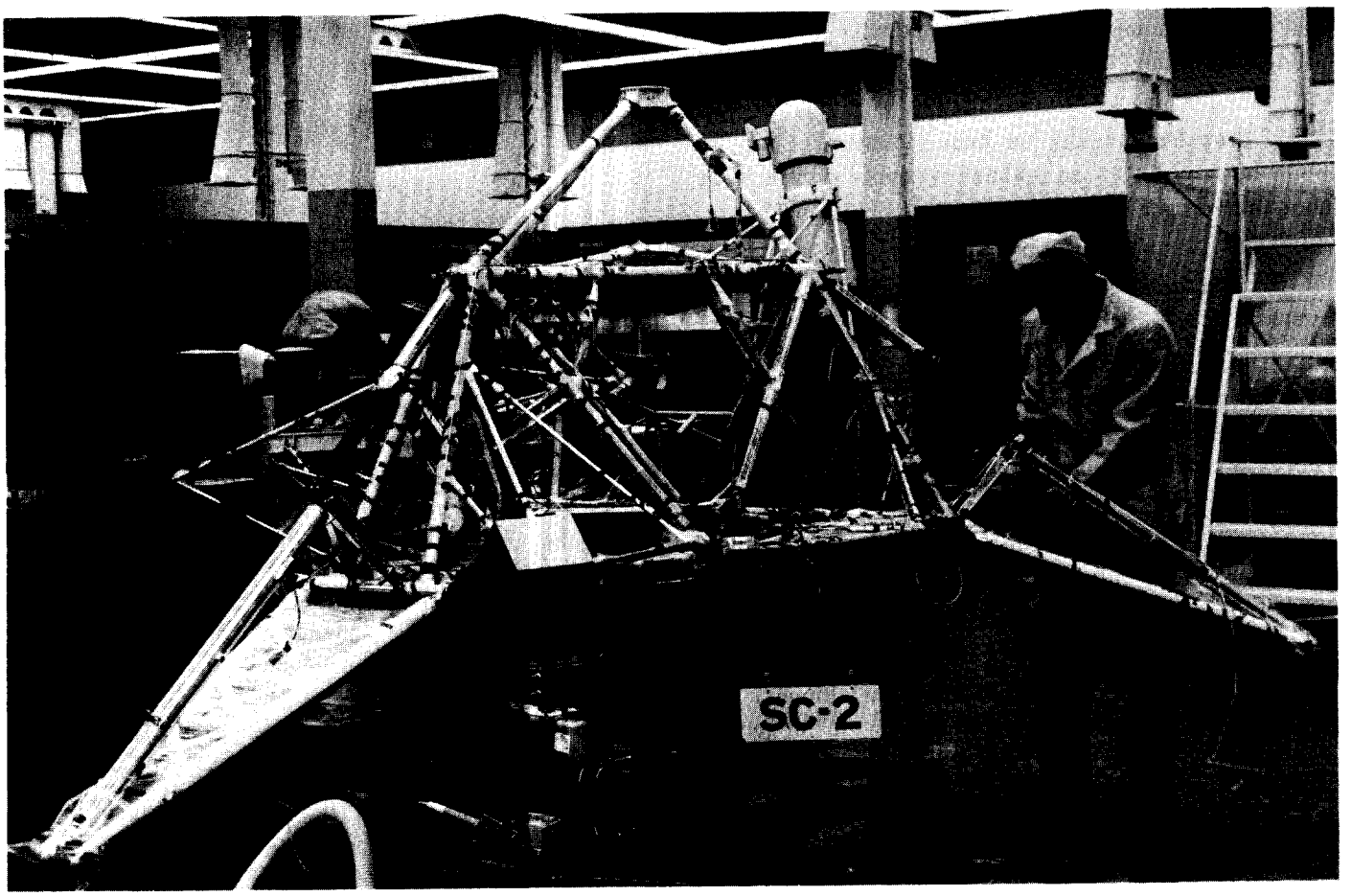

Fig. 64. SC-2 proof test model

UNCLASSIFIED
CONFIDENTIAL

UNCLASSIFIED
CONFIDENTIAL

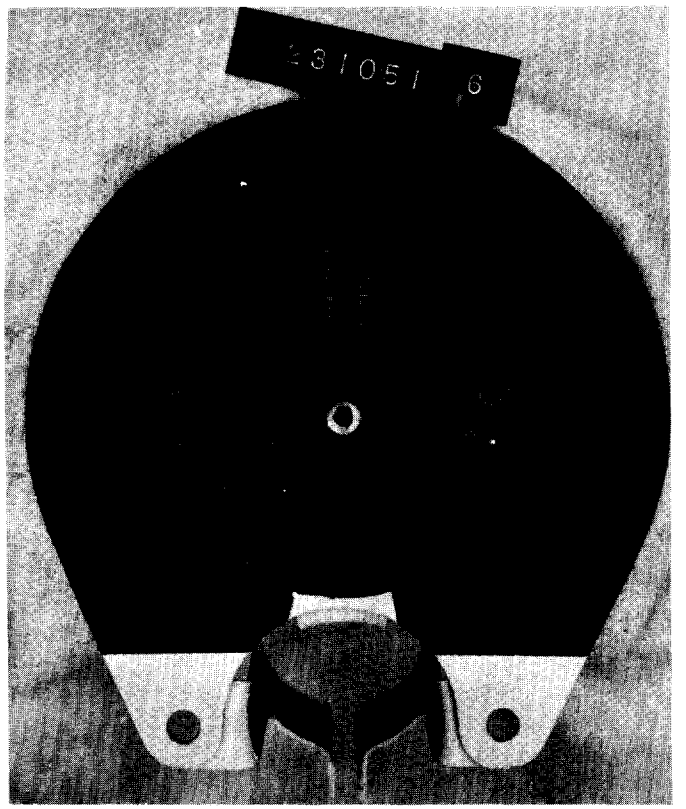

Fig. 65. TV resolution chart

The roll, elevation, and solar axis drives each utilize a three-stage planetary gear reduction. The polar axis drive uses a single-stage planetary and a double enveloping worm gear drive. Each drive uses a solenoid stepper motor for power and a wire-wound potentiometer for position indication.

The developmental unit X-1, upgraded to include a strengthened elevation housing (Fig. 66), solar panel tube support fittings, and a vibration damper between the solar panel and mast have completed successful type-approval vibration tests in the x- and y-axes while installed on the S-2A spacecraft. The damper reduced the motion of the solar panel and antenna, at the positioner resonant frequency, to within the required dynamic envelope. The damper arms fit into sockets on the back of the solar panel (Fig. 67). When the solar panel is erected to the transit position the damper arms pivot down under spring tension to a position next to the mast.

An outdated positioner is being upgraded for use in the TCM thermal evaluation program. The positioner drive mechanisms are being modified to provide the torque required for operation in the Earth's gravitational field.

Several pin pullers with spring-loaded taper pins (Fig. 68) have been fired under load at −216°F. A slight deformation of the microswitch actuator has occurred as a result of the firings. A relocation of the switch, allowing it to be released instead of being depressed by the taper pin retraction, is being investigated. Tests are continuing to determine the force required to pull the 1- and 2-in./ft taper pins under extreme load and temperature conditions.

c. Separation sensing and arming device. These devices (three per spacecraft) provide redundant interruption for the postseparation squib firing circuits and the vernier engine solenoid circuit until after the spacecraft separates from the *Centaur*.

Six sets of flight hardware (three devices per set) have been flight-acceptance tested and delivered for spacecraft assembly. The next set of units is in final assembly and will be delivered following flight-acceptance testing.

d. Pyrotechnic devices.

Squibs. The squib type-approval test program was completed. Postfiring tests on the squib glass header sealing characteristics were completed on a sample basis. The results are:

(1) Squib configuration 236472-4 (3 units out of 10 tested) met the minimum gas leakage of 0.01 cm^3/hr at 200 psig.

(2) Squib configurations 236472-1 and 236472-2 (15 out of 20 and 8 out of 10, respectively) met the minimum gas leakage requirements at 3000 psig. In the total 270 squib firings there was no evidence of any blown-out or loosened connector pins, expulsion of glass or debris, or blown-out or deformed mating connectors.

Pyrotechnic switch. The pyrotechnic switch type-approval test program is approximately 85% complete. Four switches, two normally open and two normally closed, were exposed to RFI environments without any adverse effects. The units fired normally with all functional and postfiring data within specification.

Fifty-six switch assemblies have been exposed to the following environments: vibration, hot storage, cold stor-

CONFIDENTIAL
UNCLASSIFIED

UNCLASSIFIED
CONFIDENTIAL

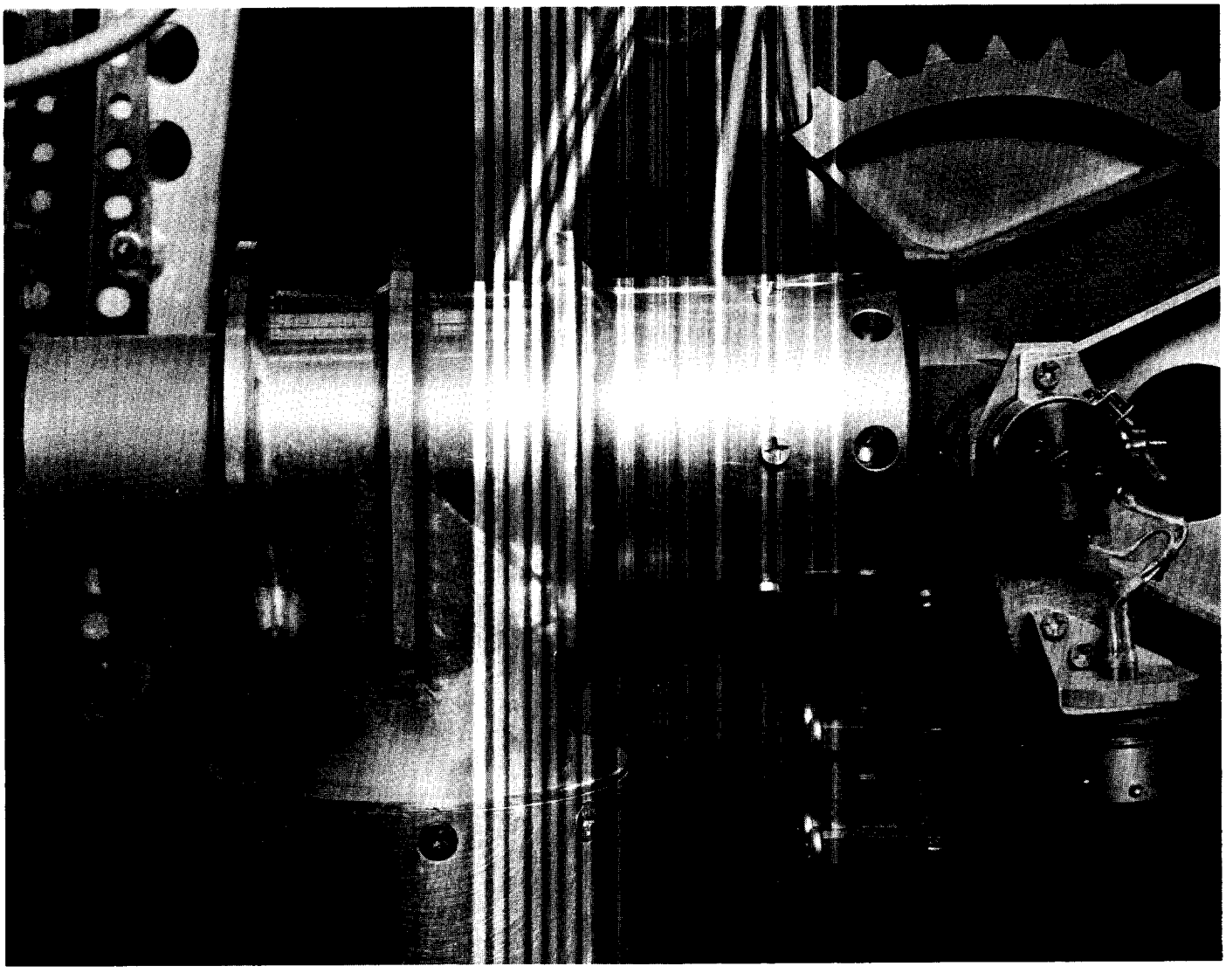

Fig. 66. Redesigned elevation axis housing

age, sealing, temperature shock, acceleration, mechanical shock, and 5-ft drop. After each test environment, a set number of units was fired; all functioned within the specified requirements.

Twenty-two assemblies are being subjected to a thermal-vacuum environment after which they will be fired in this environment. Following postfiring tests, the units will be vibrated and the switch contacts monitored for any chattering, opening, or closing.

e. T-2 oxidizer manifold dump device (OMD). OMD devices on signal-to-noise G1 and G16 were analyzed to determine the probable cause of failure. Signal-to-noise G1 failed to function during system test and signal-to-noise G16 failed during the T-2 drop. Pins B and C, normally open, were shorted in both units after firing.

Dissection of both devices isolated the shorts to the potted connector assembly. All squibs of each device showed normal electrical characteristics. The squibs fired properly when energized with the specified system all-fire current. In the complete disassembly of the connector pins and associated wiring, the excessively tinned and uninsulated wires were almost overlapping or touching the other wires as well as the connector pins.

It was concluded that the excessively tinned and uninsulated wiring, poor assembly procedures (which could not be inspected), and lack of process and material controls contributed to the unreliability of the unit.

UNCLASSIFIED
CONFIDENTIAL

CONFIDENTIAL UNCLASSIFIED

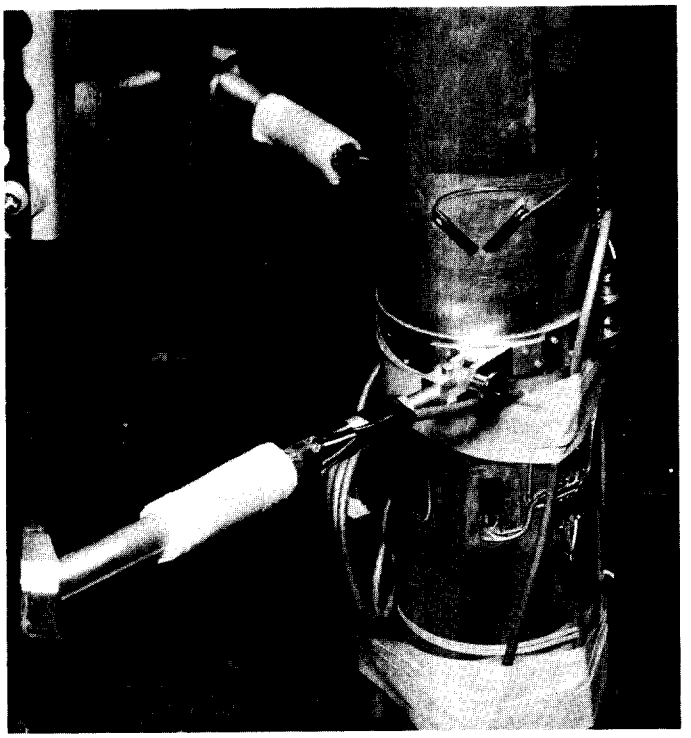

Fig. 67. Solar panel damper installation

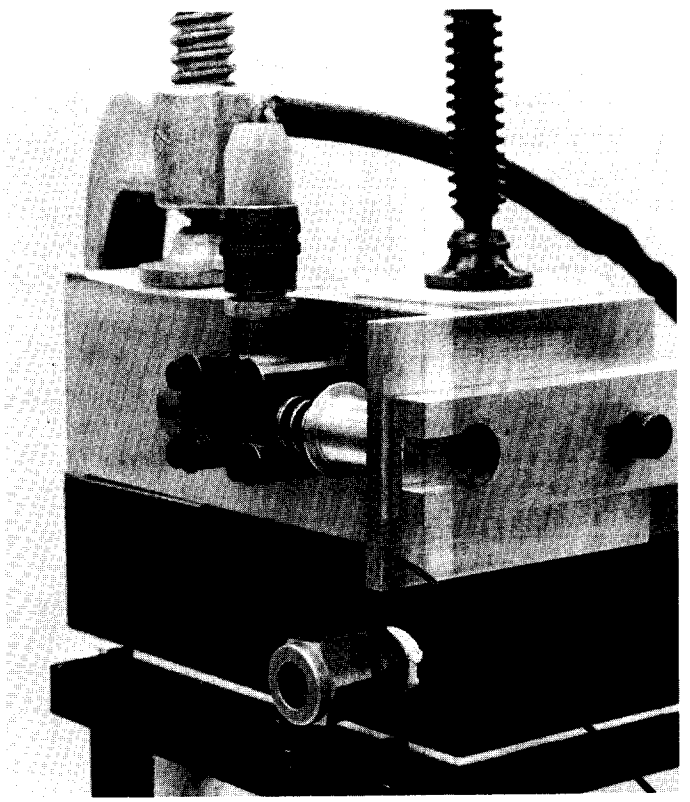

Fig. 68. Pin-puller with spring-loaded taper pins

J. Reliability and Quality Assurance

1. Reliability

The A-21 spacecraft system *a priori* estimates and minimum requirements are given in Table 18. The system *a priori* estimate increase is the result of a reevaluation of the reliability of the engineering mechanisms auxiliary based on a failure analysis mode. Table 19 shows the current and allocated subsystem *a priori* reliability estimates for the flight and landing phase. Reliability estimates for all subsystems (flight and landing phase) based on the latest available test data are presented in Table 20.

Following is the status of significant activities in subcontractor programs:

(1) *Vector Electronic Company.* Five subcarrier oscillators were analyzed; control, test, and quality assurance action was taken. The inherent problem

Table 18. System *a priori* estimates and requirements

Phase	Minimum system requirements	Current estimate	Preceding estimate
Flight and landing[a]	0.78	0.856	0.836
First 80 hr of lunar operation[b]	0.95	0.922	0.922

[a]Excludes vernier engine thrust chamber assemblies.
[b]Excludes payload.

Table 19. Subsystem *a priori* reliability estimates for flight and landing phase

Subsystem	Current estimate	Allocated reliability
Command decoding	0.990	0.991
Signal processing	0.997	0.997
Structures[a]	0.994	0.972
Thermal controls	0.998	0.995
Telecommunications	0.996	0.994
Flight controls	0.956	0.961
Propulsion[b]	0.957	0.937
Electrical power	0.963	0.949
Mechanisms	0.996	0.986
System	0.856	0.80

[a]Includes wiring harness and interconnections.
[b]Includes Hughes Aircraft Company portion of vernier engine system only.

CONFIDENTIAL UNCLASSIFIED

UNCLASSIFIED
CONFIDENTIAL

Table 20. Reliability estimates for flight and landing based on test data[a]

Subsystem	Current estimate	Preceding estimate	Comments
Command decoding	0.969	0.965	Additional test time with no relevant failures
Signal processing	0.959	0.924	Additional test time with few relevant failures
Structures	0.842	0.734	Previously relevant failures for wiring harness now judged irrelevant
Thermal controls	0.998	0.998	No change; *a priori* estimates used
Telecommunications	≈1.000	0.985	Additional test time with no additional relevant failures
Flight controls	0.824	0.794	Additional failure-free test time on RADVS and flight control sensor group
Propulsion	0.959	0.959	No change
Electrical power	0.344	0.828	Change due to limited test data on battery charge regulator (1 relevant failure in 84 operating hr)
Mechanisms	0.967	0.964	
Probability of system success $= \prod_{i=1}^{i=9} P_i$	0.205	0.391	

[a]Where relevant test data are not available on a unit, the *a priori* estimate of the unit was used.

of the subcarrier oscillator center frequency shifting out of tolerance continues to be of primary concern. Hughes Aircraft Company has initiated a detailed failure mode analysis study of subcarrier oscillator circuitry, component application, and packaging in an attempt to determine possible failure modes and potential problem areas.

(2) *Magnetic Research Corporation.* Design review of the altitude marking radar magnetron modulator was conducted. Potential failure modes were uncovered that may have been caused by packaging difficulties with the larger components. It was decided that the present box size would be enlarged with some rearrangement of components. All units will be sealed at Hughes to prevent leaks experienced around the header of the hermetically sealed modulators. The mica capacitor has been redesigned to meet reliability requirements.

(3) *Ryan Aeronautical Company.* Reliability estimates for the radar altimeter and doppler velocity sensor (RADVS) based on recent test data indicate an improvement from 0.985 to 0.991. Due to failure of the AM-2 doppler velocity sensor antenna, special vibration tests are being conducted at Hughes using the entire AM-2 RADVS system mounted on test spacecraft S-8. Type-approval tests, with the exception of the system level life test and the final electrical acceptance test, were completed on SN-1. At Hughes direction, System SN-1 has been diverted temporarily for a temperature study program. A potential crystal holder corrosion problem is also being studied.

(4) *Systron-Donner Company.* The reliability point estimate for the linear force balance accelerometer based on test data remains at 0.802. Since the accelerometer is now required to measure both plus and minus accelerations caused by superimposed vibration, new reliability improvements have been incorporated: (1) all components in the accelerometer will be *Surveyor*-qualified, and (2) Templac (temperature indicating paint) will be applied to the case of the accelerometer as a positive means of identifying any unit subjected to temperatures in excess of 200°F.

(5) *Kearfott.* The reliability estimate for the gyros based on test data increased from 0.839 to 0.865. A program was initiated to investigate the effectiveness of the revised "flush and fill" procedure. Equipment will be measured quantitatively for contamination before and after each cleaning operation; the particle counts will then be analyzed.

(6) *Endevco Corporation.* The reliability estimate for the accelerometers based on test data remains at 0.994, which is above the required value of 0.975. All accelerometers have been delivered and reliability requirements complied with.

(7) *Santa Barbara Research Center.* The reliability estimate for the Canopus sensor based on test data taken over the last six months increased from 0.500 to 0.970. Two units were operated a total of 3894 hr without a relevant failure. In the reliability demonstration test, SN-3 and -9 demonstrated a reliability of 0.970 with 80% confidence. The units were subjected to further environmental testing to increase confidence. SN-3 was vibrated followed

UNCLASSIFIED

UNCLASSIFIED

by a 66-hr thermal-vacuum-simulating flight sequence. After this sequence, a leak was induced in the case allowing it to depressurize and the unit was operated for 114 hr in a vacuum. The unit was then placed in a Sun-star simulator. The Canopus-indicates signal was strong and clear but the motor was noisy. Disassembly revealed the bearings were dry, the torque was high, and the lubricant had sublimed on the window. The unit was cleaned, the gears were oiled, and the motor was replaced. SN-3 again performed satisfactorily. SN-9, subjected to three additional mission profiles including vibration, still meets specifications.

2. Material and Process Studies

Activities continue in the evaluation of the suitability of materials for the *Surveyor* lunar environments. Efforts to improve testing techniques for a more quantitative measure of the products of outgassing on critical spacecraft surfaces were initiated. This method involves controlling the temperature differential between the sample material exposed and the condensing surface; it also provides a natural flow of the "outgassed" vapor past the temperature-controlled surface instead of condensing the gas in a small volume.

a. Thermal-vacuum testing. Dow Corning RTV 882 silicone rubber was subjected to a thermal-vacuum environment of 5×10^{-6} torr at 125°F for 72 hr. The weight loss was only 1% in 72 hr; however, condensation from outgassing was observed after 24 hr of exposure. Results of tests to determine the temperature limitations of vacuum aluminization coatings indicate that the surface starts to degrade on an epoxy laminate substrate at 300°F. On an aluminum substrate this coating is satisfactory to 400°F. The test results of five polyurethane foam materials evaluated to determine the most suitable product for vibration damping in the space environment are shown in Table 21.

b. Thermal control coatings. Results of tests showing measurements of the thermal characteristics of white organic paint from a rebaking cycle are shown by Table 22. Rebaking is required when an adjacent surface is repainted. Additional test results showing the characteristics of 3M white velvet organic paint to resist degradation from exposure to ultraviolet radiation in the thermal-vacuum environment are shown in Table 23.

3. Mechanical and Power Subsystems

a. Electropyrotechnics. Holex Inc., completed the analysis of two helium dump valve squibs which failed during type-approval tests. The squib failed as a result

Table 22. Thermal characteristics of white organic paint

Number of curing cycles	Solar absorptance, α	Infrarad emittance, ξ
1	0.23	0.92
2	0.22	0.91
3	0.23	0.91

Table 21. Physical properties of flexible polyurethane foams

Material	Density, lb/ft^3	Water vapor absorption (24 hr, 98% relative humidity, 160°F), %	Compression set, %	Ball rebound, in.	Outgassing at 160°F, 10^{-6} torr
Foamflex, yellow (Pacific Latex Corp.)	1.0	27.5	12.5	5.75	No deposit after 8 days
Foamflex, white (Pacific Latex Corp.)	1.17	18.3	24.0	Not determined	Deposit in 1 day
Califoam X-SS (Califoam Corp.)	0.93	13.8	9.4	7.5	No deposit after 8 days
Califoam X-SS (Califoam Corp.)	0.95	12.6	7.75	4.5	No deposit after 8 days
CPR-SS (CPR International)	1.10	21.7	2.5	Not determined	Deposit in 1 day

UNCLASSIFIED

UNCLASSIFIED
CONFIDENTIAL

Table 23. Effect of ultraviolet on thermo-physical properties of 3M-white velvet paint

Ultraviolet exposure	Solar absorptance, α		Infrared emittance, ξ	
	Initial	Final	Initial	Final
70 hr at 1 solar constant	0.23	0.28	0.91	0.89
150 hr at 1 solar constant	0.24	0.28	0.91	0.89
400 hr at 1 solar constant	0.23	0.32	0.91	0.93
Specimen baked three times at 250°F for 1½ hr, then exposed 70 hr to 5 solar constants = 350 solar equivalent hr	0.23	0.34	0.91	0.91
Specimen soiled, cleaned with aluminum oxide paste, then exposed 70 hr to 5 solar constants = 350 solar equivalent hr	0.26	0.38	—	0.91
Specimen soiled, cleaned with silica abrasive paper, then exposed 70 hr to 5 solar constants = 350 solar equivalent hr	0.25	0.36	—	0.91

of a movement of the ceramic cup which sheared the bridge wires. Fig. 69a illustrates the mode of failure. Fig. 69b shows the redesigned squib. Each of the redesigned squibs will have an aluminum press-fit ring to retain the ceramic cup. The ceramic cups will be cemented to the squib body. Future valve firing tests will be performed with the valves mounted on simulated tank and regulator masses.

b. Retrorocket engine mathematical model. The mathematical reliability model includes probabilities of successfully surviving prefiring environments, fulfilling dynamic operating requirements, and achieving the thrust decay performance necessary to enable successful ejection of the engine prior to lunar landing. Since each probability term in the model represents a statistical independent event, the terms are joined into a series reliability expression as follows:

$$R = [P_{TG}\, P_V\, P_{TC}\, P_{ALT}\, P_{ACC}\, P_S\, P_H]_I \times [P_i\, P_I\, P_{AT}\, P_{TE}]_{II} \times [P_{TD}]_{III}$$

where R represents the reliability of the retro-engine, and P is the probability of successfully complying with the requirements designated by the subscripts:

TG = thermal gradient	H = humidity
V = vibration	i = ignition
TC = temperature cycling	I = total impulse
ALT = altitude	AT = action time
ACC = acceleration	TE = thrust excursion
S = storage and handling	TD = thrust decay

Subscripts I, II, and III refer to prefiring, thrust-time period, and postfiring period, respectively.

Retro-engines used during the development and qualification test programs were reviewed to determine applicability for the mathematical model. Engine attributes and test parameters were identified so that data from the various engine tests could be matched with appropriate entries in the mathematical model. Engine A21-F, an inert engine, was selected as having been subjected to typical mission vibration and shock environments. Results of environmental testing in terms of effects on structural capability of the engine were considered valid in calculating vibration and shock probabilities.

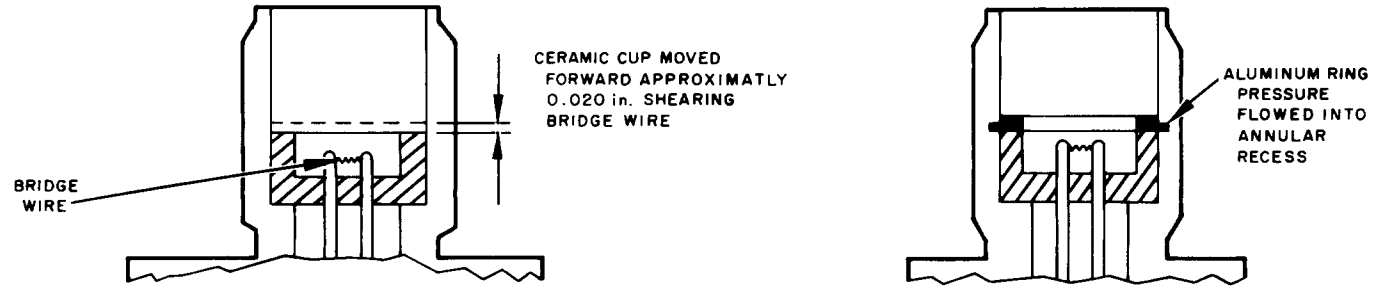
CERAMIC CUP MOVED FORWARD APPROXIMATLY 0.020 in. SHEARING BRIDGE WIRE
BRIDGE WIRE
ALUMINUM RING PRESSURE FLOWED INTO ANNULAR RECESS
(a) SQUIB FAILURE MODE
(b) REDESIGNED SQUIB

Fig. 69. Helium dump valve squib

UNCLASSIFIED
CONFIDENTIAL

UNCLASSIFIED
CONFIDENTIAL

K. System Testing

1. T-21 Prototype Vehicle Tests

a. Checkout. Checkout of the T-21 control items continued in preparation for the solar-thermal-vacuum test phase. A malfunction of the yaw gyro required repair of the flight control sensor group. A failure of the Canopus sensor was corrected. Erroneous gains in the 2.3-kc subcarrier oscillator (SCO) data channel occurred. Investigation showed that the SCO output was connected to both the frequency- and phase-summing amplifier; this resulted in the SCO having improper central signal processor output. Action is underway to correct this problem.

During integration of the television and telecommunications subsystems, an interface problem between the approach camera and signal processing was encountered. Three telemetry lines would not accept adequate back current, resulting in a full-scale telemetry signal at all times. The approach camera was removed from the spacecraft for correction of this problem.

A similar problem was encountered in the RF subsystem. The filament ON telemetry signals from both transmitters were not accepting adequate back current, resulting in a filament ON signal at all times. This signal satisfied the transmitter high-voltage ON logic and allowed high voltage to come on with no filament voltage. A change presently under development to correct this problem will be incorporated in the T-21 vehicle prior to solar-thermal-vacuum testing.

b. T-21 QA-1 RADVS group testing. The cause of perturbations observed previously in the V_y and V_z dc analog outputs was traced to the Beam 3 preamplifier. When this preamplifier gain-switched, a transient was produced that affected the Beam 3 tracker and, therefore, the V_y and V_z analog outputs. A modification incorporated in the high-voltage power supply section of the klystron power supply modulator (KPSM) reduced the system noise contribution of the KPSM by approximately 6 db.

A complete radar altimeter and doppler velocity sensor (RADVS) group test was performed on the QA-1 system installed on the T-21 vehicle. A problem of excessive system noise was traced to improper installation of the doppler velocity sensor (DVS) waveguide at the KPSM. Also, system noise increased to a level that caused tracker acquisition after approximately 30 min of operation with forced air cooling. However, it was determined that the system would operate satisfactorily without cooling for a period in excess of 5 min, which meets the specification requirements.

Although data obtained from the various test requirements indicated a few out-of-tolerance conditions, overall system operation was deemed satisfactory for continued testing.

c. T-21 solar-thermal-vacuum test phase. Solar-thermal-vacuum (STV) test equipment checkout using the M-12 spacecraft mockup was completed (Fig. 70). The equipment is being installed in the actual T-21 STV vehicle test phase. Chamber emergency shutdown modifications were completed and functional testing of these modifications was performed. The operations techniques and modifications to the chamber demonstrate that the system is able to satisfactorily accomplish a shutdown in event of total power failure.

d. Data analysis. Following Upgrade III, the areas affected by the modifications were rechecked. Phase modulation, sensitivity, and bandwidths are the only retest items of the RF group which failed to meet specifications. Flight control group test results showed the improvement expected of the updated hardware. A large number of previously incomplete intergroup integration and mission sequence test requirements was also met.

2. System Test Equipment

a. Stray energy monitors. Vibration testing of stray energy monitors was conducted for the purpose of verifying mechanical survivability under expected spacecraft vibration levels. Three tests on each of the three major axes were performed on 29 units. Three mechanical activation-type failures occurred, all at levels in excess of 30 g. These three failures occurred during the first two sweeps of a total of three performed at this g-level. No additional failures were experienced during six succeeding tests at greater than 20 g.

It is believed that the three failures were random in nature and that a confidence level of about 95% could be attained if a preconditioning vibration test were performed on each device before actual test use. This test would remove marginal units before installation on the spacecraft. Should an activation occur during spacecraft vibration test, a look under a microscope at the end of the test would reveal the cause of activation (either mechanical or electrical).

UNCLASSIFIED
CONFIDENTIAL

UNCLASSIFIED
CONFIDENTIAL

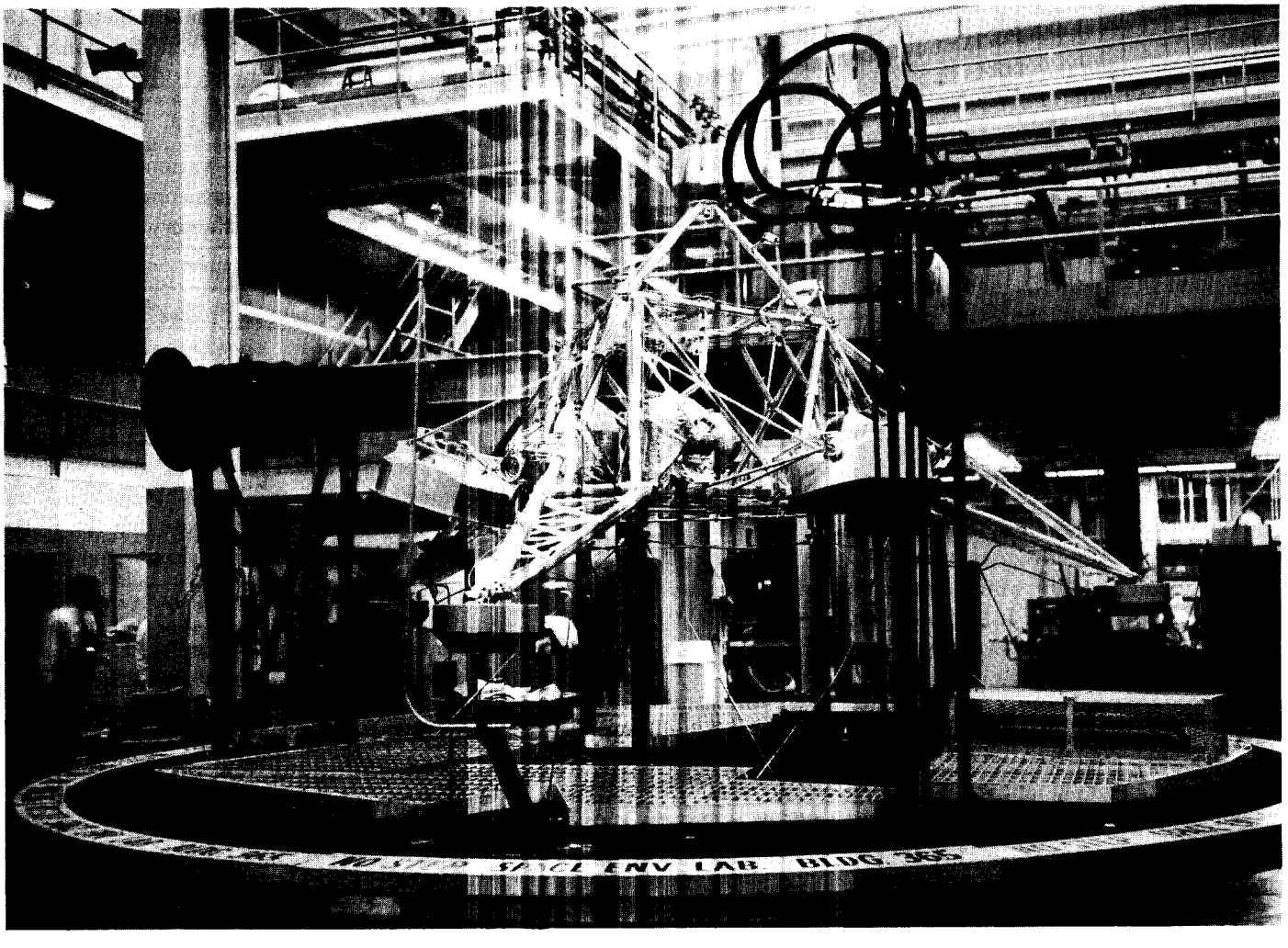

Fig. 70. STV test equipment checkout on chamber end-bell

b. Landing shock hardware. A portable drop ramp was designed and fabricated for the T-21 landing shock tests. The ramp is built in five modules, each consisting of a heavy wooden platform bolted to a structural steel frame. The platform is 4 × 20 ft in size and is inclined at 15 deg. Its surface is studded with wooden cubes 4 in. on a side and spaced 16 in. on centers in staggered rows 8 in. apart (standard lunar surface). A maximum ramp width of 20 ft can be obtained with all modules bolted together.

The drop release mechanism is in final design. For the drops, the vehicle is suspended from a pyramid-shaped spreader formed of tubular steel members. Support cables are fastened at each of the three landing gear hinges, angled out to clear all vehicle interferences, and then routed up the three inclined spreader tubes to a single release point at its apex. Support cables are released by a pneumatic actuator and then travel down the inclined tubes until captured by a restriction at the lower end. This facilitates immediate retrieval of the vehicle after a drop, thereby curtailing the excessive stresses on the landing gear shock struts associated with Earth gravity.

c. TV test pattern illuminator. The test pattern illuminator was designed as a source of approximately 6000°K light for testing the following characteristics of the survey television system: sensitivity, dynamic range, photometry, colorimetry, signal output, and vidicon spectral response.

The unit consists of a lamp chamber which contains two 650-w, quartz-iodine lamps and two reflectors (Fig. 71). Between the lamps and the test-pattern holder are six slots for insertion of filters. The standard complement of filters consists of: (1) three sandblasted pyrex panes which are used purely for diffusion, (2) three nickel-

UNCLASSIFIED
CONFIDENTIAL

UNCLASSIFIED

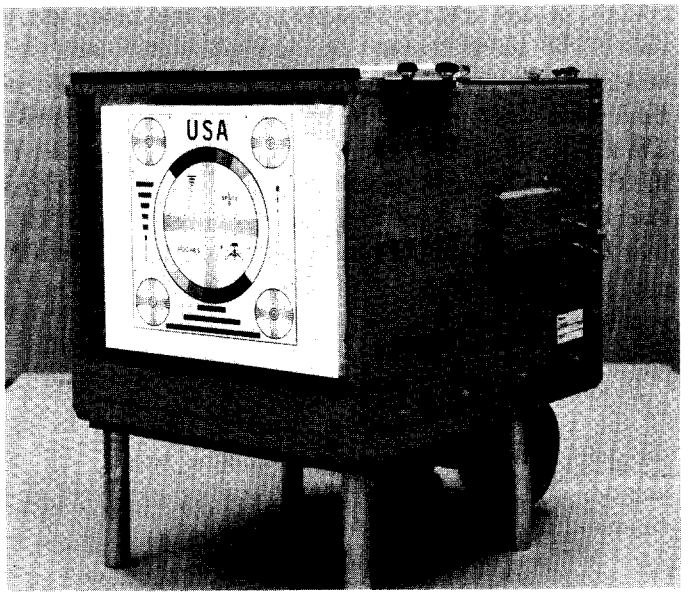

Fig. 71. TV test pattern illuminator

screen absorption filters at 50, 25, and 10% transmittances, (3) a blue, color-corrective filter made of Corning 5900 glass, and tentatively, (4) a filter of Libbey-Owens-Ford heat-absorbing glass, sandblasted, which can provide additional diffusion and color correction. Nearly all interior surfaces of the box which are exposed to incident light rays are made of polished aluminum to minimize light losses. Several choices were provided within the lamp chamber for locations of the lamps and reflectors since the optimal locations for these parts cannot be predicted conclusively in advance.

Initial checkout tests of the first unit were completed. Design of the cooling system was evaluated first; structural adequacy of the unit was checked throughout the tests; and brightness levels, brightness uniformity, and spectral characteristics were measured for various combinations of adjustable features.

In the first part of the test, temperatures were measured at critical parts of the unit. Maximum temperatures were reached within 15 min of turn on. The hottest location, aside from the lamps themselves, was 220°F at the pyrex diffusion filter in front of the lamps. The most sensitive part in the unit, which is the Corning blue filter, reached a uniform temperature of about 145°F, which is safe as long as the glass is allowed to expand properly.

The basic structural design of the unit was found to be adequate. Improvements were recommended in the floor of the lamp chamber, the covers, and the mounting design of the reflectors. The reflector surfaces, which were designed to spread the light from the central to the top and bottom areas, were left unchanged.

The brightness measurements were taken with a Spectra Model SB1-1/2 brightness spot meter. Spectral test results were presented in terms of chromaticity coordinates and blackbody color temperatures. Color measurements were made with a Perkin Elmer Model 112U spectrophotometer, using a blackened thermocouple as a detector. The estimated accuracy of color temperature measurements is ±100°K.

The design objectives of the test pattern illuminator were fulfilled. For the proposed standard configuration, the average brightness is 3340 ft-L and the variation over the whole 8 × 8-in. control area is within ±5% of the average. This standard configuration consists of three pyrex diffusion filters in Slots 1, 3, and 5, where Slot 1 is nearest the lamps, and a Corning blue filter in Slot 6. (The test pattern fits in Slot 7 at the front of the unit.)

For the standard configuration the color temperature is a little over 5400°K in most of the control area, although it drops to an estimated 5100 deg in the right and left margins outside of the control area. This is apparently caused by a differential loss of blue light at low-angle reflections. The nickel absorption screens also cause an appreciable red shift. The same explanation is probably applicable.

Opalized glass diffusion filters were originally to be included in the unit to complement the sandblasted pyrex filters. They were eliminated as a result of the tests, however, for three reasons: (1) their transmission was nonuniform, (2) they reduced the luminance about 25% compared with sandblasted pyrex, and (3) they caused a red-shift of approximately 200°K in the color of the light. The Libbey-Owens-Ford filters of sandblasted heat-absorbing glass were able to raise the color temperature to 6000°K or slightly above, but at a cost of an appreciable green bias and a loss of brightness.

3. Data Acquisition Center

The increasing work load, which often involves more than one spacecraft undergoing systems test simultaneously, has created the following requirements: (1) increased real-time test control, test monitoring, and data acquisition visibility; and (2) increased capability to perform near real-time data playback and processing for analysis. To meet these requirements, a data acquisition center conceptual design was completed.

UNCLASSIFIED

UNCLASSIFIED

The facility will consist of two real-time test monitoring and data acquisition stations, one off-line data playback and editing station, and a data analysis station which will support both the real-time and off-line functions. Adequate digital data analysis equipment will be utilized to properly sort, scale, and limit-check the telemetry and hard-line data. The output format of the data to the analysis station will assure that quick-look and detailed analyses can be performed promptly during test operations.

The development of the data acquisition center is planned in two phases. The first-phase installation will consist of one command and data handling console (CDC) and peripheral equipment, augmented with four FR-1200 tape recorders, a command decoder, and a time code translator. The second phase will include digital data analyzers, additional telemetry processing equipment, and more extensive data displays.

4. SC-1 Flight Acceptance Testing

Group tests were completed on the SC-1 flight spacecraft power subsystem, then the remaining group tests, except RADVS, were performed using the spacecraft power subsystem. Because of the lack of spacecraft units, the flight control, altitude marking radar, and signal processing group tests could not be performed prior to the start of the upgrade period.

System problems encountered to date are:

(1) An interface problem exists between the approach TV camera and the TV auxiliary. Bias on the TV auxiliary input circuits caused the camera telemetry readings to be out of specification.

(2) In checking the automatic solar panel deployment circuits, it was found that no return point existed for the switching logic circuits.

Improvements to correct these problems will be incorporated during the upgrade period. The spacecraft harness will be thermally wrapped in preparation for the solar-thermal-vacuum testing to be accomplished on completion of the system functional test phase.

5. S-8 Vehicle Testing

a. S-8 flight control/vernier propulsion system test. Bracket design for the 26 accelerometers to be used in acquiring vibration data in testing of the S-8 vehicle was completed and the mounting brackets are being fabricated. The accelerometer amplifier packages (each containing three amplifiers) will be located in groups of three near each of the three vehicle leg attachments. Circuit modifications have been made to the amplifier to increase the input impedance and improve the low frequency response. Test and calibration results indicate that the desired flat frequency response from 5 to 2000 cps can be obtained with the Endevco model 2213 accelerometer.

Strain gage instrumentation will be installed on each of the three vernier engine brackets identical to the installation on flight spacecraft. Engine thrust will be monitored and compared with chamber pressures and commands.

Vehicle position and dynamic instrumentation, consisting of two pendulous inclinometers and three low-frequency accelerometers mounted at or near the center of gravity, will be attached to a special bracket. This bracket will replace the separation and arming device at the top of the main retrorocket for the midcourse configuration and will attach to a tripodal bracket mounted at the three retro attach points for the landing configuration (no retro engine). Fabrication of these brackets is progressing.

Fabrication of the signal processing and internal control unit is complete except for the installation of a time delay relay not yet delivered. An emergency automatic engine shutdown feature has been incorporated. This will turn off all engines if one or more of them does not build up to 63-psi thrust chamber pressure within 300 ms $\pm 10\%$ after engines have been commanded on.

The E-2 antenna/solar panel positioner is being upgraded for use on the S-8 vehicle. This includes modification of the collar and base ring to fit the current flight-type spaceframe. Also included will be incorporation of dummy motors, pin puller brackets, and polar axis manual positioning provisions.

The original Compartment A design, which will hold the boost regulator, telemetry unit, signal processing and internal control unit, and battery, is being replaced with a flight-type compartment. This change is based on recent test evidence which indicates that the stiffness of the main box of Compartment A does contribute to the mounting stiffness.

UNCLASSIFIED

UNCLASSIFIED
CONFIDENTIAL

The design change in the flight-type vernier engine mounting has necessitated a design change in the suspension system-to-vehicle attachment bracketry. It was planned to use a solid shaft through the landing gear journal which would pick up the attachment bracketry. Since the new vernier engine bracket now attaches to the journal, a solid shaft through the journal would change the mechanical vibration coupling from the engine to the frame. Redesign of the vehicle attachment bracketry is in progress.

Suspension system modifications resulting from recent tests at AFMDC are being incorporated. They consist of correction of minor problems, such as covering cable clamps to prevent fouling, and relocating the lower tether winch from being directly beneath the vehicle.

b. S-8/RADVS vibration test. This test was conducted to demonstrate satisfactory operation of the radar altimeter and doppler velocity sensor (RADVS) subsystem on a flight-type spaceframe when subjected to the vibrational environment expected to result from firing the vernier engines. The presence of any radar interference attributable to vibratory excitation of the footpads or crushable blocks was explored. Data were taken to establish adequate functional performance criteria for individual antennas when subjected to random vibration.

Equipment arrangement. To meet test objectives, it was necessary to operate the RADVS system in a free field. This was accomplished by mounting the S-8 vehicle (Fig. 72) in an inverted position on a shock cord suspension system (Fig. 73) with the vibration exciters coupled to the vernier engine dummies. The vehicle was mounted with legs extended and crushable blocks installed. Testing took place at the Hughes Culver City plant adjacent to the hangar, Building 45. A RADVS checkout facility was established inside the hangar.

Three Ling A280 shakers, an RP3/5 power amplifier system, and a random console system were used. Drive link assemblies attached the shakers to the vehicle. Endevco piezoelectric-type force gages were installed between the drive links and the vernier engine dummies.

Operation of the RADVS was monitored during random vibration inputs on the basis of engine firings and T-21/QA-1 vibration data from AFMDC tests. Single-engine and multiple-engine vibration testing was conducted to evaluate the effects of correlated and uncorrelated random inputs as test parameters.

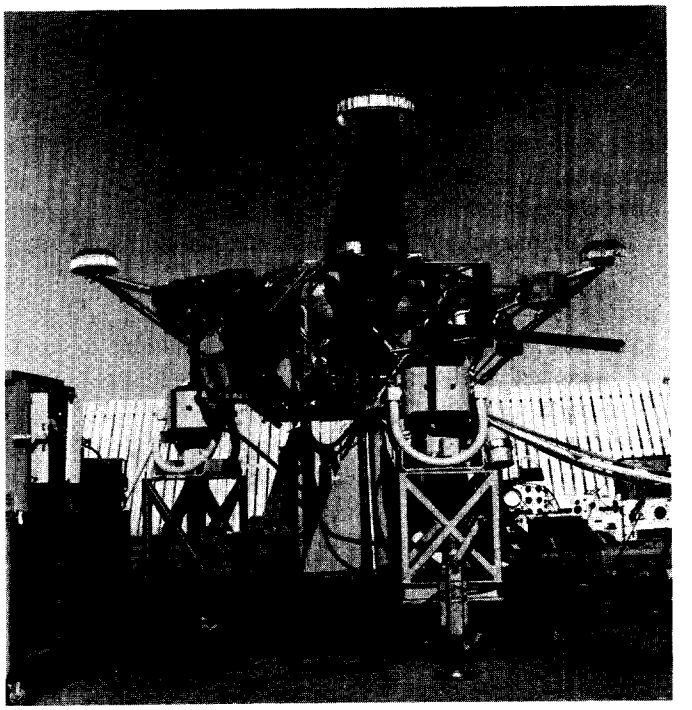

Fig. 72. S-8 vehicle inverted on test fixture with shakers attached to vernier engine dummies

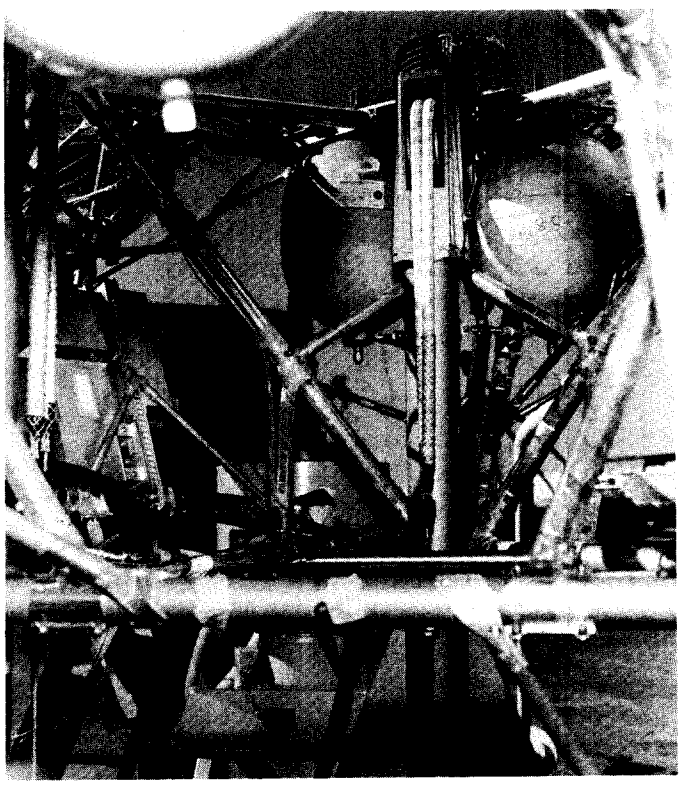

Fig. 73. Shock cord suspension attaching to three *Centaur* interface points

UNCLASSIFIED

UNCLASSIFIED
CONFIDENTIAL

Test configuration. The S-8 vehicle configuration represented the spacecraft just after retro-engine ejection and during vernier engine operation. Vernier engine dummies were installed and used as the vibration input points. Referee fluids (isopropyl alcohol and Freon TF) were used as ballast for the fuel and oxidizer tanks of the vernier propulsion system. The RADVS system tested during this program is to include the AM-1, AM-2, and SN-1.

Vibration instrumentation included piezoelectric-type accelerometers and force gages. The force gages were used to monitor force input at the vernier engines while accelerometers were used to monitor responses at the engines, antennas, KPSM, Leg 1 footpad, and on the power splitter (nonflight type). Endevco 2213 type accelerometers were used except on the power splitter where miniature Columbia Research accelerometers were installed. Fig. 74 shows the transducer locations and provides the annotation for each channel of data.

The vibration data were recorded on two 14-channel tape recorders (Ampex FR100 and Series 800 airborne tape recorder). These channels were recorded on FM from 0 to 2 kc at 15 in./sec. Some RADVS signals were recorded on the FR1300 Ampex tape recorders on FM from 0 to 10 kc at 30 in./sec. Other RADVS signals were recorded on the Honeywell 1612 Visicorder.

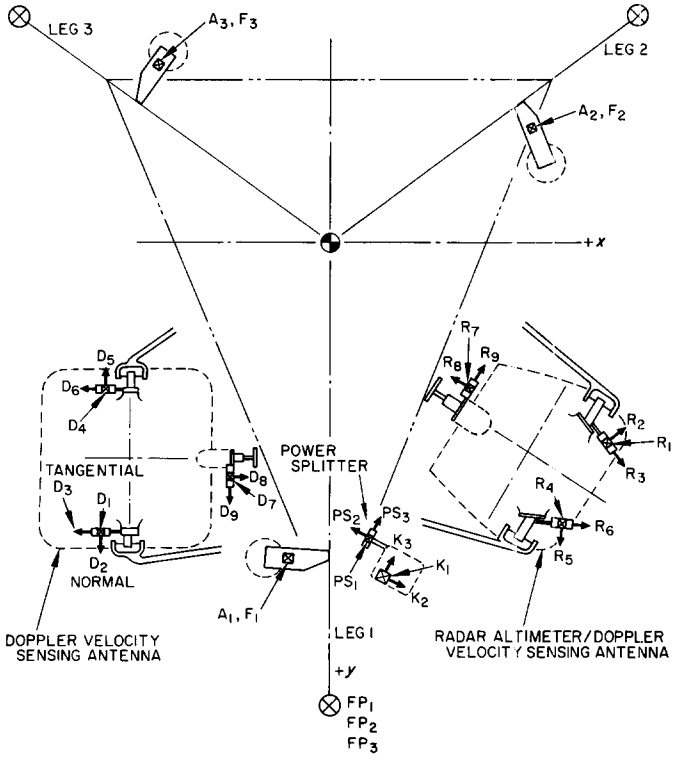

Fig. 74. Transducer locations for *Surveyor* S-8 RADVS test

Calibration tests. The excitation to be simulated during these tests is the force excitation due to operation of the vernier engines. This excitation is believed to be a "white" (i.e., constant) random force spectral density which is unaffected by the response of the spacecraft to this excitation. Further, it was assumed that the excitations from the individual engines are independent, i.e., uncorrelated.

Because of variations in both vibration shaker characteristics and mechanical impedance match between each shaker and the spacecraft, the force spectral density will differ, as a function of frequency, from one engine location to another. This is true even though the same armature current flows through each shaker. However, the three excitations will be correlated. Because of this correlation, the response at a particular point of the spacecraft will be different than the response to three uncorrelated inputs with the same spectral density. The difference will depend on the complex transfer functions between the response point and the three excitation points, as well as the cross correlation between excitations, and may increase or decrease the response compared to the uncorrelated excitation.

Therefore, to simulate the three white, independent vernier engine excitations, a nonwhite spectral density excitation was derived empirically from five calibration tests. In three of these five tests, white noise excitation at 7-lb rms overall was applied singly to each of the three engine locations, with the other two shakers disconnected from the spacecraft. White noise at 7-lb rms was then applied to all three engines simultaneously, with the excitation at Engine 1 used for control and equalization. This excitation was then repeated, except that the sum of the output signals of the three force gages (summed and averaged signal, ΣF_i) on an instantaneous basis was employed for equalization and control. Control by both these methods was used to determine the better control method for the operating tests. Engine 1 was chosen, since it caused the greatest response of the RADVS antennas during the T-21/QA-1 vibration tests. The responses at five representative points of the spacecraft were measured for determination of the correction factor to be applied to the nominal white noise spectral density. A correction factor was computed for each of

UNCLASSIFIED
CONFIDENTIAL

UNCLASSIFIED

the 25 equalization bandwidths between 84 and 2000 cps, based on the responses at the five spacecraft locations and the relative vibration sensitivity at each point.

Vibration test operations and results. After equalization of the random vibration spectrum to the desired level, the instrumentation tape recorders were started and the "on-line" spectral density analysis of the control signal initiated. Vibration was applied continuously for approximately 9 min to permit recording of a sufficiently long data sample for later spectral analysis. The "on-line" analysis, used to check the equalization, consisted of an x-y plot using a 6-min sweep from 50 cps to 2.5 kc, a 20-cps bandwidth filter, and a 2-sec time constant. The filter output was squared and detected prior to log conversion for x-y plotting. Except when reequalization was necessary, test level control was achieved by control of the overall rms level at the control signal.

In general, the RADVS system was operated during the first 2 min of each test run. Equalization for the tests was performed at 10-lb rms overall (the quoted level for the summed and averaged signal is also approximately the level at each engine location). The tests at higher levels were controlled by increasing the rms signal by the appropriate factor, without any attempt to reequalize the system, to reduce both the elapsed test time as well as the cumulative vibration exposure of the spacecraft. Checking of the "on-line" spectral analyses indicated that the system is quite linear over the range of excitations employed since the equalization is not greatly changed up to 56-lb rms.

Detailed spectral analyses at the force excitations and acceleration responses for the numerous test runs have not yet been completed. However, the overall rms levels for the force gages and accelerometer signals have been measured. While the force gage and vernier engine accelerometer levels (F_i and A_i) followed the summed and averaged level quite well, it appears that response levels at locations remote from the vernier engines were less linear.

In general, the results to date seem to indicate that the excitation method, using three shakers driven from a single power amplifier, has proven to be quite satisfactory. Use of multishaker excitation for random vibration testing, particularly with force rather than acceleration control, has not been used previously so far as can be determined.

RADVS test operations and results. Preceding the vibration tests, an abbreviated RADVS group quantitative checkout was conducted. This pretest checkout required a special RADVS system test equipment assembly (STEA) arrangement and waveguide connection (Fig. 75). At the completion of a vibration phase, the vehicle was returned to the hangar for a posttest checkout and reinstallation of the succeeding RADVS system.

On line RADVS testing consisted basically of monitoring the RADVS signals. This information related preamplifier residual noise. Therefore, preamplifier outputs which locked up could be observed during the various phases of vibration testing. Since this was the first time the RADVS system was vibrated in a spacecraft while operating in a free field, additional tests were conducted with antenna dummy loads installed. Results of these tests provided calibration for the RADVS for future vibration tests when dummy loads may be required. Prior to vibration tests on a particular RADVS system, a check was made on site to verify adequate system operation by using a blitz wheel, a test instrument that creates a known doppler shift.

Detailed spectral analyses of the preamplifier outputs for the test runs have not been completed. However, both AM-1 and AM-2 RADVS systems operated satisfactorily, going to 5 times actual anticipated vernier engine excitation levels.

The AM-1 and AM-2 RADVS systems were subjected to random inputs of 10-, 14-, 20-, 28-, 40-, and 56-lb rms at each engine in the frequency range of 50 to 2000 cps. Tests on the AM-1 included both an instrumented and flight-type power splitter. AM-2 was tested with a flight-type power splitter only.

Calibration runs were conducted on the AM-1 RADVS system with dummy loads on the antenna. Test runs included excitation levels of 10-, 20-, 28-, 40-, and 56-lb rms per engine with no lockups encountered in the radar system.

The instrumented power splitter on the AM-1 RADVS system was replaced by the flight-type power splitter. Tests were run at 10-, 28-, and 56-lb rms with successful operation of the flight RADVS system. The vehicle was returned to the hangar test area and an abbreviated checkout of the RADVS system was performed with satisfactory operation.

UNCLASSIFIED

UNCLASSIFIED
CONFIDENTIAL

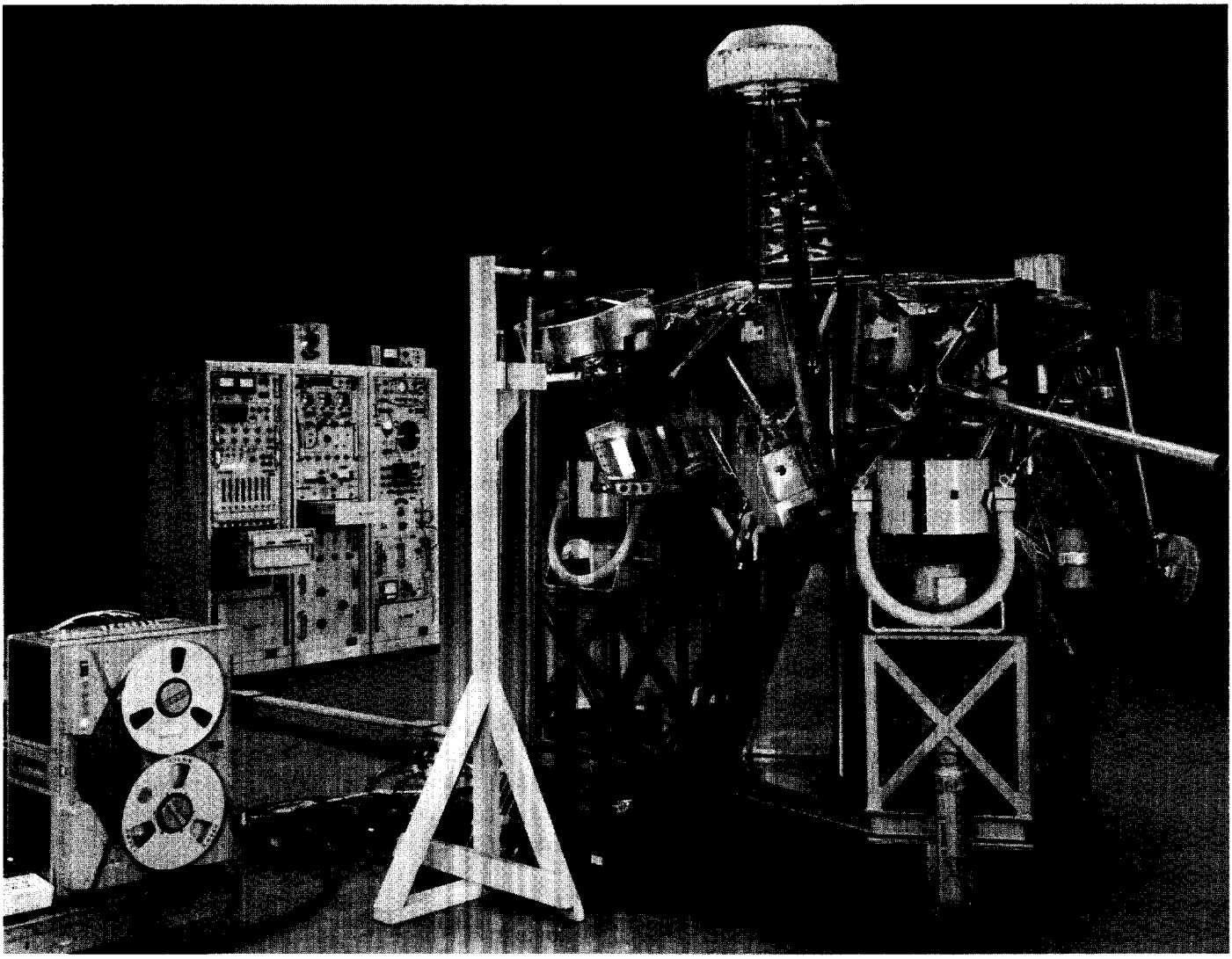

Fig. 75. RADVS/STEA setup for RADVS checkout

After AM-2 RADVS installation, the system was instrumented and checked out satisfactorily in the hangar area. The AM-2 system was moved to the test site. Tests were run at 10-, 14-, 20-, 28-, 40-, and 56-lb rms per engine with satisfactory operation of the RADVS system. Calibration tests were conducted on the AM-2 RADVS at 10-, 28-, and 56-lb rms per engine with dummy loads attached to the antenna feedhorns.

From the results of T-2 firings at AFMDC the engine accelerometer level measured was on the order of 1.8-*g* rms. Engine responses for the S-8/RADVS vibration tests measured as high as 10.5-*g* rms, indicating a rather large margin of satisfactory RADVS operation.

6. *T-2 Closed Loop Test Program*

The T-2 closed loop test program was initiated to improve evaluation of the flight control electronics to increase confidence in performance of the system and hardware in a configuration as close as possible to the mission. The tests were conducted at AFMDC, where the T-2 vehicle, cables, test equipment, and hardware could be used in the flight configuration. The closed loop simulation equipment was modified from the T-21 STEA for the T-2 configuration and mission profile.

The tests were performed as a mixed simulation in which the closed loop equipment was utilized to simulate the electrical analog of the T-2 vehicle geometry and

UNCLASSIFIED
CONFIDENTIAL

UNCLASSIFIED

dynamics, the vehicle mass, aerodynamic drag, and engine thrust. The gyros and accelerometer were electrically torqued. The RADVS was alternately replaced by the electrical transfer function and included in the system such that only the microwave operation was simulated by the STEA. Velocity and rate loops were closed and examined for stability and performance in simulated mission profiles. The equipment was exercised in the simulated mission and examined for conformance to the performance requirements.

The test program was designed to evaluate the flight control electronics in a simulated dynamic condition in the planned T-2 drop missions. The tests were arranged to meet the following three configurations: (1) radar attitude control, (2) acceleration loop, and (3) trajectory control. The program included testing of the flight control electronics with simulated radar response to close the velocity loop and a series of tests with the RADVS hardware included. Acoustic and radar noise were introduced to evaluate system performance. The noise was derived from actual tapes of acoustic noise taken during vernier engine firings and radar electronic noise taken during the T-2H helicopter flights. The radar was studied in the closed loop configuration with varying signal strengths.

The acceleration loop was investigated with varying initial conditions of specific impulse, mass, time delay, and initial angle. The effect of the radar signal strength was also examined.

A series of tests was conducted to measure the characteristics of the inner rate loop stability. The high and low crossover frequencies and associated gain margins were recorded. The phase margin was measured by introducing disturbances into the loop. The effect of a step response was also measured. The tests were conducted for both the pitch and yaw channels.

The T-2 closed loop test program verified that the T-2 vehicle flight control hardware performs in accordance with the design requirements and mission objectives. The equipment is stable under simulated system operation. The system parameters were measured to correspond to the results of the analog computer and design analysis studies which define the T-2 flight control system. The integration of the RADVS with the flight control electronics resulted in a compatible system in closed loop operation. Injection of acoustic and electronic radar noise at system operation levels resulted in performance which is acceptable for mission success.

7. T-2S Descent Testing

The test profile was programmed to separate the T-2S vehicle with the vernier engines in low thrust. Constant high thrust was programmed 5 sec after separation, providing radar lockon was acquired. The test was programmed for termination at 22 sec after separation and at an altitude of approximately 600 ft.

Because of onboard malfunctions, high thrust was not accomplished nor was engine shutoff accomplished at the programmed altitude. Emergency recovery was commanded, but the main parachutes were not deployed. The vernier engines remained on until touchdown. The resulting impact represented a 40- to 45-g landing.

Table 24 lists the five discrete failures which occurred in the onboard equipment, summarizes the specific nature of each malfunction, and shows localization of the failure down to the subunit level.

Table 24. Malfunction summary

Failure number	Observation	Malfunction	Failure location
1	Continuous slow roll (0.1 revolutions/sec)	Roll control loop not working after engine ignition	Failure of roll amplifier inflight control electronics unit
2	RADVS shutoff	13-ft mark prematurely generated at 3.5 sec	Intermittent failure of range converter circuitry in RADVS/SDC
3	Oxidizer manifold dump not activated	Squib failed to fire	Short between bridge wires in squib
4	Recovery chute not deployed	Drogue chute properly deployed but could not pull main chute out of pack	Tow wire was 20 deg from vertical at release and moved above spacecraft during drop; this combined with roll caused twisting around recovery drogue chute shrouds preventing breakaway force from deploying main chute
5	No engine shutoff at emergency recovery	Recovery bus power not received at engine valve power relay	Diode failure in turnoff circuitry of electronic auxiliary

UNCLASSIFIED

UNCLASSIFIED
CONFIDENTIAL

L. System Analysis

1. Marker Radar Backup Analysis

The purpose of the altitude marking radar is to provide an accurate measure of distance from the spacecraft to the Moon in order to initiate terminal descent operations. It is also possible to fire the retro based on orbit determination alone, in which case ignition would occur at the expected time that the altitude reached the desired ignition altitude. However, the variation of the actual altitude from the expected altitude is about 27,000 ft (3σ), based on a 3-sec (3σ) accuracy of time of flight. Such a variation of ignition altitudes would frequently result in burnout altitudes far beyond the capability of the *Surveyor* descent system. That is, burnout would occur in an acceptable region (from the point of view of vernier fuel and thrust constraints) only about 60% of the time. Therefore, the altitude marking radar is used to generate a much more accurate measure of ignition altitude. However, if the radar has failed, it is clear that the retro-engine should be ignited on the basis of orbit determination, thus increasing the probability of success from zero to about 60%. If, during a mission, the expected marking time is passed without a mark having occurred, there comes a time when the probability of a bad radar is sufficiently great that the probability of successful descent is increased by ignition on the basis of orbit determination.

It is evident that this time depends on the reliability of the radar and the accuracy of the orbit determination. For example, if the accuracy of the orbit determination is low, a long time should be allowed to elapse between the expected marking time and the time that the Earth command for retro ignition is transmitted. On the other hand, if the radar reliability is low and the orbit determination accuracy is high, optimum performance would be expected if the ignition command were transmitted shortly after the expected marking time.

The optimum waiting time as a function of these two parameters has been determined using the theory of probability. If the signal denoting a mark has not been received by the Deep Space Instrumentation Facility (DSIF) prior to a certain time t, the ignition signal is transmitted to the spacecraft. By this means, it is possible to increase the probability of success above the reliability of the radar. If this reliability is 0.99, the maximum gain is 1%. However, if, because of an in-flight test or an unusually severe liftoff environment, the reliability estimate is reduced to 75 or 50%, substantial benefit can be achieved.

2. Effect of Removing the Marker Radar

As orbit determination capability increases, the question arises as to the possibility of initiating the terminal descent by Earth command, without benefit of the marker radar. This possibility is evaluated by assuming the reliability of the radar to be zero. The optimum ignition time is then

$$t_i = t^* + T \tag{1}$$

where t^* is the expected time at the marking altitude and T is the delay between mark and fire signals. The resulting probability of mission success is then found to be

$$P_s = \frac{1}{(2\pi)^{1/2}} \int_{-a}^{a} e^{-x^2/2}\, dx \tag{2}$$

where

$$a = \frac{3\sigma_h}{(\sigma_h^2 + V^2\,\sigma_t^2)^{1/2}} \tag{3}$$

σ_h^2 and σ_t^2 are variances of the burnout altitude (given ignition altitude) and arrival time (based on orbit determination). V is the vertical component of the approach velocity.

Eq. (2) is evaluated by means of a table of the normal probability integral. In particular, if $\sigma_t = 0$ (perfect ignition), then $a = 3$ and $P_s = 0.997$. This results from the assumption that only enough fuel is provided to take care of the current 3σ altitude dispersions.

Fig. 76 shows the effect of orbit determination accuracy on probability of success when $V = 8800$ ft/sec and $\sigma_h = 3000$ ft.

3. DSIF Acquisition Time Constraints

The original *Surveyor* spacecraft design was based on the assumption that a maximum time of 5 min would be required for initial acquisition of the spacecraft by the Johannesburg DSIF station. More recent estimates give times appreciably longer than the earlier estimates. A study was undertaken to establish DSIF acquisition time requirements consistent with the spacecraft design to assure acquisition with a high level of confidence. The requirements were based on doppler tracking demands, command capability, and telemetry needs (Fig. 77).

a. Spacecraft to ground acquisition threshold. For normal conditions (assuming automatic Sun acquisition), the spacecraft roll axis will be oriented toward the Sun during DSIF acquisition. For worst-case geometry and

CONFIDENTIAL
UNCLASSIFIED

UNCLASSIFIED

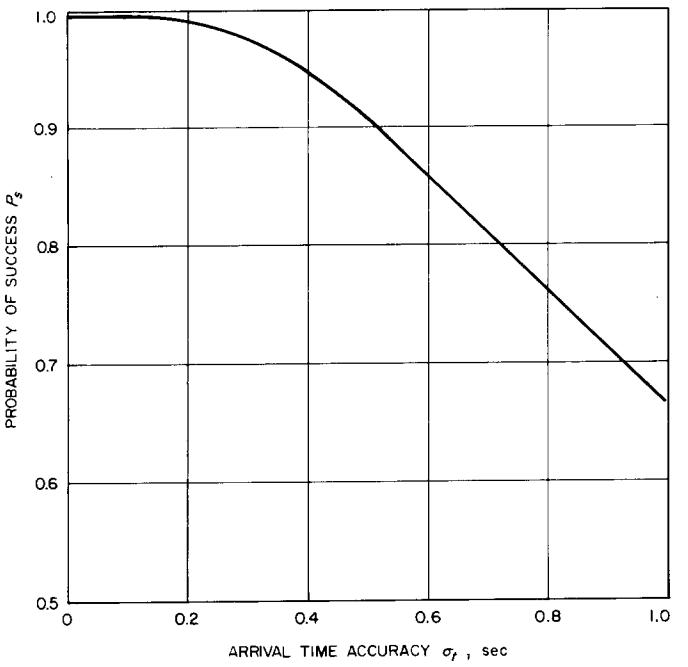

Fig. 76. Probability of success vs arrival time accuracy (marker radar removed)

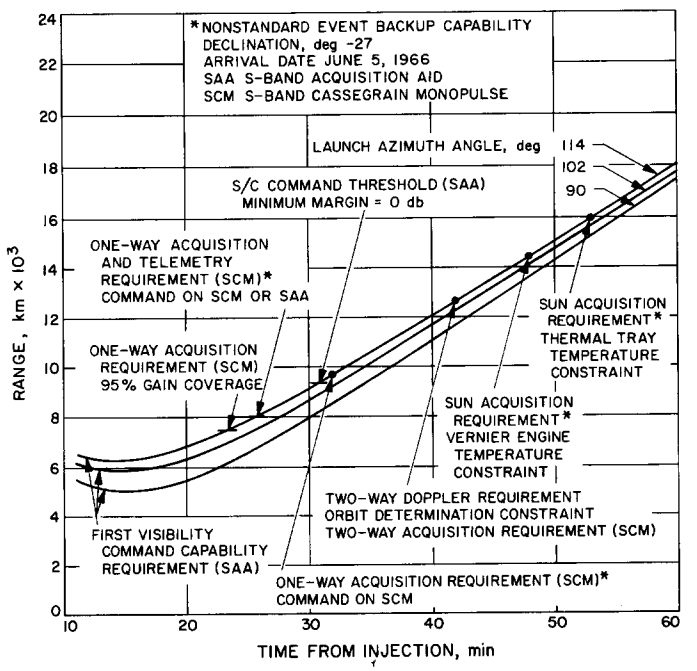
*NONSTANDARD EVENT BACKUP CAPABILITY
DECLINATION, deg -27
ARRIVAL DATE JUNE 5, 1966
SAA S-BAND ACQUISITION AID
SCM S-BAND CASSEGRAIN MONOPULSE
LAUNCH AZIMUTH ANGLE, deg
114
102
90
S/C COMMAND THRESHOLD (SAA)
MINIMUM MARGIN = 0 db
ONE-WAY ACQUISITION AND TELEMETRY REQUIREMENT (SCM)* COMMAND ON SCM OR SAA
ONE-WAY ACQUISITION REQUIREMENT (SCM) 95% GAIN COVERAGE
SUN ACQUISITION REQUIREMENT* THERMAL TRAY TEMPERATURE CONSTRAINT
SUN ACQUISITION REQUIREMENT* VERNIER ENGINE TEMPERATURE CONSTRAINT
TWO-WAY DOPPLER REQUIREMENT
ORBIT DETERMINATION CONSTRAINT
TWO-WAY ACQUISITION REQUIREMENT (SCM)
FIRST VISIBILITY COMMAND CAPABILITY REQUIREMENT (SAA)
ONE-WAY ACQUISITION REQUIREMENT (SCM)* COMMAND ON SCM
RANGE, km × 10^3
TIME FROM INJECTION, min

Fig. 77. DSIF acquisition requirements

with a random roll orientation, the spacecraft antenna gain level that will be exceeded approximately 95% of the time is −24 db. With this gain level, threshold conditions on the S-band acquisition aid (SAA) antenna are reached at a range of 7450 km, which occurs at approximately 24 min after injection. Thus one-way acquisition on the big dish [S-band Cassegrain monopulse (feedhorn and bridge system)] (SCM) should be completed by this time. If not, the probability of acquisition on the SAA antenna will start decreasing as the range increases.

b. Ground-to-spacecraft command threshold. There are numerous spacecraft failures for which corrective action is possible if commands can be sent to the spacecraft. Table 25 lists these possible nonstandard events which could occur prior to acquisition and which could cause difficulty in acquiring the spacecraft. Command capability is required in these conditions to activate the redundant equipment or initiate the backup modes.

The command link threshold signal condition, when using the S-band acquisition aid (SAA) antenna, occurs at a range of 9200 km, which is reached at approximately 31 min after injection. Thus all "blind" commands (those transmitted over the SAA antenna without knowing the spacecraft angle location or receiver frequency) must be transmitted prior to this time to have a high probability of being successful. That is, command capability over the SCM antenna (which implies at least one-way acquisition) must be established by this time to provide continued backup command capability.

A nonstandard condition of special note is the failure to acquire the Sun automatically. To overcome such a failure before any permanent damage to the spacecraft occurs because of the wrong Sun orientation, spacecraft telemetry and command capability must be established prior to 32 min after injection. This leaves just enough time to perform the required manual operations and achieve the proper orientation before the first susceptible item in the spacecraft (the vernier engine system) reaches its survival temperature limit for worst-case solar orientation.

c. Telemetry requirements. In addition to command capability, it is also necessary to receive spacecraft telemetry to use the spacecraft nonstandard capability effectively. Telemetry is essential to recognize certain malfunctions, determine the corrective action, and evaluate the results. Thus it is required, somewhat arbitrarily, that telemetry be received at least 5 min before the command threshold is reached. That is, telemetry should be available (which implies at least one-way acquisition on the SCM antenna) at least by 26 min after injection.

UNCLASSIFIED

UNCLASSIFIED
CONFIDENTIAL

Table 25. Nonstandard event possibilities

Nonstandard event	Event known at time of acquisition	Acquisition possible with failure	Effect of malfunction	Backup capability
Transmitter fails to go to high power	Yes (downrange)	Unlikely Probably <70%	Spacecraft will not be acquired unless antenna gain is above —5 db	Blind command high power on
Transmitter fails completely	Yes (downrange)	No (without backup)	No acquisition unless blind commands are effective	Blind command to other transmitter
Spacecraft in deep antenna null	No	No (without backup)	Spacecraft will not be acquired unless the spacecraft rolls out of the null	Blind command to other antenna
Omnidirectional antennas not extended	Yes (downrange)	Yes	Possible degradation in antenna gain coverage Uncertainty in antenna patterns resulting in bad prediction data	Command omni-directional antenna extension
Landing gear not extended	Yes (downrange)	Yes	Spacecraft will not Sun-acquire automatically Spacecraft may be tumbling at 3 deg/sec (3σ) Omnidirectional antennas will not be extended Gas jets not enabled	Command leg extension, omni-extension, Sun acquisition
Gas jet system not enabled	Yes (downrange)	Yes	Spacecraft will not Sun-acquire automatically Spacecraft may be tumbling at 3 deg/sec (3σ)	Command gas jet enable, Sun acquisition
Automatic Sun acquisition failure	Yes (downrange)	Yes	Thermal problems may occur	Command Sun acquisition

d. Conclusions. The acquisition requirements are given in Fig. 77. One-way carrier acquisition on the 85-ft dish should be completed within 24 min from the time of injection (which is 12 min from first visibility for direct ascent trajectories) to have no degrading effect on mission success. Telemetry should be acquired within 26 min from injection (14 min from visibility) with command capability of the 85-ft dish being required 6 min later or at 32 min after injection (20 min after visibility). Finally, two-way acquisition on the 85-ft dish should be accomplished by 42 min from injection (30 min after visibility) to meet present orbit determination requirements.

4. Automatic Sun Acquisition Considerations

In the initial spacecraft design, Sun acquisition and orientation was initiated manually by ground command and took place while being monitored via the spacecraft-to-ground telemetry link. Thus DSIF acquisition was a prerequisite to Sun acquisition. In addition, proper spacecraft thermal control is dependent on proper Sun orientation, and early Sun acquisition is required to establish the proper thermal environment.

Recent concern about the time required for DSIF acquisition and the possibility of this acquisition being delayed as long as 30 to 60 min has led to several studies regarding the advisability and feasibility of incorporating an automatic Sun acquisition mode that does not require any commands or monitoring by the DSIF. Study conclusions indicate that it is desirable to add a new acquisition Sun sensor which is not affected by other than direct sunlight and which will eliminate the threat of Earthlight interference during early Sun acquisition. Placing this unit on the flight control sensor group eliminates dependence on previous proper positioning of the solar panel and permits earlier Sun acquisition initiation.

CONFIDENTIAL
UNCLASSIFIED

UNCLASSIFIED

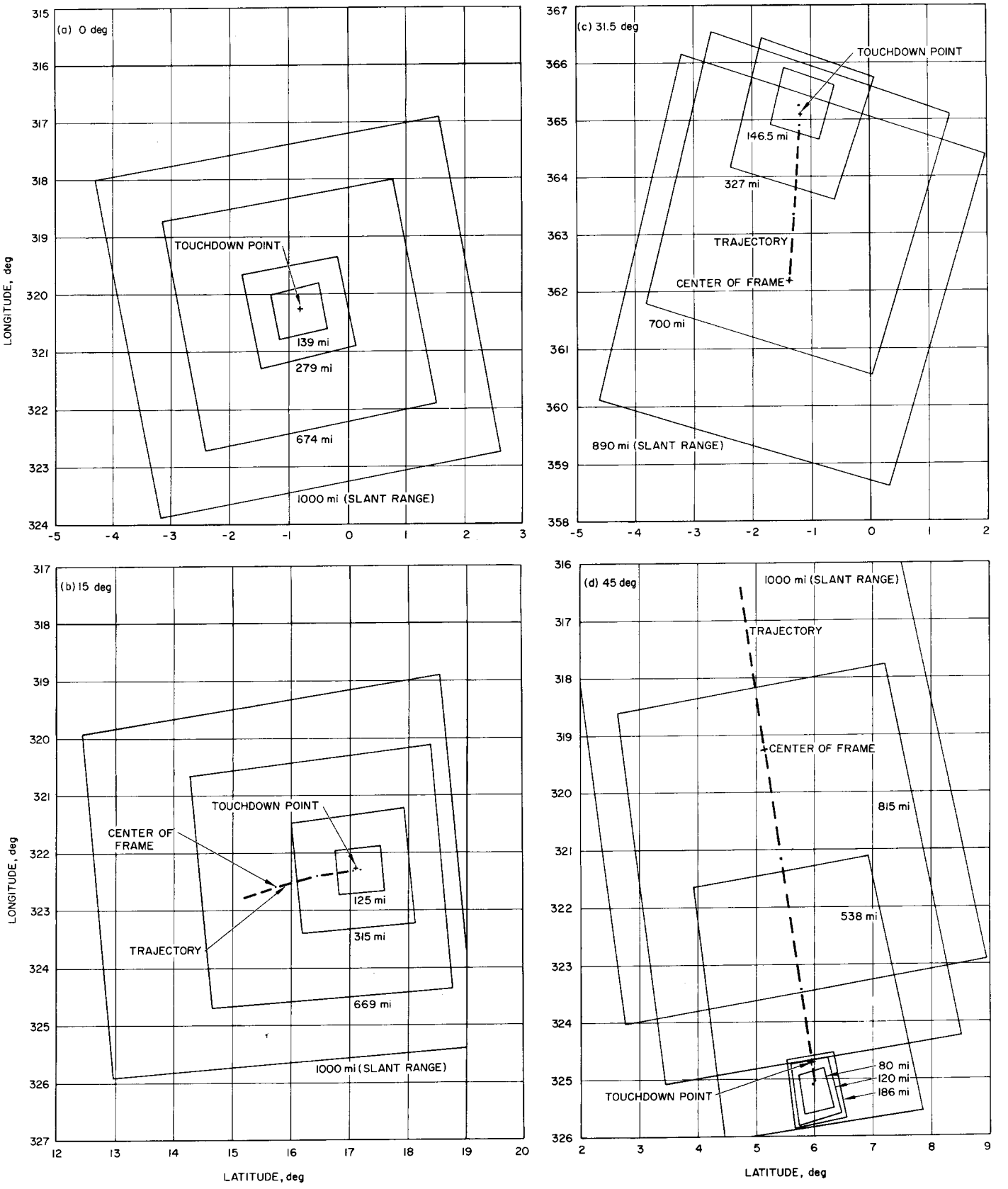

Fig. 78. Descent TV coverage unbraked impact angle

UNCLASSIFIED

UNCLASSIFIED
CONFIDENTIAL

Addition of the capability to acquire the Sun automatically will eliminate the threat of temperature extremes as long as Sun acquisition takes place within 60 min after launch. The present secondary Sun sensor should be retained on the solar panel to serve both as a backup for Sun acquisition and for necessary lunar operations.

5. Descent TV Picture Plots of Lunar Surface Coverage

Fig. 78 shows descent TV picture coverage of the lunar surface for unbraked impact angles of 0, 15, 31.5, and 45 deg. For 0, 15, and 31.5 deg, the touchdown point is contained in the last frame shown. For these three cases, although the last frame at 80-mi (statute) slant range is not shown, the touchdown point is contained within this frame. In the 45-deg unbraked impact angle case, the touchdown point is contained within the frame at 120-mi slant range, but not in the last frame at 80-mi slant range. At this last frame, the distance between the touchdown point and the edge of the TV picture is approximately 1.86 statute mi.

6. Processing of System-Test Telemetry Tapes Using Surveyor Management Computer Programs

One of the major objectives in the development of engineering management computer programs (Fig. 79) is the processing of system-test spacecraft data. Engineering management computer programs necessary to perform a complete analysis of system-test spacecraft telemetry data are: (1) engineering data reduction program, (2) sequence translator program, (3) power management program, and (4) thermal management program.[8]

System-test telemetry data will consist of a command sequence tape and a spacecraft telemetry tape. The command sequence tape will consist of commands given to the spacecraft, each with an associated time in order of increasing time. The spacecraft telemetry tape will be composed of frames of actual spacecraft data corresponding to the sequence of commands contained in the command sequence tape. The spacecraft telemetry tape will be processed in the engineering data reduction program (EDR). The EDR will reduce a number of samples of each telemetry data point to arrive at a mean and variance for each data point interval, having discarded those samples which are more than 2.5σ from the mean or have bad parity. With each set of data, point means and variances will be the associated time. The EDR will also read the command sequence tape and eliminate or discard data which occur during the execution of a command by the spacecraft. The processed data provided by the EDR (PDATA and TDATA Tables), i.e., power and thermal data tables, will be in a form acceptable by the power management and thermal management programs, respectively.

The command sequence tape will be processed by the sequence translator program (STP) for use by the power management program. The STP will reformat the command list of the command sequence tape, eliminating

[8] For the first T-21 thermal vacuum tests, processing of system-test telemetry data will not include utilization of the thermal management program because of the amount of work required to provide a transit model (parameters) that will match the thermal vacuum simulation.

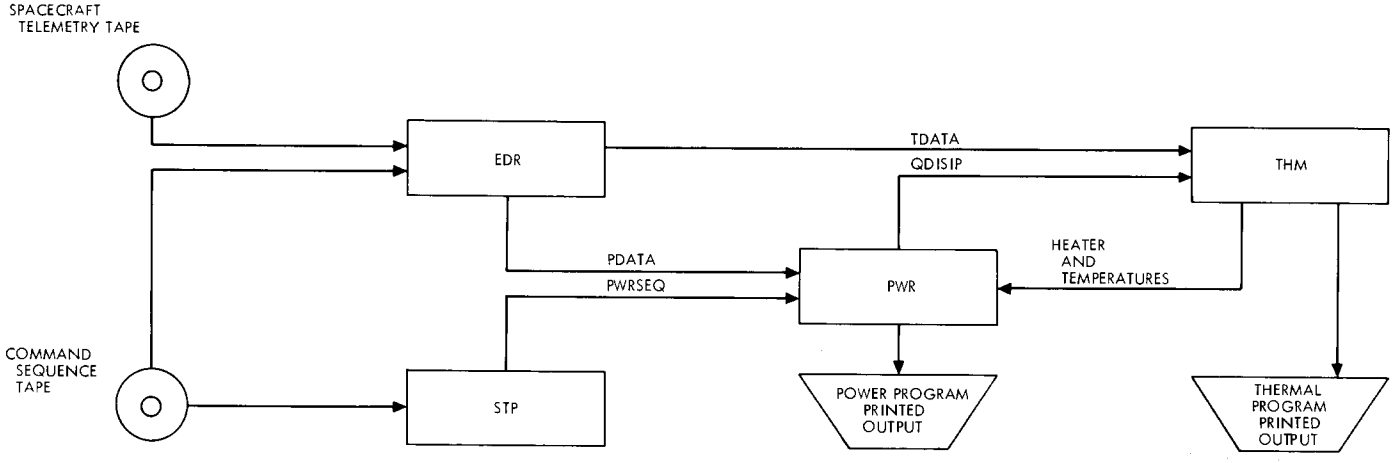

Fig. 79. Engineering management program interface

UNCLASSIFIED
CONFIDENTIAL

UNCLASSIFIED
CONFIDENTIAL

commands which do not affect the spacecraft power system. This abridged and reformatted command list (PWRSEQ Table) will be in the form acceptable to the power management program.

The power management program utilizes both the PWRSEQ and PDATA Tables (the processed command sequence tape and spacecraft telemetry tape, respectively) to predict values of spacecraft telemetry data points as a function of the command sequence, to compare predicted values with actual values at equivalent times in the command sequence, and to bookkeep important power system parameters such as battery energy. After each command, the power management program will compute the values of power system parameters, including most spacecraft telemetry data points, and compare the computed values to the actual values from the PDATA Table.

The power management program outputs dissipation information for use by the thermal management program (THM) in the QDISIP (power dissipation table). The THM uses the QDISIP information and the TDATA temperature data points and outputs temperatures of power systems elements (TEMPS Table), as well as heater temperatures (HEATER Table), for use by the power management program.

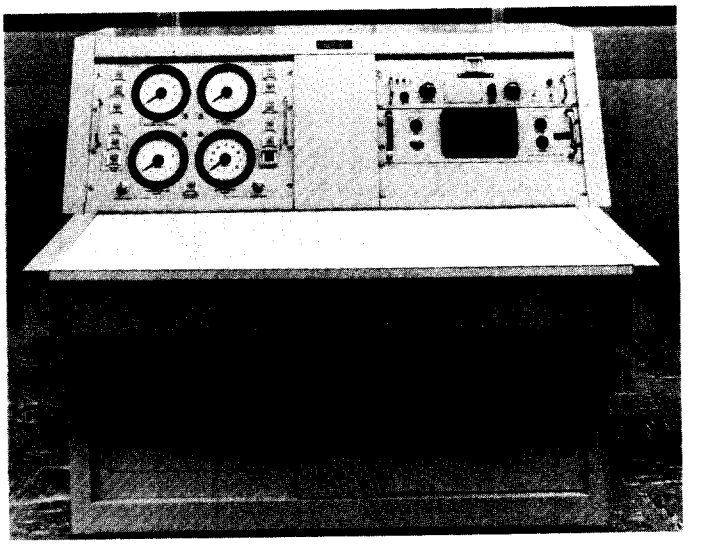

Fig. 80. *Surveyor* operations console

continuity and isolations checks (conductor-to-conductor and conductor-to-electrical ground) were made on all hardline connections. A complete operational checkout of the equipment was made, and the following functions were monitored to the simulated *Surveyor* spacecraft: transponder system *on* command, transponder system *off* command, transponder transfer-switch low power, transponder transfer-switch high power, battery pressure parameters simulation, ready-to-launch command, and prelaunch power supply commands.

Shipment was made to the Air Force Eastern Test Range for installation in Launch Complex 36A. The operations console received considerable damage during transit; the dynamic-model-unique panels (i.e., ready-to-launch, digital voltmeter, and control and monitor) were packaged separately and appeared to be undamaged. These units were returned to Hughes Aircraft Company and are presently undergoing checkout and recalibration.

M. Launch Operations

1. *Surveyor* Operations Console and Launch Control Rack

The SN-1 *Surveyor* operations console (Fig. 80) and launch control rack were completed in the dynamic-model configuration and accepted by JPL and Air Force Quality Control. Preparation for technical acceptance was accomplished by simulating blockhouse and transfer room installation by hardline connections between the *Surveyor* operations console and the launch control rack. A test breakout box enabled insertion of line and load impedances simulating launch complex cabling impedances on the required signal characteristics. Electrical

2. Safety Console

The safety console (Fig. 81) has been completed and is undergoing quality-control and engineering evaluation testing to verify that the unit is capable of meeting the operational requirements. The operating characteristics of the toxic gas detector, emergency power system, and the pulse generator utilized in dumping spacecraft high-pressure gases will be determined, and correct operation of all controls and monitoring devices will be verified. The evaluation testing also provides an opportunity to conduct an operator familiarization program.

UNCLASSIFIED
CONFIDENTIAL

UNCLASSIFIED
CONFIDENTIAL

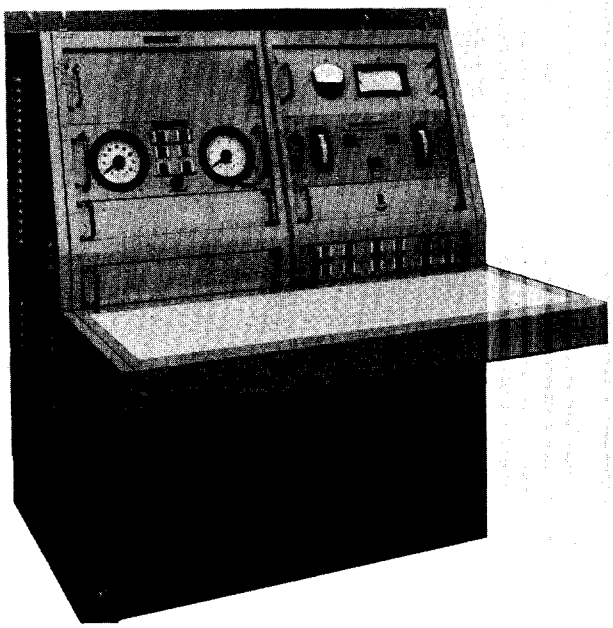

Fig. 81. Launch operations safety console

N. Space Flight Operations

1. Command and Data Handling Console/Deep Space Instrumentation Facility Compatibility

Progress was achieved by Hughes Aircraft Company (HAC) personnel at the Goldstone Tracking Station toward resolution of the problem areas uncovered by the compatibility test series. Action was completed on the following:

Deep Space Instrumentation Facility (DSIF) serial time code. Interim field modifications were incorporated to allow the count up–down clock to respond to negative pulses as supplied by the DSIF (rather than the positive pulses which were originally specified by JPL) and to prevent loading of the DSIF timing signal by the command and data handling console (CDC) low-frequency oscillograph. Subsequent tests indicated that these modifications satisfactorily corrected the problems. However, another problem was uncovered: lack of index markers in the DSIF time code, causing the clock to run slow because 2 pps for sync is not actually being supplied. This problem is currently being resolved.

Low-bit-rate instability. An interim field modification to the pulse-code modulated (PCM) decommutator was incorporated to correct the marginal operation of the decommutator at 17.2 bps.

3.3-Mc filter–amplifier noise bandwidth. The frequency response of this unit was rerun to determine its noise bandwidth and its effect on the TV/RF subsystem performance. The results will be utilized to evaluate retests required of interface signal-to-noise ratios at various IF bandwidths near RF threshold.

RF voltmeter damping. Large capacitors were added across the metering circuit of the Ballantine 320A RF voltmeter to reduce the fluctuation and, hence, the measuring accuracy of noise levels. Tests and calibration were made to confirm that the basic accuracy of the voltmeter was not affected.

2. CDC/On-Site Data Processing Modification Program

A modification program that will interface the basic CDC with two on-site computers at each DSIF station and with a JPL-furnished modem at the Air Force Eastern Test Range installation is being designed and fabricated. The purposes of the program are:

(1) To present all real-time PCM telemetry received at the CDC to a SDS 910 or 920 computer in a form such that the computer can identify and process the data being received. The computer then interfaces with high-speed data lines which carry the edited data to the JPL Space Flight Operations Facility (SFOF).

(2) To present all command information, as it is being transmitted to the spacecraft, to the computer in a form such that the computer can process the message for transmission to the SFOF. Only command messages being transmitted to the spacecraft can be processed by the computer. Sequence numbers appearing in the R-register cannot be transmitted to the SFOF.

(3) To provide the capability to punch 7-level command tapes at the CDC as command messages are received from the SFOF. In addition, the tapes can be read by the CDC tape reader, sent to the computer, and retransmitted to the SFOF for verification.

UNCLASSIFIED
CONFIDENTIAL

UNCLASSIFIED

(4) To provide the capability to automatically search a command tape for any given sequence number. This is accomplished by using the input/output typewriter to send to the computer the sequence number desired. The computer, through the use of a preprepared program, determines the direction in which the tape reader should drive to bring the desired sequence number under the reader. The computer then automatically drives the tape to the desired location.

The system can be broken down into three major areas: telemetry conversion, command conversion, and switching and patching. A block diagram of the system and the interfaces with the basic CDC and the SDS 910 and 920 computers is shown in Fig. 82.

a. Telemetry conversion. This portion of the system is represented in the upper left-hand area of Fig. 82. A logic diagram of the telemetry converter is shown in Fig. 83. Modifications to the decommutator consist of bringing signals already available internally to the decommutator out to a terminal board. These signals use 12 binary multiplexed lines consisting of the 11-bit telemetered data word and a decommutator-generated parity flag bit, the

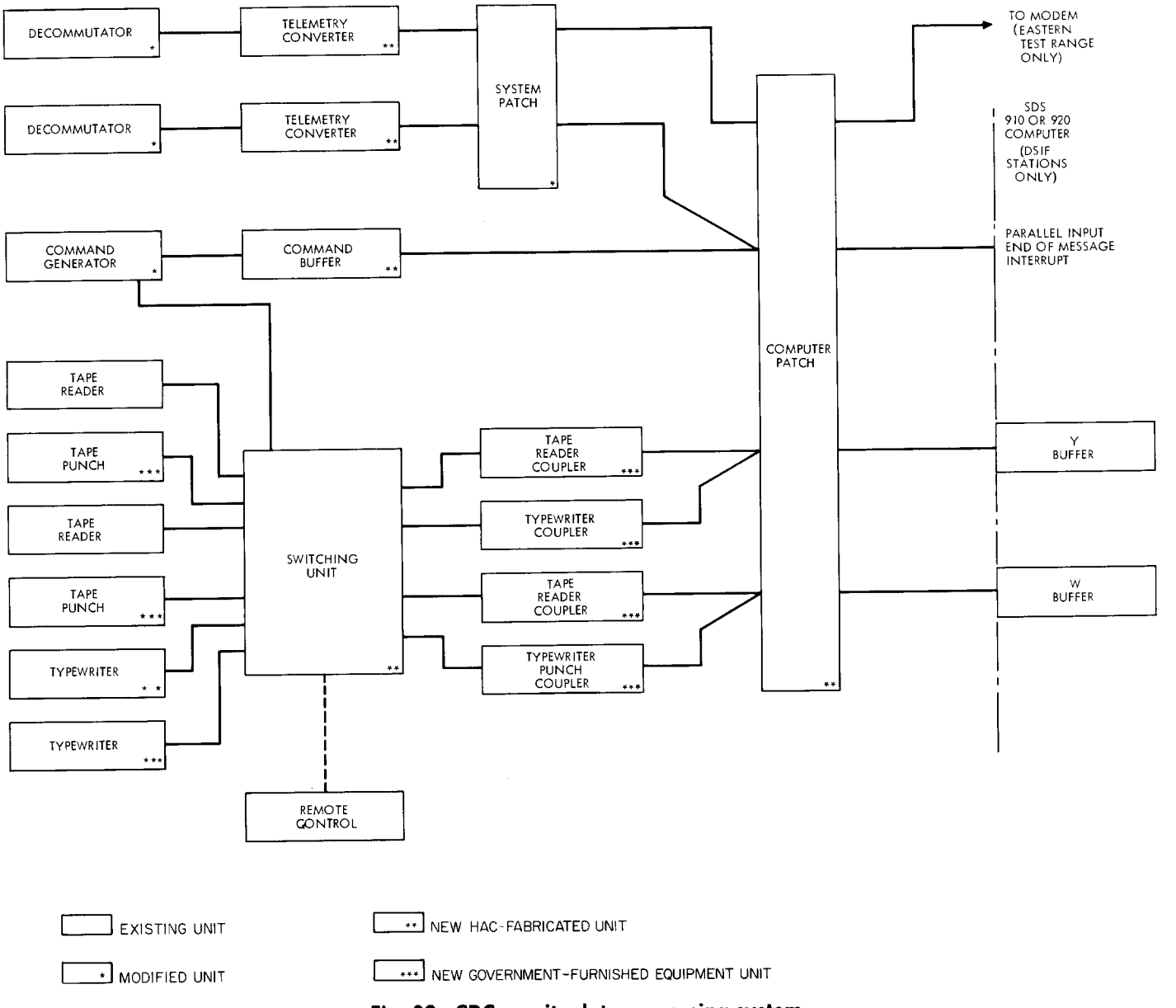

Fig. 82. CDC on-site data processing system

UNCLASSIFIED

CONFIDENTIAL

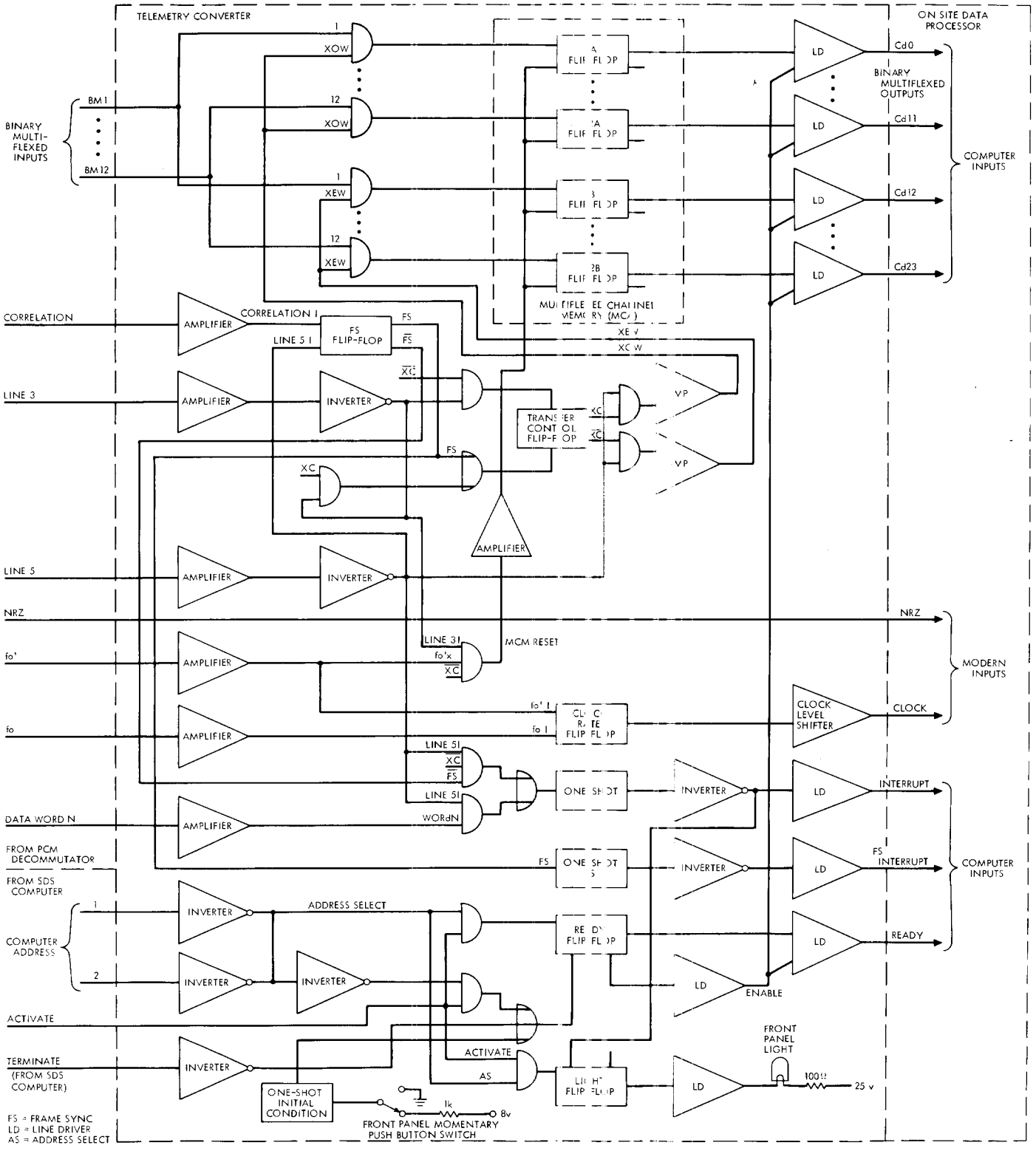

Fig. 83. Telemetry converter logic diagram

CONFIDENTIAL
UNCLASSIFIED

UNCLASSIFIED
CONFIDENTIAL

correlation pulse, Line 3, Line 5, fo, fo′, the reconstructed bit train, and the word gate for Data Word N.

The telemetry converter accepts the 12 binary multiplexed lines, the status of which is shifted into the multiplexed channel memory at the telemetry word rate. The shifting pulses are controlled such that the 12 bits associated with an odd data word are shifted into a bank of 12 flip-flops (Fig. 83). Correspondingly, the even data words are shifted into an identical set of flip-flops. These 24 flip-flops comprise the multiplexed channel memory. The odd- and even-word transfer is controlled by an alternating flip-flop which is always set to the one state prior to the transfer of all odd data words. The multiplexed channel memory outputs are fed to a series of 24 line drivers. The line drivers are enabled upon receipt of the SDS computer address and activate signals and remain enabled until receipt of a terminate pulse from the computer.

The unit instructs the computer by an interrupt signal generated when the multiplexed channel memory is ready for the processing of a pair of data words. The computer is also instructed by a frame sync interrupt signal whenever the next interrupt signal is associated with Data Words 1 and 2.

The telemetry converter also accepts the serial non-return-to-zero bit train from the decommutator, couples it to the modem, and generates a square-wave clock pulse at the telemetry bit rate from the decommutator-generated fo and fo′ pulses.

b. Command conversion. A logic diagram of the command buffer is shown in Fig. 84. Its function is to transfer the 10-bit command message and 1 bit of magnitude information from the J-register of the command generator to the SDS computer. On receipt of a print command from the command generator, the command buffer initiates the transfer process by sending an interrupt signal to the computer. The computer sends back address and activate information. When the command buffer is addressed by the computer, it sends a ready signal back to the computer and removes an inhibit from the data line drivers. After the computer has sampled the data, it sends a terminate signal to the command buffer and causes the

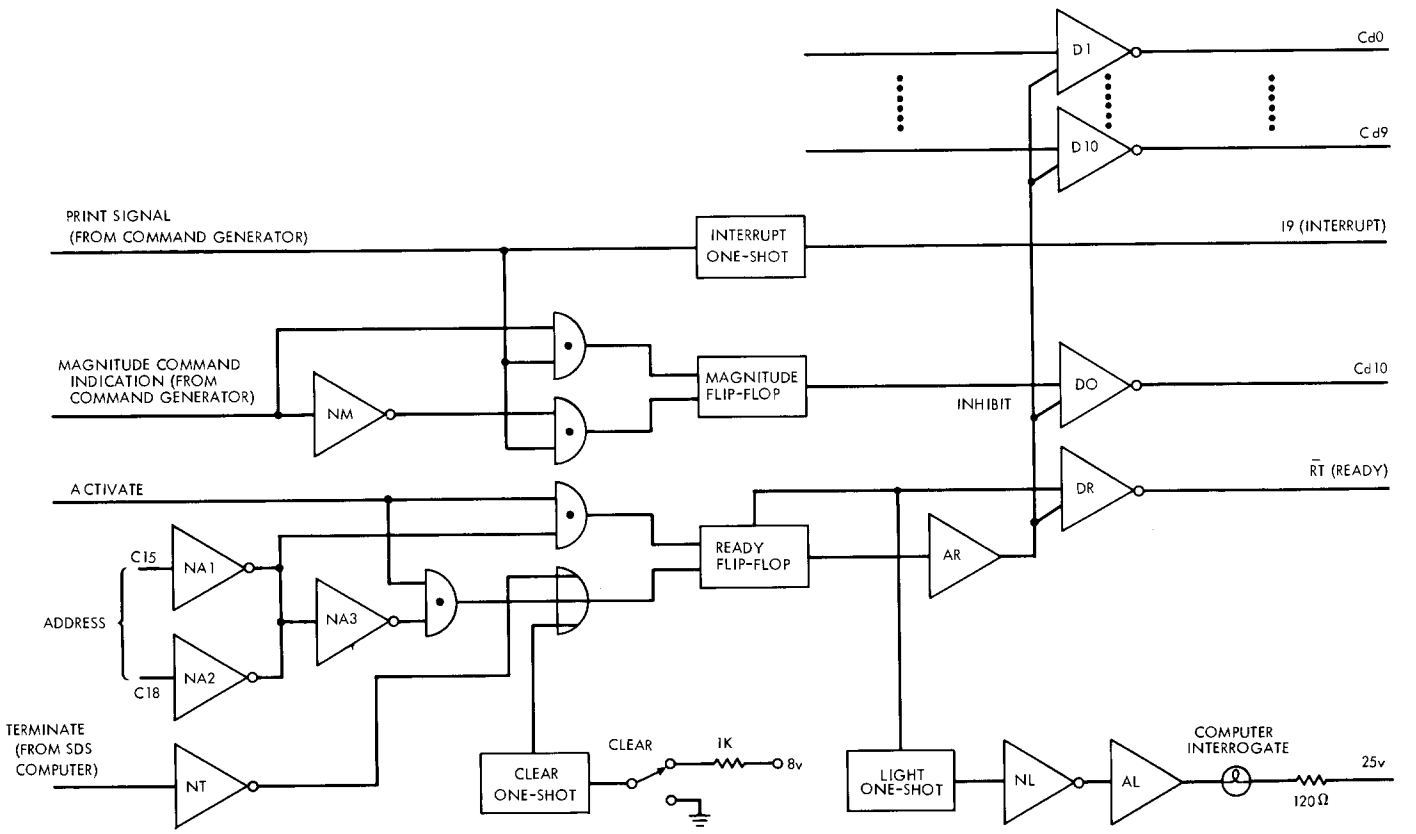

Fig. 84. Command buffer logic diagram

UNCLASSIFIED
CONFIDENTIAL

UNCLASSIFIED
CONFIDENTIAL

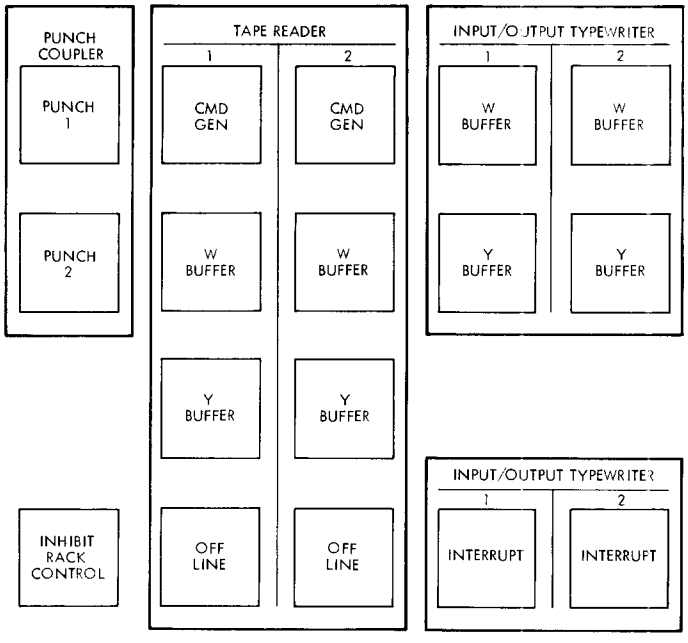

Fig. 85. Remote control unit front panel layout

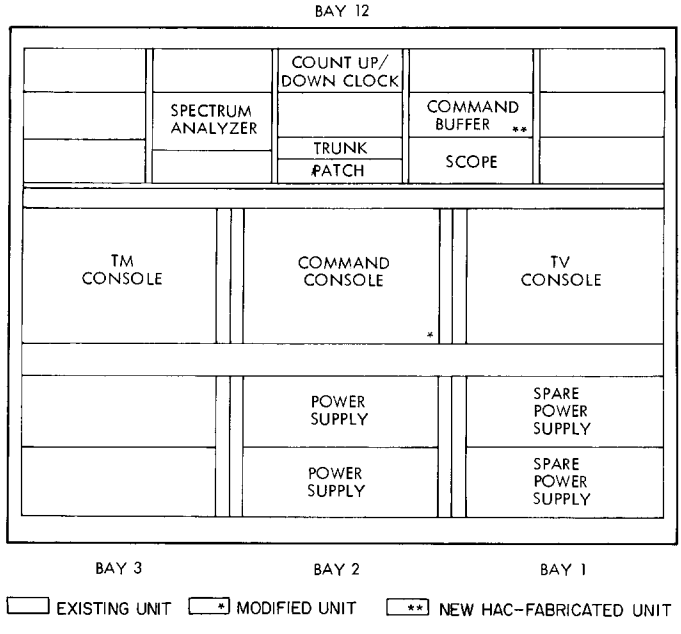

Fig. 87. Modified console layout

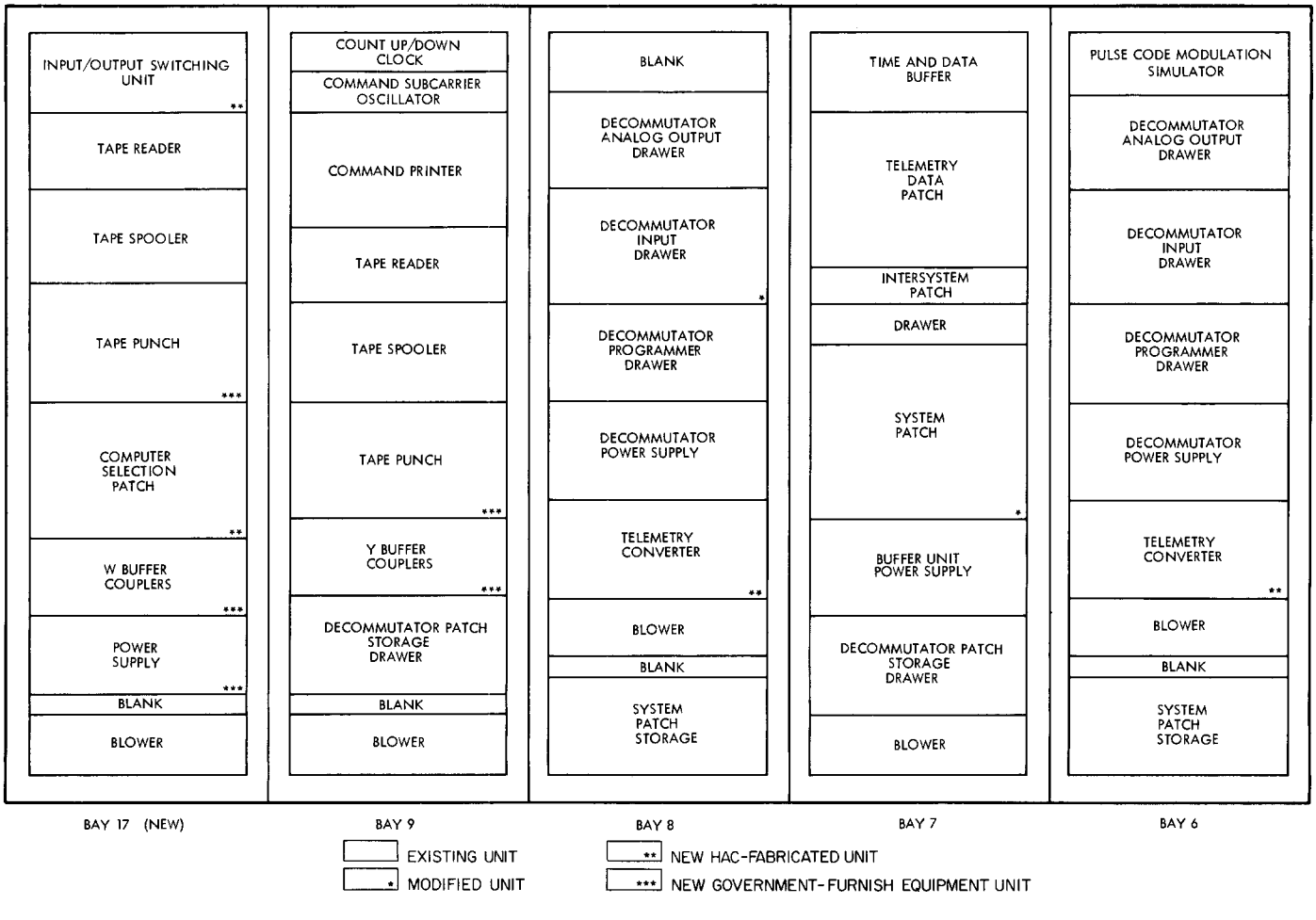

Fig. 86. Modified rack layout

UNCLASSIFIED
CONFIDENTIAL

UNCLASSIFIED

ready signal to be removed and the data line drivers to be inhibited.

c. Switching and patching. The switching function is shown in the lower left-hand portion of Fig. 82. Switching can be accomplished from either the rack-mounted unit or a remote control unit which is located between the two typewriters. The unit is capable of connecting: (1) either tape reader to either reader coupler, (2) either tape reader to the command generator, (3) either paper tape punch to the typewriter punch coupler, and (4) either typewriter to either typewriter coupler. The front panel layout of the remote control unit is shown in Fig. 85.

Patching is accomplished at two locations. The first is at the system display patch, which provides the capability to place the decommutator and its associated telemetry converter on-line. The other decommutator and telemetry converter will then serve as an on-line spare. Patching is also accomplished by the computer selection patch, which selects either the SDS 910 or the SDS 920 computer.

The new rack and console layouts are shown in Figs. 86 and 87. The remote control unit will be mounted on a shelf connected to the two input/output typewriters.

UNCLASSIFIED